AN ABSTRACT OF THE THESIS OF

Bennett Romanaggi for the degree of Master of Science in Wood Science and Civil Engineering presented on October 10 2017.

Title: Effect of Hole Edge Distance on Strength of Through-Bored Utility Poles

Abstract approved: _____

Jeffrey J. Morrell   Arijit Sinha

There are over 130 million wood poles supporting electrical transmission and distribution lines in the U.S. The vast majority of these poles are preservative treated to prolong their useful life. In some cases, however, the depth of treatment is relatively shallow, leaving a deep zone of moderately durable, untreated heartwood. This zone is susceptible to the development of internal decay that reduces pole capacity and shortens service life. Douglas-fir is one such species. Extensive efforts by Pacific Northwest utilities in the 1960's led to the development of a number of methods for improving the treatment of heartwood in Douglas-fir.   One of the most popular is through boring which involves drilling a series of holes through the cross section in critical decay areas such as the groundline, prior to treatment. The process results in nearly complete treatment of this zone.

Any process that drills holes in a pole removes cross sectional area, creating the potential for reduced flexural properties. Engineers have long been concerned about the effects of through boring. Prior studies; however, have shown that through boring produces only a minimal effect on modulus of rupture (MOR) or modulus of elasticity (MOE) and the

process has been standardized through the American National Standards Institute (ANSI) with a 5 % reduction in properties compared to non-through bored poles. However, there are still lingering questions about the process. One of these questions is the possible effect of proximity of through bored holes to the edge of the pole. Current standard specify a minimum edge distance of two inches; however, some utilities extend this distance to three inches. This increases the risk of incomplete preservative penetration that might reduce pole properties.

In order to address the issue, finite element modeling was used to examine the effect of edge distances ranging from 1 to 3 inches on pole properties. The models suggested that the current 2 inch edge distance would have no significant effect on pole properties. Forty eight air-seasoned Douglas-fir poles were used to confirm the model results. The poles were divided into 4 groups of 12 poles each. Poles in a given group were left without holes or drilled so that the through boring holes were 1, 2, or 3 inches inward from the outer edge. The poles were then tested to failure in a four point bending test and the results were used to calculate MOR and MOE. While MOE and MOR were lower than those found in previous tests, there were no statistical differences between the treatments.

The Mean Stress Method was used to simulate wood anisotropy, as stress concentration theory over-predicts stress in wood products. This was implemented as a post processing tool and used the Hoffman failure criterion to determine strength.

The numerical model or Finite Element Model was able to predict the location of failure in 36% of poles, and failure criteria within 25% of the experimental load. The model predicted failure location for 40% of poles from a previous test using the same testing

procedures, and failure criteria of 23% of the experimental load. The model predicted an observed significant difference within the previous data, but was not sensitive enough to predict a smaller difference. The model cannot predict the properties of individual pole, but may be useful for examining the relationships between anatomical and mechanical properties collected here to model changes in failure location and strength between different drilling patterns.

Effect of Hole Edge Distance on Strength of Through-Bored Utility Poles

by
Bennett Romanaggi

A THESIS

submitted to

Oregon State University

in partial fulfillment of
the requirements for the
degree of

Master of Science

Presented October 10, 2017
Commencement June 2018

Master of Science thesis of <u>Bennett Romanaggi</u> presented on <u>October 10th 2017</u>

APPROVED:

Co-Major Professor, representing Wood Science

Co-Major Professor, representing Civil Engineering

Head of the Department of Wood Science and Engineering

Head of the School of Civil and Construction Engineering

Dean of the Graduate School

I understand that my thesis will become part of the permanent collection of Oregon State University libraries. My signature below authorizes release of my thesis to any reader upon request.

Bennett Romanaggi, Author

ACKNOWLEDGEMENTS

TABLE OF CONTENTS

LIST OF FIGURES

LIST OF FIGURES (Continued)

LIST OF TABLES

Chapter 1. Introduction

Wood utility poles are a vital part of electrical infrastructure, and failure in any part of the system can affect the lives of thousands. As a result, utilities require products that are reliable and long lasting. One aspect of wood is that biological agents can cause losses of strength that increase the probability of premature failure. Poles are normally pressure-treated with preservative for protection before they are placed in service. Utilities have created several solutions to improve preservative penetration during treatment, including deep incising, radially drilling, and through boring. Through boring offers the greatest preservative penetration of the three approaches, creating complete preservative treatment at the ground-line zone, the region most susceptible to decay.

Engineers have long questioned the effects of through boring on strength, however, and there have been several studies on its effect on the mechanical properties of poles (Brown and Davidson 1961, Graham 1969, Elkins 2005, Morrell 2011). The results of these studies led to the development of a standard through-boring pattern that attempted to minimize strength losses and maximize preserved area (Elkins 2005).

Some utilities do not use the standard through-boring pattern as specified in ANSI 05.1 (ANSI 2017), and instead drill at larger edge distances. Edge distance is the perpendicular distance between the bore hole and the pole surface. Increasing the edge distance may leave gaps in the preservative envelope, increasing the likelihood of decay. However, increasing the edge distance also lowers stress concentrations. Additionally, even when the edge distance remains constant for all sizes of poles, the resultant stress concentrations can be different for each one. It would be prohibitively expensive to test all classes of poles at different edge distances; however,

developing a better understanding of the effects of edge distance on pole properties would help utilities make better decisions on through-boring patterns.

Finite-element modeling (FEM) has been used in the past to predict the strength of wood poles (Pellicane and Franco 1994), however strength predictions should be taken with a grain of salt as there are often assumptions to simplify the task. FEM has been used to predict the effects of edge distance in dimensional lumber (Falk et al. 2003) and knot location (Baño et al. 2011, Guindos and Guaita 2013) on strength, as well as trends of through-boring hole size and stress. The effects of individual parameters in drilling patterns on pole strength can be isolated, and utilities can use this information to create new through-boring and other drilling patterns.

The goal of this research was to investigate the effect of edge distance on flexural properties for a single class of Douglas-fir poles. Additionally, a strategy for predicting the effects of through boring on strength for all classes of poles was developed. A dual strategy was used to accomplish the following research aims:

1. Evaluate differences in strength of and failure patterns between poles through bored at different edge distances.
2. Numerically predict the strength and failure locations of through-bored poles.

By validating the finite element model with the full-size test data, the model can be modified to predict strength losses for different classes of poles, through-boring patterns, or species.

Scope of Study

An experiment was designed to investigate the effect of the edge distance (control, 1 inch, 2 inch, and 3 inch) of through-bored holes on pole strength. A linear elastic finite model was

developed to predict stress concentrations manifested at through-bored holes. The failure

location and strength of poles were predicted with stresses found with the Mean Stress Method.

Validation of the model included the experimental data in this study, as well as previous results

by Elkins (2005).

Chapter 2. Literature Review

Development of Through Boring

The development of modern society was spurred by accessible electricity. A reliable electrical network has been required since the invention of the first light bulbs. Moving electricity requires a distribution network, and wood poles have been an important component of that system. There are over 150 million wood poles supporting the wires that make up the electric grid in the United States (Mankowski et al. 2002). These poles are largely composed of three wood species: southern pine, western redcedar, and Douglas-fir. Wood is a biological material that is susceptible to degradation from a variety of agents. As a result, most poles are artificially impregnated with preservatives to extend their service life.

The species used for wood poles have different performance attributes. Southern pine is the most commonly used species; it has a thick band of very treatable sapwood surrounding a small, untreatable heartwood core. Once treated, the thick shell of treated wood provides good protection for the untreated core. Western redcedar has a thin shell of sapwood surrounding a naturally durable heartwood core. This species was initially used without supplemental treatment, but the thin sapwood shell is now artificially impregnated with preservative.

The expansion of the burgeoning electrical distribution system after the Second World War led to shortages of western redcedar and the substitution of Douglas-fir. However, there were a number of problems with this substitution. Douglas-fir is difficult to treat; this species has a thin band of treatable sapwood surrounding a moderately durable heartwood core, which poses the greatest protection challenge. The thin layer of preservative treatment can be compromised by

checks while in service. Furthermore, poles were not being sufficiently heated during the treatment process, allowing decay fungi already present in the wood to continue to degrade the poles once they were placed in service. The poles were often not properly seasoned prior to treatment, leading to skips in the preservative barrier. These wet poles also continued to season in service. As they did, deep checks opened that often penetrated beyond the depth of the original preservative treatment. These checks created pathways for fungi and insects to enter and degrade the moderately durable heartwood.

A 1959 survey of 74 pressure-treated poles that had been service for an average of 11 years in Portland, Oregon found that 19% of the poles had rot pockets, while a separate survey by the Bonneville Power Administration (BPA) found decay rates closer to 50% (Merz 1959). These surveys led to a cooperative effort by BPA, Pacific Power, and Portland General Electric Co. (PGE) to identify solutions to what was viewed as a very large, emerging problem. Among the developments from this process were the identification of fumigants for the internal treatment of poles in order to arrest decay and the requirement that poles be heated for a sufficient time period to kill any fungi present inside the wood. In addition, there were efforts to develop improved methods for achieving more complete treatment of Douglas-fir heartwood. Among the processes developed were deep incising, radial drilling, and through boring prior to preservative impregnation.

Incising is the practice of driving sharpened metal teeth into the wood to a specific depth (usually 0.40 to 0.75 inches). The process exposes more end-grain to preservative penetration, improving the depth and uniformity of treatment. Deep incising substitutes 5- to 6-inch-long teeth to produce much deeper penetration. Radial drilling involves drilling 0.25-inch diameter holes to a

depth of 3 to 5 inches into the wood in a pattern that produces nearly complete preservative penetration of the bored area.

Through-boring was developed by George Merz of PGE, and it has increased the service life of Douglas-fir poles to 60 to 70 years (Morrell 2011). Through boring involves drilling holes of 0.50 to 0.56 inches in diameter at a slight angle completely through the pole in the groundline area (Figure 2-1). While all three practices were and continue to be used, through boring has been the most widely adopted. At first, only the local utilities employed through boring for their Douglas-fir poles, but the practice slowly spread across the country for pre-treatment of large Douglas-fir transmission poles, ultimately leading to its inclusion in the American National Standards Institute Standard ANSI 05.1 (ANSI 2017).

Conceptually, drilling holes in the critical groundline region of a pole creates concern among engineers, and there have been a limited number of tests to evaluate the potential effects of these groundline treatments on the flexural properties of poles. Brown and Davidson (1961) tested the bending strength of Class 4, 40-foot poles with several variations of groundline boring. The poles were drilled before treatment with one of either two different radial drilling patterns or two Merz through-bored patterns. The poles were set in the ground to a normal depth (about 6 feet) and tested full length in cantilever loading. They found that the breaking strengths of the poles with varying Merz patterns were 91% to 96% of those for the untreated controls. Radial drilling to a depth of 4 inches from the surface or to the pole center resulted in breaking strengths that were 73% to 76% of the controls. This is counterintuitive that holes drilled partway are weaker, but could be due to the creation of multiple radial failure planes in the pole.
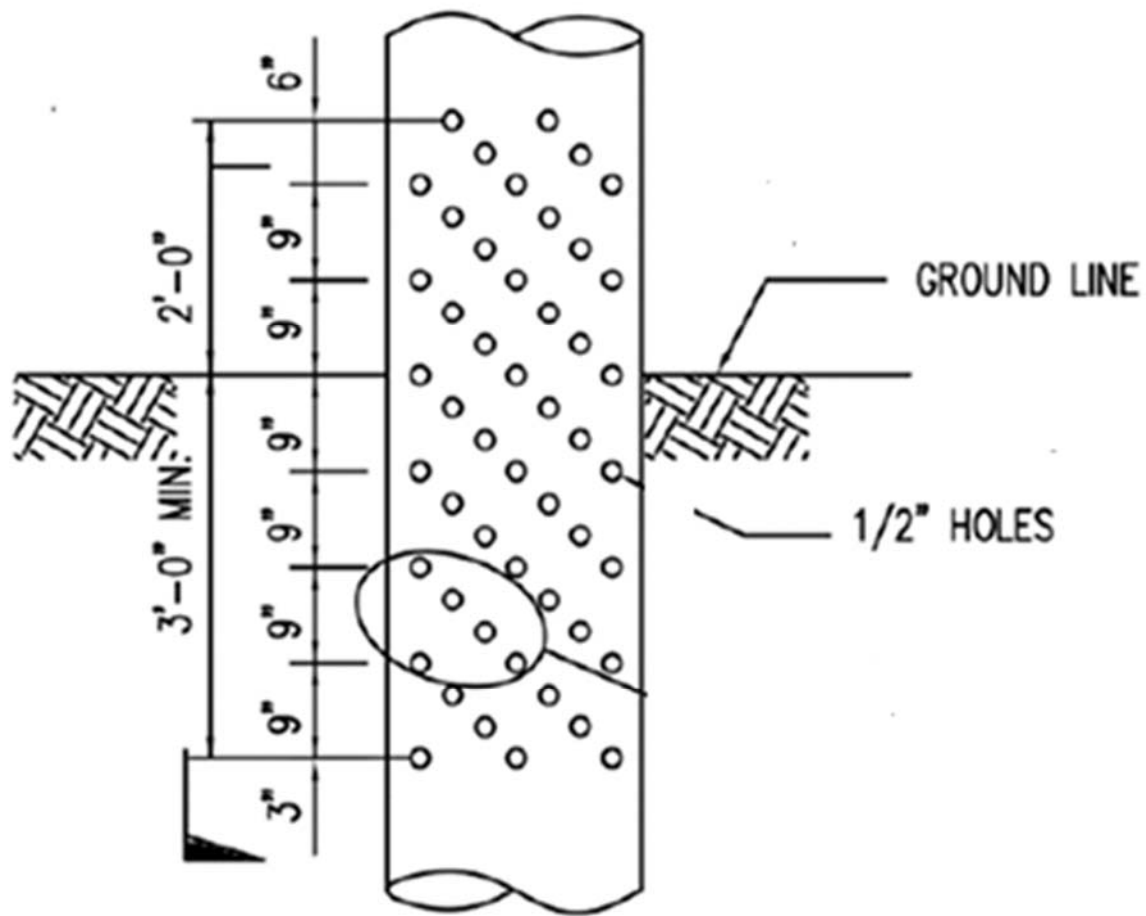
Figure 2-1: The through-boring pattern used today. (ANSI 2017)

Graham et al. (1969) tested shorter Douglas-fir pole sections that had been deep incised, through bored, or radially drilled, and found minimal effects for deep incising, but 16% to 24% losses in modulus of rupture (MOR) for poles with various boring patterns. These poles were tested in bending, but it is unclear if the results bear directly on the properties of a full-length pole tested in cantilever loading, which is more reflective of in-service loads. These limited test data largely

formed the basis for supporting the use of through boring and radial drilling in utility specifications.

In 2002, the effects of through boring on lodgepole pine were investigated; this species has similar durability and treatment characteristics as Douglas-fir (Morrell 2002). The pole sections were small (average diameter was 4.77 inches) with 0.25-inch diameter holes drilled 0.5 inch from the edge, at a spacing of 1.97 inches (50 mm) or 5.91 inches (150 mm) horizontally and 2.95 inches (75 mm) longitudinally. The poles were tested in four-point bending, both parallel and perpendicular to the holes. Modulus of elasticity (MOE) was found to be 88% of that found for non-through-bored controls; MOR was found to be 90% to 96% of the control when poles were tested parallel to the holes and 70% to 82% when tested perpendicular to the holes. The results indicated that through boring could negatively affect the flexural properties of smaller diameter poles, and that the effect was directional.

A number of studies showed that through-boring largely eliminated decay in the drilled region and markedly extended pole service life (Newbill 1993, Morrell and Schneider 1994). While there were periodic concerns about losses in flexural properties, the trade-off in terms of improved treatment at the ground line was believed to largely offset any strength losses. However, periodic pole failures of through-bored poles subjected to overloads such as strong winds or ice generally occurred in the through-bored zone, leading engineers to question the potential effects of this practice on strength. In addition, there were a number of patterns used by utilities, making it difficult for wood treaters to standardize practices.

Kent (2003) used loss of section modulus from through boring to estimate possible strength effects, and estimated a maximum 17.5% to 23.5% reduction in strength. These calculations did

not take into account stress concentrations, and he recommended modeling and testing to determine the actual effects.

In order to address the issues highlighted by Kent (2003), Elkins (2005) undertook a large-scale test to determine the effects of through boring on pole properties. Elkins began with finite-element modeling to study stress concentrations around through-bored holes. The goal was to determine the sizes of and distances between holes that would minimize stress concentrations. These data, along with prior studies, showed the minimum distances needed to result in full preservative penetration in a through-bored zone, which were then used to develop an optimum boring pattern. The effects of through boring on flexural properties were then evaluated, using four different hole sizes on Class 4, 40-foot pole sections. One hundred and thirty-two poles were tested in four-point bending in a configuration developed in Australia (Crews et al. 2004). The results indicated that through boring had no significant effect on flexural properties when the holes were less than or equal to 0.5 inches in diameter. These results, along with a follow-up test evaluating the effects of the orientation of the load direction (parallel or perpendicular to the holes) were used to support the inclusion of through boring in the ANSI 05.1 standard, using a standard pattern, 0.5-inch diameter holes and a reduction in properties of 5%, in order to account for the directional effects.

While through boring continues to be used and adopted by utilities, there are still lingering concerns about its possible effects on pole properties. One particular area of concern is the distance from a through-boring hole to the edge of a pole. Elkins (2005) examined this factor using finite-element modeling and used test data to arrive at a minimum 2-inch edge distance. However, some utilities have chosen to use larger edge distances. This practice moves the holes farther into the pole and increases the likelihood of unpreserved wood between the surface and

hole. This is important because the potentially affected area is located close to the surface, where most of the bending strength of a pole lies. There appear to be no data supporting the larger edge distance, and there is concern among treaters that this practice will make it more difficult to obtain acceptable treatment. In order to address this issue, the following study was undertaken.

Pole Kiln Drying and Moisture Content

Utility poles are often kiln-dried before treatment to reduce the moisture content (MC) from green to near fiber saturation. Kiln-drying affects strength, MOE, and checking. The ANSI 05.1 standard recognizes that kiln-dried wood has a 0.9 reduction factor on strength. This 0.9 factor seems to be a conservative estimate derived from two series of tests on southern pine poles (Eggleston 1952, Thompson 1969). Electric Power Research Institute (EPRI) authors saw a 10% reduction in MOR (Philips et al. 1985) and a 14% to 34% reduction in MOE. In practice, kiln drying is performed on green poles to bring the shell below the fiber saturation point (FSP) before treatment, but it is not frequently used on Douglas-fir or western red cedar.

Wood et al. (1960) looked at the effects of Boultonizing, steaming, and air drying for several species. The authors found that the strength decreased more between treated and untreated poles compared to small, clear specimens cut from both groups. Additional defects, such as shakes developed in treatment, exacerbated strength loss. Steamed southern pine poles developed pith checks and lost 20% strength, compared to green controls. This was greater than for other treatments, which lost less than 10% strength. Wood et al. (1960) recognized that checks affected the shear area, and that shear stress in bending was typically low. Shakes would reduce bending strength. The authors also stated that the strength of treated Douglas-fir decreased radially

inward. They did not hypothesize why; however, differential shrinkage would create tension cracks that would reduce strength.

Philips et al. (1985) examined the difference in strength between air-seasoned southern pine poles and poles in a previous kiln-drying study (Thompson 1969). The authors found kiln drying at 152° and 182° F led to a decrease of MOR by 12% to18% and MOE by 34% and 39%. Matched samples were not used, and the presence of pith checks and shakes was not recorded. The species in the study were southern pine, but a reduction in strength would also be expected for Douglas-fir.

Graham and Womack (1972) dried 8-foot sections of green Douglas-fir at temperatures from 220° to 290° F. The authors found that the largest checks extended the length of the section, and that internal checks formed. Internal checks were caused by differential shrinkage between the dry shell and wet core. However, no mechanical testing was performed; the researchers estimated the loss of strength to be between 5% and 12%. Kozlik (1982) kiln dried 8-foot sections of Douglas-fir to find strength reductions, testing three pole diameters at three kiln schedules, which ranged in severity. The largest checks extended the length of the pole in 75% of the kiln-dried samples, but air-seasoned poles had similar checking patterns. Small, clear specimens were cut, and were tested in three-point bending. The authors found that there was a reduction of 15% in the severely kiln-dried specimens and only a 5% drop at the less severe schedule, compared to the air-dried specimens. At all temperatures, MOE was reduced by 4%. Based on the conclusions from this study and the ASTM 1960 (Wood et al. 1960) test, greater drops in strength would be expected for a full-size pole than for small, clear samples. Checking was similar for all sizes, but no tests were performed on differences in strength between sizes.

Kiln drying reduces the strength of wood, but as wood dries, its strength increases. As Douglas-fir dries from green to 12% MC, the strength increases by 60% for tension parallel to grain, 90% for compression parallel to grain, and 25% for shear parallel to grain (Forest Products Laboratory 2010) for small, clear specimens. The effect of moisture decreases as size increases. This conclusion is based on wet service factors (C_M), a safety factor for MC above 19% for an extended period. In dimensional lumber, the maximum C_M for bending is 0.85, for shear parallel to grain is 0.97, and for compression parallel to grain is 0.8 (National Design Specifications 2015). For posts and timbers, C_M is one except for compression perpendicular to grain and compression parallel to grain. A similar non-loss of strength is seen for poles and pilings. Although pole design values may not change with moisture content, individual strengths may. Philips et al. (1986) showed an increase in strength properties of air-dried poles of 1% to 10%, with MOR being significantly greater.

Madsen (1975) examined the effects of MC on the distribution of strength in dimensional lumber. Madsen found that dimensional lumber that was weaker than the average was not affected by MC, while stronger specimens experienced changes in strength. Although material properties increased, defects still controlled the point and strength at failure. Utility poles under the fiber saturation point may increase in strength, depending on the frequency of defects. As both air seasoning and kiln drying were used in the experiment, the mechanical effects of both may cancel.

Stress Concentrations

Stress is a way in which a body reacts to external forces. The stress field within a body is the distribution of internal tractions that balances the external forces that are applied. In a solid body under tension, a plane normal to the load will contain a constant distribution and magnitude of these traction fields or stress fields. However, the stress fields are redistributed when there is a discontinuity, and there is a sharp rise in stress around those regions. The redistribution and increase in stress is greatest near an abrupt discontinuity, such as a hole. Stress fields and magnitude are near normal farther from the distribution, shown by Saint-Venant's Principle (Boresi and Schmidt 2003). Stress concentrators can occur in many locations, such as notches, holes, or corners.

Equation [1] describes the magnitude of stress concentration, called the stress concentration factor (SCF),

$$SCF = \frac{\sigma_{max}}{\sigma_{nom}} \qquad [1]$$

where σ_{nom} is the stress without the discontinuity and σ_{max} is the maximum stress created by the discontinuity. The most common example is an isotropic bar with a hole under tension loading (Figure 2-2). The bar is defined by width D, hole diameter d, and thickness t. The nominal stress is simply the tensile force divided by the cross-sectional area.
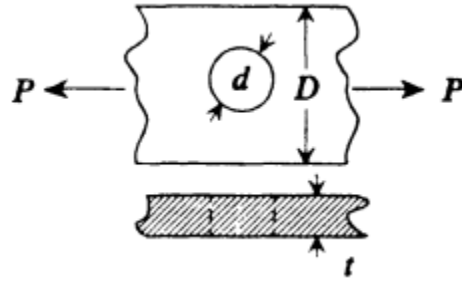
Figure 2-2: Bar under tension (Roark and Young 2011).

Stress can be predicted for different ratios of D and t (Figure 2-3); these predictions indicate that

the maximum stress for an isotropic material can increase threefold. This is important, as a small

hole or notch causes a large increase in stress. If SCFs are not considered in the design,

premature failures can occur. Although SCF have been listed for a variety of different shapes and

loading conditions (Pilkey 1997), there are still a number of scenarios that have not been

examined.
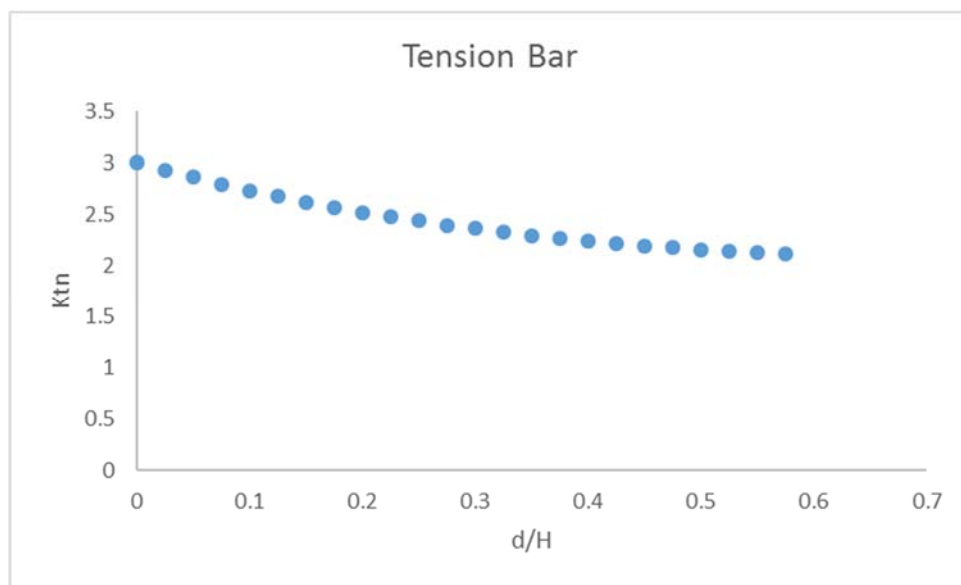
Figure 2-3. Maximum stress concentration for a bar under tension.

Stress concentrations can occur together, and this magnifies the stress. For example, a utility pole in bending contains multiple stress concentrations. Each through-bored hole creates a stress concentration, and the edge distance of each hole creates additional stress. In addition, most SCFs are only applicable for isotropic materials, although solutions do exist for some loadings of anisotropic materials.

A utility pole can also be idealized as a cylinder under bending, where curvature adds additional stresses compared to a rectangle. Figure 2-4 describes an isotropic cylinder in bending, derived from Pilkey (1997); the curve has a minimum at $d/D = 0.1$. The optimal hole diameter is 1.05 inches for a Class 4 pole with a diameter of 12 inches. However, the experimentally optimal hole size is smaller, 0.5in (Elkins 2005). These results suggest that stress concentrations alone do not explain the results of previous testing.
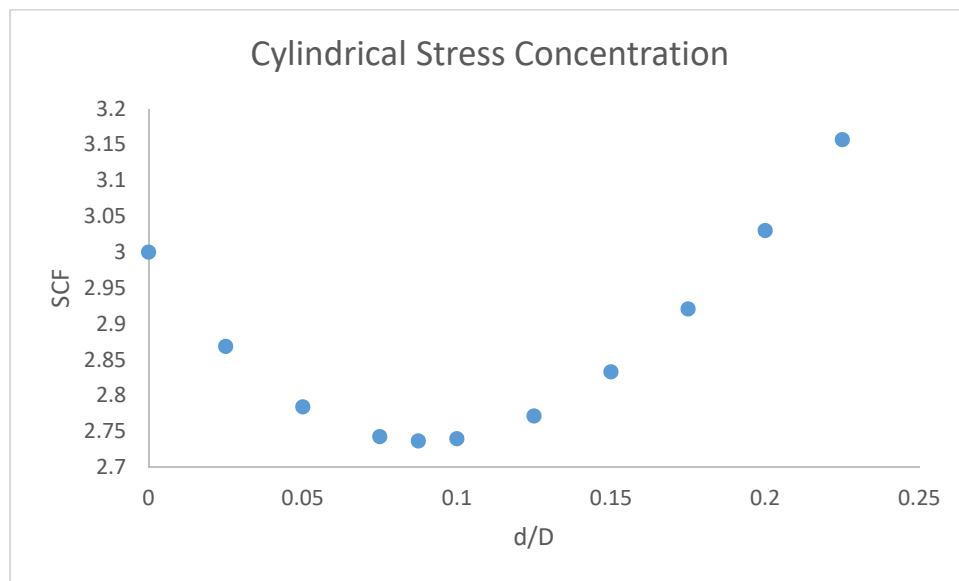
Figure 2-4: Stress concentrations created for a cylinder in bending: d/D is a normalized hole diameter, where d is the hole diameter and D is the cylinder diameter.

Pilkey (1997) also described the effect of edge distance for a rectangular beam with a hole in bending (Figure 2-5). There is no minimum stress value, as was the case in the cylindrical member above. This is important in utility poles since moving the holes farther from the edge increases the likelihood of gaps in the treated area. Thus, there is a tradeoff between stress and treatment quality.
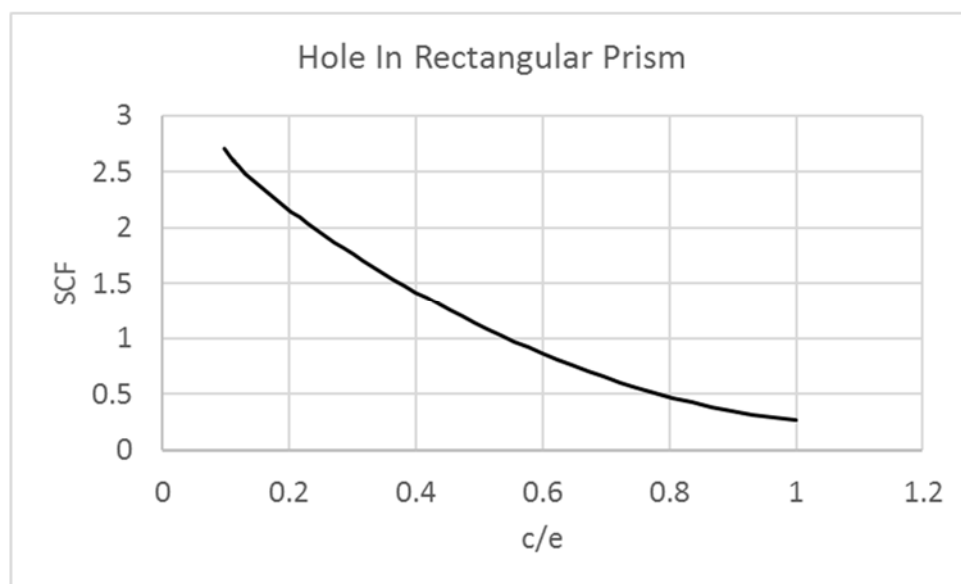
Figure 2-5: SCFs for a rectangular prism in bending with a hole at the edge distance, c/e, where c is the edge distance and e is the width minus the edge distance.

The effect of edge distance on properties has been previously investigated on dimensional lumber (Williams et al. 2000, Falk et al. 2003). Falk examined the effect of 1-inch diameter holes drilled into Douglas-fir nominal 4- by 8-inch (88.9-by 184-mm) beams tested in bending and

found that a small edge distance significantly affected the strength. They hypothesized that edge distance was more important than hole size. However, the parameters were only tested in a few configurations, and the authors suggested the need to test more configurations. Williams et al. (2000) modeled Douglas-fir nominal 4- by 8-inch (88.9- by 184.0-mm) beams using finite element analysis with two different edge distances and used Falk's experimental data to validate the model, comparing ultimate load, load-deflection, and mode of failure. They found holes to be at a critical stress near the edge of the beam, and subsequently estimated the stress ratios. This model only predicted failure for rectangular dimensional lumber with a single hole, however. A different model would need to be developed for a cylindrical member.

In addition to causing an increase in stress, holes can produce a change in the neutral axis. Davis et al. (2012) investigated the effect of knots in the tension and compression faces, and tracked the location of the neutral axis. A change in neutral axis depth means that traditional beam mechanics are less accurate. The neutral axis can change for both small and large samples due to differences in MOE in tension and compression (Davis et al. 2012); however, the true neutral axis for large specimens should remain nearly constant, due to nearly equal knots and holes in both the tension and compression faces,

Most SCF derived in the literature are for isotropic materials and are solely dependent on the geometric properties of those materials. Stress concentrations for orthotropic materials also depend on the material properties. The first prediction for stress concentrations in wood was by Smith (1944), who predicted the stress distribution in plywood under tension. Smith used mechanics to show that there was an increase of $5.84\sigma_{nom}$, compared to $3\sigma_{nom}$, as previously derived for an isotropic material. This stress increase was a multiplier based off the difference of Young's Modulus in the x and y direction, and the shear modulus in the xy direction. This stress

increase was 16% greater than the experimental results because of mathematical assumptions and the difficulty of measuring strain at a point. Measured stress concentrations in wood have been shown to be accurate, although they do not address wood's heterogeneity. Chiang (1998) predicted SCF for an edge-notched orthotropic plate using a multiplier factor of the material properties to predict the stress increase and found good correlations with experimental results.

The orthotropic multiplier factor is not the only multiplier in this process. Wu (2003) examined stress concentrations in orthotropic cylinders with a hole in tension, where no SCF existed for this system; however, factors do exist for plates, cylinders, and orthotropic materials. Wu (2003) determined the stress concentration using two scaling factors: the ratios between (1) an isotropic cylinder and an isotropic plate and (2) an orthotropic plate and an isotropic plate. These factors were multiplied together with the SCF for an isotropic plate to find the SCF for an orthotropic cylinder under tension. The results showed good convergence with finite element predictions. More SCFs for other loadings and geometries could be developed using this approach.

As a non-homogenous material, wood already contains natural stress concentrations in the form of knots and checks. Knots radiate outward from the pith and are weaker than the surrounding wood. Differences in stiffness result in knots acting similarly to holes when under tension (Guindos and Guaita 2013). Additionally, knots redirect the flow of grain and change the direction of normal stresses. Natural stress concentrations may be greater than the manufactured stress concentrations. Elkins (2005) tested through-bored utility poles and found that the majority of failures initiated at knots. The initial stress concentrations created by the knots were greater than the manufactured concentrations, and they dictated the type of failure.

Although minor in comparison with large defects such as knots, the cellular structure of wood may also affect stress concentrations, depending on how the cells are sheared by a manufactured defect such as a hole. Stress concentration theory assumes that the maximum stress will occur at a point, which is a limitation of FEM, requiring an infinitesimally fine mesh, although it produces close estimates. Additionally failure can only initiate at a finite area, compared to traditional homogeneous stress concentrations (Danielson 2007). This idea will be further explored in the failure criteria section.

Stress concentrations can occur near each other, and introducing stress concentrations may occasionally increase the strength. An example of introducing stress concentrations to increase the strength is with crack remediation in concrete and steel, which can be explained as follows. A small hole is drilled at the crack tip. This hole produces a smaller stress concentration than the prior crack tip. This hole can also be drilled near another hole, which then smooths the stress field around both of the holes. This use of holes for defense was first introduced by Heywood (1952), was optimized later by Erikson and Riley(1978), and was further optimized with Finite Element Analysis by Meguid (1986). One of the main conclusions from Meguid's (1986) work was that to act defensively, holes have to be one to two hole diameters apart. However, Pilkey (1997) stated that holes would continue to interact at distances of 10 diameters apart. Wang and Bodig (1991) explored this idea with wood, examining interactions between pairs of knots on a two-dimensional plate. They found that knots needed to be close together and that the larger the difference between the two knots, the greater the stress decrease. They also noted that at least one interacting knot pair existed in half of the poles surveyed, and that their interaction increased the stress induced in bending.

The defense hole theory was one of the explanations for the decreased variation found in through-bored utility poles (Elkins 2005). The through-boring holes redirect stress around the knots, and the pattern and spacing of the holes ensure that there will nearly always be a hole near a knot to redirect stress.

Fracture Mechanics and Failure Criteria

All materials fail under extreme loading, and it important to understand how this process occurs. Materials can experience many types of stresses under loading. Failure theories attempt to determine how the combination of stresses cause the material to fail. The simplest stress theory is the maximum stress criterion, which states that a material will fail when a principal stress exceeds the yield stress (Boresi and Schmidt 2003). This theory ignores components of any secondary stresses and is not useful for anisotropic materials.

More realistic examples combine multiple stress components in order to create more accurate stress states. The most common example of this approach is the von-Mises yield criterion (Boresi and Schmidt 2003), which gives an equivalent stress based on differences in principal stress. The problem with this theory is that it does not recognize stresses in different directions, and it uses only the largest principal stresses and again is only for isotropic materials.

Strength can differ in all directions for an anisotropic material. A failure theory then must account for strength differences in every direction. Hill's (1948) yield criterion uses all stress components, with coefficients that represent strength in three directions. Hill's yield theory does not consider differences between tensile and compression stresses, however, so is not applicable to wood. The Tsai-Azzi criterion is a special case of the Hill yield criterion that looks at individual quadrants of stress to account for the difference (Carbero 2012). The Tsai-Wu criteria

is similar to the Tsai-Aziz, but it contains a linear term. The Tsai-Wu contains coefficients for the differences in tension and compression for each direction of stress, products of those directions, and shear. Additionally, there are components that need to be determined by using a biaxial test. These methods work when biaxial components are assumed to be equal to zero (Patton-Mallory 1997,Williams et al. 2000). The criterion is similar to the Hill approach when the biaxial term = 0 (Carbero 2012); however, other researchers have determined biaxial components to be between 0.08 (Eberhardsteiner 2002) and 0.5 (Tsai 1992). The Hoffman criterion (ANSYS 2017) is similar to the Tsai-Wu criterion, but does not contain the term for differences in tension and compression and instead uses a linear multiplier.

Researchers have recognized that traditional stress criteria must be modified when applied to wood. Theories for stress concentrations assume that maximum stress will occur at a singularity. In wood, the smallest distance is determined by the size of the wood cells (Guindos and Guaita 2014). Wood grain around knots and holes also change the direction of stress. One approach to address these issues is to acknowledge the size effect by using fracture mechanics.

Masuda and Honda(1988) and Landelius (1989) developed similar methods to calculate the stress in a region rather than at a point. The "mean stress method" averages stresses over an area or volume. This method was developed through testing notched beams, while Landelius created a theoretical solution. This method uses an additional variable, the theoretical integration size, which is dependent on the orthotropic stiffness for Mode 1 fracture, the perpendicular tensile strength, and the critical energy release rate (Landelius 1989). However, changing the magnitude of this variable does change the averaged stresses around the area, another variable to be aware of.

Gustafsson et al. (1996) used the mean stress method to predict the strength of glulam beams with holes and it has also been used to predict the effects of knots on strength in bending using finite element analysis (Guindos and Guaita 2014) . The best strength prediction was made with the Tsai Hill criterion and an integration volume, using an 8-mm cube. Correct integration volumes are still under discussion, and differ for hardwoods and softwoods because of the differences in cell arrangement. Masuda (1988) used 2 mm in the longitudinal direction, while Thelandersson (2003) suggested using 20 mm along the grain and 4 mm in radial/tangential directions for softwoods. This method increases the computational time, but may provide valuable information at a small scale.

Finite Element Modeling of Wood and Utility Poles

The orthotropic nature, heterogeneity, and nonlinearity of wood make predicting strength difficult. Wood requires testing many more samples as it comes from a living organism, resulting in inherent variance not present in steel or other materials. Computer modeling can be used to predict the strength of wood products and thereby reduce the need for physical tests. Nonlinearity, natural defects, grain direction, and failure mechanism have all been modeled for wood.

The material behavior of wood is orthotropic and nonlinear. Nonlinear behavior occurs in compression, and wood behaves differently in compression as the cells either buckle or are crushed. Methods to define the nonlinear behavior include using bilinear and trilinear functions (Patton-Mallory et al. 1997, Moses and Prion 2002, Guindos and Guaita 2014), power functions (Tabiei and Wu 2000), or more terms (Baño et al. 2011). Bodig and Goodman (1973) showed that longitudinal MOE was proportional to the other elastic parameters, and these ratios have

been used in several models (Cramer and Goodman 1983, Cramer and Goodman 1985, Pellicane and Franco 1994). Some researchers reference the work of Vallippan et al. (1976) and Shih and Lee (1978). Vallippan et al. (1976) created an anisotropic work-hardening material model, for which Shih and Lee (1978) created an extension of the Hills yield criterion in order to account for strength differences in tension and compression. Patton-Mallory et al. (1997) created a constitutive model to account for the effects of changing elastic parameters on other directions for a bolted connection. The nonlinear behavior was modeled using a trilinear curve for Douglas-fir; in addition to changing E_L, the authors also reduced the Poison's ratio. The authors modeled both shear and tension perpendicular to grain as nonlinear, in order to maintain symmetry. This model produced a good match between the stress strain curves. However, it is not a true constitutive model, due to negative stiffness coefficients, which show that the model is unstable. Tabiei and Wu (2000) examined nonlinear compression of wood, and attempted to create a symmetric, nonlinear stiffness matrix. Changes to the elastic modulus were based on previous experiments that used the same species with different orientations, producing reasonable results. The anisotropic model created by Moses and Prion (2002) improved upon the Patton-Mallory model in order to more accurately predict strength, using a constitutive model. The authors used the TB, ANISO option in ANSYS, which does not modify the stiffness matrix. This anisotropic option assumes a bilinear curve in each direction for compression, tension, and shear. The tangent moduli and yield moduli in each direction can be different. This option reduced the tension-perpendicular-to-grain stress, compared to the Patton-Mallory model, but overestimated the failure properties of Douglas-fir. The Moses-Prion model uses 3.2 MPa, compared to 2.3 MPa, for tension perpendicular to grain, and 7.6 MPa, compared to 5.5 MPa, for compression perpendicular to grain (Forest Products Laboratory 2010). A number of researchers have used

inflated strength values for their small clear samples, but other strength values remain relatively close to reference values.

The nonlinearity of wood has also been addressed using an effective section technique. Cramer and Goodman (1983) characterized the tensile strength of a beam with a knot in it by decreasing the stiffness of an element to near zero when the element stress reached the designated tensile strength in any direction. After this initial failure, the load will continue to increase until a maximum has been reached. This technique was coined "the effective section technique" and predicted the stress within 20%, an improvement compared to ASTM tests. Removing material as it yielded created a nonlinear stress strain curve. This work laid a good foundation, but the stress was essentially dictated by the clear wood area after material was removed due to perpendicular to grain stress. Cramer and Goodman (1985) improved the model to use stress intensities to create cracks. Zandbergs and Smith (1988) included grain direction while Williams et al. (2000) predicted the bending strength of a beam with a single hole using the Tsai-Wu strength theory and the stress limits found in the Wood Handbook (2010). Element reduction occurred when an element reached the Tsai Wu criteria on all nine integration points. This minimized the potential for one stress to dominate a single location. Williams et al. (2000) found good results for stress strain curves, and replicated the nonlinear behavior. The maximum load fell within one standard deviation of test specimens, and the model remained conservative. Ghan and Zhu (2004) used the effective section technique to predict the strength of OSB I-beams with different sized openings. Failure was dictated by the Tsai-Hill criteria. The authors found good correlations between the stress strain curves and failure loads.

Finite element modeling has been used to predict the stress concentrations around knots. Knots are commonly modeled as holes when the knot is in tension (Cramer and Goodman 1985, Baño

et al. 2011, Guindos and Guaita 2013). Cramer and Goodman (1985) found that using the maximum stress concentration for an orthotropic material was inaccurate, with a maximum SCF of 8. The authors used the effective section technique to predict strength. Wang and Bodig (1991) looked at the knot interaction in wooden poles, using at a planar model and superimposing the stress fields of the two knots together. Baño et al. (2011) modeled knots as both holes and knots and compared the model to experimental results. The authors found that knots could be safely modeled as holes when in tension; however, the material behavior and contact should be modeled in compression. This was significant, as it suggested that there were already many holes existing in a pole that are creating stress concentrations. Their nonlinear model predicted the maximum load with an error of 9.7%. One error in the model is that the strength properties for tension perpendicular to grain (10 to 3.2 MPa) and in shear (14 MPa to 10.4 MPa) are larger than for species similar to *Pinus sylvestris* found in the Wood Handbook (Forest Products Laboratory 2010). The authors later determined the influence of size and position on knots in another set of experiments in 2013. The knots were placed on the tension side at varying heights in a beam. They found that there was a 250% decrease in MOR as the knot moved from the neutral axis to near the edge, showing the importance of edge distance on strength.

Guindos and Guaita (2013) further developed the model created by Baño et al. (2011) to include grain orientation. Grain deviation was modeled as a liquid flowing around a knot, and the velocity vectors acted as the grain direction around knots. The authors then compared several failure criteria with the experimental failure load of *Pinus sylvestris* beams and found an error of less than 5%. However, there was no distinction between yield stress and the tangent modulus in the tension and compression. Guindos and Guaita (2014) addressed this in the next model by

adding fracture mechanics using the mean stress method. The authors compared the magnitude of stress components of knots at different orientations, finding orientation to be as important as edge distance.

Pellicane and Franco (1994) created a model to simulate cantilever bending of utility poles and verified through the testing of full-size poles. The model consisted of 20-sided isoparametric elements and 15 node wedge elements. Knots were modeled in the poles as decreases of the MOE, with the knot area based on the affected area, using the flow grain analogy. The poles were 50 to 60 feet long and were tested as cantilever beams. After testing, small, clear samples were cut from along the cross-section. The samples were broken in bending, and the moduli of elasticity and rupture were determined. The MOR of small samples were compared to the maximum stress parallel to grain in the model segments to find a proportional factor. The predicted strength was a 1-kip load multiplied by this proportional factor. The authors found less than 7% difference between the predicted and experimental strength, and predicted the failure location in 66% of samples. However, the method, which was supposed to predict strength, was only used for two-thirds of the samples; when the same method was used for the remaining samples, predicted strength was off by 32% to 44%.

Elkins (2005) used finite element modeling to predict the effects of distance between holes, the size of holes, and edge distance in utility poles. She predicted trends for the above information, but the presented SCF were not meaningful due to not considering size effects of wood. Her results provide a starting point to investigate how edge distance affects pole strength.

Chapter 3. Experimental Materials and Methods

Summary of Experiment

The goal of this research was to determine the effect of the distance of through-boring holes from the edge of Douglas-fir utility poles on flexural properties.

Materials

Forty-eight poles were obtained from a facility located in Arbuckle, California and shipped to Oregon State University (OSU) in Corvallis. The poles had been obtained from Douglas-fir stands near Lebanon, Oregon. The poles were a mix of Class 1 40-foot, Class 2 35-foot, and Class 4 40-foot, and the butts were cut into 20-foot sections. The poles had been air-seasoned prior to arrival.

Typically, through-boring holes are drilled parallel to the reference face, or the face of greatest curvature. This is important, as the greatest wind loads will bear perpendicularly against the pole. Many of the poles were heavily checked in one direction, and this face was marked as the reference face. Orienting the pole according to the largest check minimized the creation of a shear plane.

A drilling apparatus was created (Figures 3-1, 3-2, 3-3) to allow accurate drilling for holes at a constant edge distance. Holes were drilled at 1, 2, or 3 inches (25, 50, or 75 mm) inward from the pole edge (Figure 3-3 and 3-4). Holes were drilled in both the tension and compression faces at the defined edge distance (Figure 3-5). The Merz pattern (1959) additionally has holes in the center (crossed circles in Figure 3-4); however, these holes were not drilled in the test poles in order to isolate the effect of edge distance. Additional holes also increase the probability that

these holes will interact with knots, causing failure due to the interaction. This would obfuscate

the role of edge distance on flexural properties.
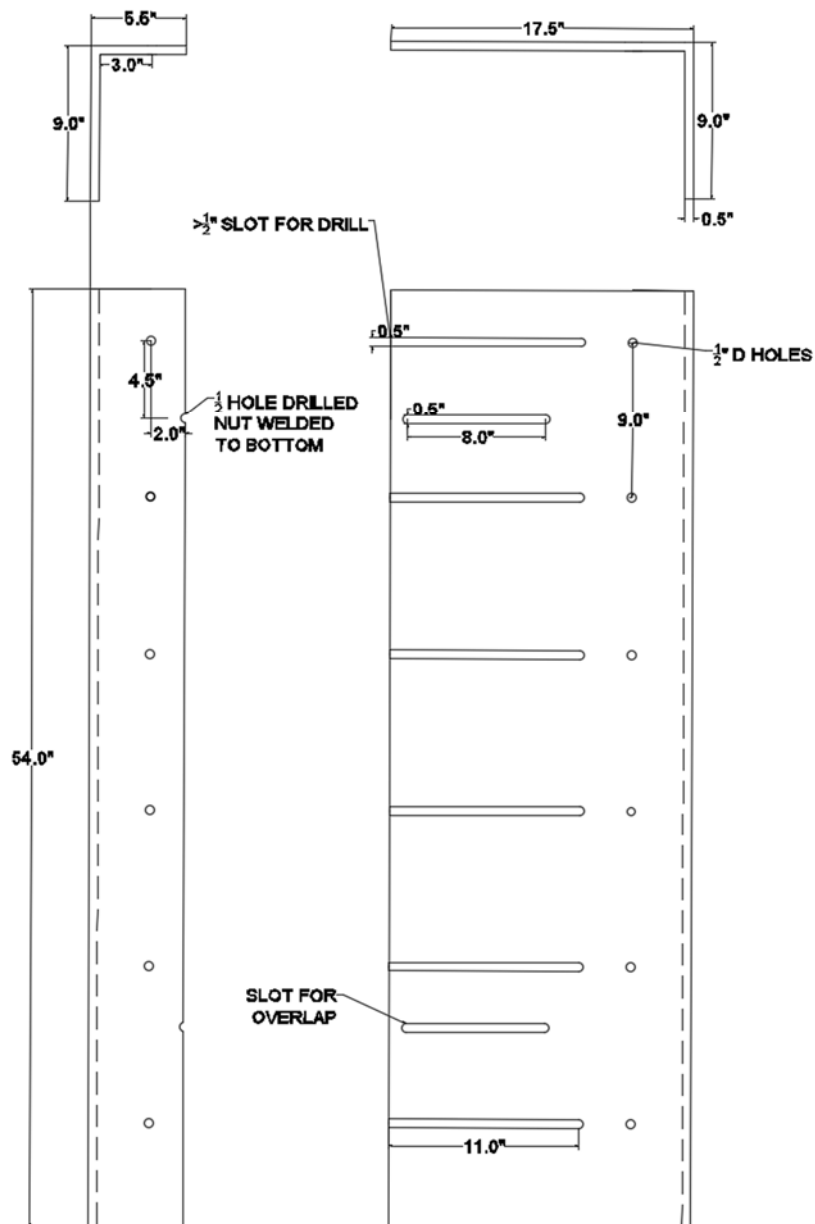
Figure 3-1. Diagram of the drilling rig created for drilling holes at a constant edge distance for any size of pole.

Figure 3-2 and 3-3. Photos of the drilling apparatus created for drilling holes at a constant edge distance. The plate can slide in and out to fit any size. Blocks cut to 1 and 2 inches are placed in the interior edges to drill at different edge distances. Holes are drilled downward through the pipes.
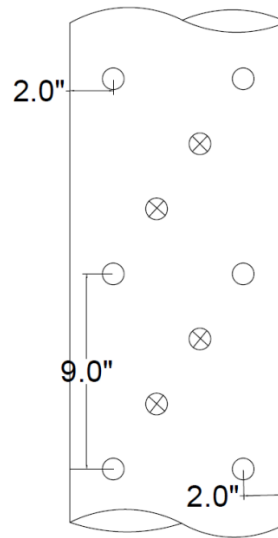
Figure 3-4. Example of a hole pattern used to through bore Douglas-fir poles. Holes with an "x" were not drilled.

Figure 3-5: Position of the holes in the tension and compression sections of the pole

Twelve holes were drilled at 9-inch (225 mm) intervals along the pole length, from 36 to 96 inches (900 to 2400 mm) above the butt, following the Merz (1959) pattern, as defined in ANSI Standard 05.1 (2017). Six holes were drilled parallel to the tension face, and the other six were drilled on the compression face of each pole.

The initial moisture content (MC) of the poles ranged from 14% to 28%, as measured from the outer 1.5 inch (38.1 mm). Due to the range of MC and the influence of moisture on mechanical properties, the poles were kiln dried at OSU. This option was chosen over wetting all poles above the FSP, due to time limits and the difficulty associated with obtaining a uniform high moisture content. Generally poles are tested in the green condition to derive ANSI properties.

The poles were dried in three charges of sixteen poles each. The first charge of 16 poles was exposed to a dry-bulb temperature of 160° F for 48 hours, with no steam applied, resulting in severely checked poles with an average MC of 8%, as measured from the outer inch. The first charge was then conditioned to 14% before testing. The second and third batches of poles were subjected to a dry bulb temperature of 120° F and wet bulb depression of 15° F for 2 hours, followed by a dry bulb of 140° F and depression of 15° F for 72 hours. The resulting MC was 14% to 16% in the outer inch of these poles.

Test Apparatus

The poles were tested using a method first developed by Crews et al. (2004), and adopted by Elkins (2005). The test is an asymmetric, unequally loaded four-point bending test. The load is biased 1:5 to the bottom end (Figure 3-4). The asymmetric and unequal loading conditions create a nearly constant moment across the groundline, mimicking the stress at the groundline observed in the field. The 1:5 ratio is created by the cylinder pushing asymmetrically on a beam, and by lever arms producing the 1:5 ratio. The moment in this test is not constant, and shear is present. Rounding of the loads was done for ease of construction of the beam lever arm. This test setup has advantages over the three-point bending test, as it stresses the entire groundline region rather than a small section directly beneath the load. This nearly constant moment will affect both

natural and manufactured stress concentrations, with the cause of failure being easily traced at the point of origin, which should be the highest stress concentration present in the loaded section.
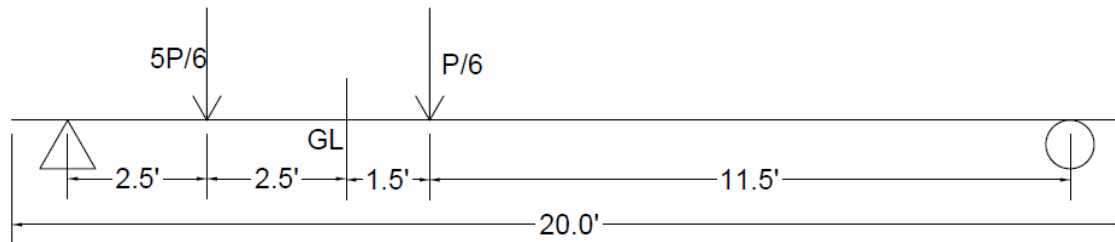
Figure 3-4: Diagram illustrating the support position and loading direction.

The supports were Douglas-fir saddles, with rotation allowed. This configuration allowed the pole tests to be modeled as a simply supported beam. The use of Douglas-fir for both the supports and the load heads minimized stress concentrations and limited material bearing. The test was not shear critical; the length was calculated to produce a depth-to-length ratio greater than 14.

Testing Procedure

The poles were grouped to maintain a constant average diameter and standard deviation. Additionally, all poles in Charge 1 were distributed across all groups, to keep variability caused by drying stresses constant through all groups. This was done for Charge 2 and Charge 3 as well.

The poles were weighed, and the diameters at the tip, bottom, and the loading locations were measured. Multiple diameters were measured, since taper was not constant across the pole

length. Knot maps were created for each pole, noting the longitudinal location and size of every t knot (>12.5 mm in diameter) near the groundline. The minimum diameter was defined by ANSI 05.1, as contributing to the maximum number of knots per 300-mm-long section. The circumferential distance was defined by the arc distance from a straight line on the compression face.

These parameters were needed to create the finite element model for each pole. The largest checks and their distance, width, and arc position were reported. The checks were not included in the finite model nor were other defects such as splits, crushing, and sweep were noted, but were not included in the model. The edge distances of the through-bored poles were measured, with both ends of the holes being measured, to give the average through-bored distance. Additionally, the average edge distance of at least two holes was measured for both the tension and compression faces in every pole.

Some poles were too large for the load heads, and supports had to be cut to fit. This was done by using an angle grinder to remove material at the location. Pole diameter, length of pole, locations and edge distances of through-bored holes, knot maps, and test MOE data were all input into the finite element model. These data were used to predict failure location, the failure load, and mode of failure and these results were compared to the experimental results.

Each pole was loaded with the through-bored holes perpendicular to the applied load. Each pole was loaded in four-point bending at a rate of 6.25 mm/min, with a 250 kip hydraulic actuator attached to a steel moment frame bolted to a concrete reaction floor. Linear variable differential transformers (LVDTs) measured the displacement at each support caused by compression of the saddles. The settlement from both ends was averaged and subtracted from the total deflection.

Additionally, a potentiometer measured deflection at a point 9.5 feet from the butt, which was calculated as the point where the greatest deflection occurred. Load, the two deflection measurements, and support settlement were recorded continuously at a rate of 5 Hz.

Failure was defined as the point when the maximum strength capacity of the pole was reached. The test was stopped after a loss of 15% of strength (post peak) or after a catastrophic failure. The ultimate mode of failure was recorded for each pole, in addition to any previous failures. Modes of recorded failure included tension, hole shear, compression, or end-shear failure. The failure area was photographed for each pole segment. Possible causes of failure, such as knot, knot cluster, hole, or check were noted for each pole. The diameter of the failure location was determined from the known taper, and was used for the section modulus and edge distance calculations. (Appendix 4)

A 50-mm-thick disk was cut near the failure zone of each pole. The disks were weighed, oven dried at 102° C, and weighed again to determine MC (oven dry basis). The thickness and diameter of each disk were measured. For disks with large voids or holes, disks were cut into halves or quarters. The oven-dry volume and mass for each disk were found by using the above method, and these data were used to calculate the specific gravity. The number of annual rings and number of rings in the outer 2 inches of the pole were counted, and the diameter of the heartwood was measured.

The MOR was calculated by using the section modulus of the through-bored region and the maximum moment. This was done to remain consistent with the method used in previous papers. The section modulus was calculated using a gross section, rather than subtracting the area removed from through-bored holes. Many poles did not fail at a section with through-bored

holes, negating the need for using a net section calculation. The effect of grinding larger members only changed MOR by 1% to 2%. The post-grinding MOR was not used, as many sections did not fail at a section with removed material.

The MOE was derived by using equations for a tapered beam and superposition of two loads. The equation, derivation, and validation can be seen in Appendix 4. The recorded MOE was used for elastic properties in the finite element modeling and to examine correlations between MOE and MOR.

Sample Size Determination

Sample size was determined by using a power-based calculation, which is typically used for hypothesis testing (Cornish 2006). Both power-based and precision-based samples were considered, but power calculations compare two groups directly to each other. δ was the smallest detectable difference, s was the standard deviation, and α and β represented the significance and power of the test, respectively. The data produced by Elkins (2005) were used to determine standard deviation by multiplying MOR and the coefficient of variation for a 50-mm diameter hole. δ was estimated so that a 15% difference in the sample MOR would be detected. These analyses indicated that 12 samples were sufficient for each group.

$$n = f(a, B) * \frac{2s^2}{\delta^2}$$

$$\alpha = .05$$

$$\beta = .1$$

$$f(\alpha, \beta) = 10.5$$

$$n = f(a, B) * \frac{2s^2}{\delta^2} = 11.29 \rightarrow 12$$

Chapter 4- Finite Element Materials and Methods

Previous 2D and 3D models, considered a variety of defects such as knots and slope of grain. However, they were very computationally expensive. Since then, increased computational power makes is easier to model many parameters quickly and efficiently. The goal of our work was to detect differences among multiple parameterized models; that included failure load, failure location, and failure mechanism. Detecting strength differences can be used to optimize the geometry of through-boring or other drilling patterns, decreasing the need to test many pole sections.

Pole diameter, length of pole, locations and edge distances of through-bored holes, knot maps, and test MOE data were all input into the finite element model. These data were used to predict failure location, the failure load, and mode of failure and these results were compared to the experimental results.

Geometry

The FEM was built in ANSYS (version 16.0) with a Top Down approach. Cone primitives replicated the shape of a utility pole. Three cone primitives were created, representing sections in four-point bending from the butt to the first load point, the width between the two loading heads, and between the second loading head and the tip. The diameter was measured for all poles at those points. The intersection between the cones provides geometry for loading to be applied.

The through-bored holes were modeled as cylinders slicing through the pole using the sketch function in ANSYS workbench. The holes were then extruded to cut through the cones with the edge distance kept constant through the entire bored section.

Knots were modeled as cones drilling out radially from the center of the cone. The position and direction of the cone were parameterized from knot maps to yield the longitudinal distance from the butt and circumferential distance from the reference face. Knots were not modeled to have a longitudinal inclination, since visually measuring the longitudinal inclination was not possible visually without cutting into the pole. This assumption was reasonable as the largest bending stresses occur at the pole surface.

Additional models were created using rectangles and cylinders with holes to verify and predict bending stress concentrations in plates and cylinders. A model with a parabolic curve was created to simulate the sweep of a utility pole to check for circumferential differences in stiffness.

Meshing

Meshing was done primarily with the Proximity and Curvature function, a size function in ANSYS. This function allows the user to refine the mesh near holes, and to mesh curves correctly. The minimum element size at the holes was 0.05 inches and the minimum element size at knot vertexes was 0.02 in. The maximum element size was 1.4 in. The stiffness matrix decreased in size and consequently reduced processing time by only refining the mesh near holes (Figure 4-1). The mesh could not converge at vertexes in knot. so a small face was introduced to provide correct meshing. The mesh was verified in post processing using the default ANSYS convergence tools, and by hand calculation for orthotropic materials, since this property is not

supported in ANSYS. Symmetry was not used, due to the lack of symmetry in a utility pole with defects.
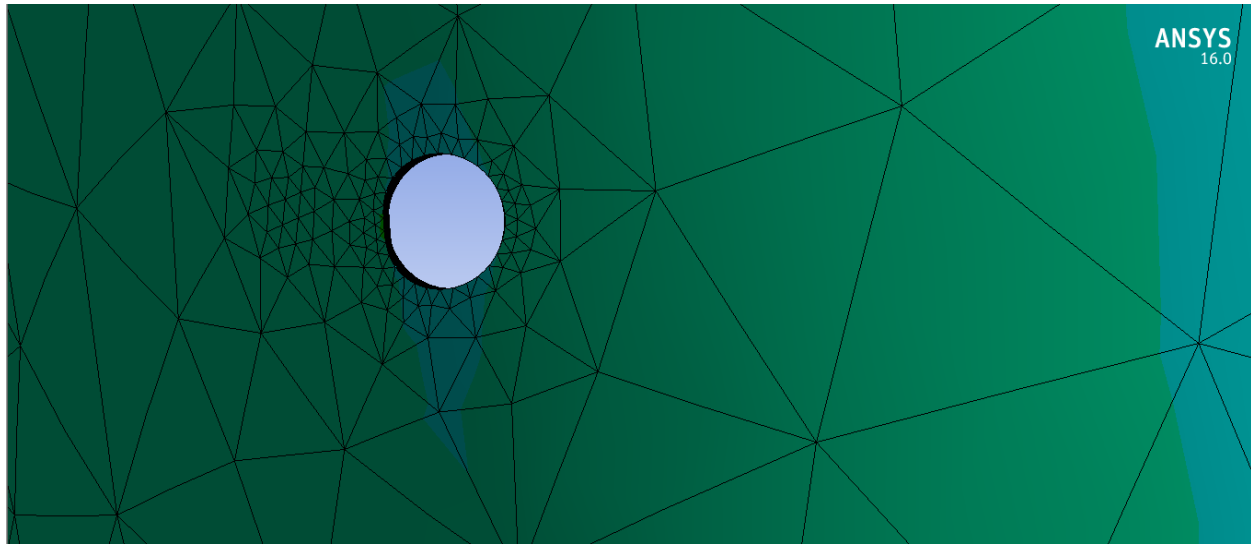
Figure 4-1: Meshing around a hole is finely meshed

Elements

Determining the element that fits all requirements required several iterations starting with SOLID186. This is a 20 node quadratic cube, with options for tetrahedrons, pyramids and prisms, needed to correctly model curvature. This element is capable of large strains and birth/death. The 20-sided node is one of the most computationally expensive elements, having 60 total DOF but midsized nodes are needed to capture curvature. The cylindrical orthotropic material properties were defined by a cylindrical coordinate system. This element does not support anisotropic plasticity. For this reason, SOLID 92, a tetrahedral 10 node quadratic solid was used. It proved to be a better choice as it supported non-linearity and element birth and death. The program automatically added additional elements too. SURF156 is a quadratic surface load element, used to apply loads in the structure. CONTA174 connects cone primitives together.

Boundary Conditions and Loading

Four-point and cantilever bending were created, representing two common methods for pole testing. For four-point bending, the model is restrained transitionally in the X, Y, and Z directions, and rotationally in the X direction. The cantilever model it is fixed in all directions with the remote displacement tool with the deformable option, which allows the model to converge easier.

The load was applied as a force acting downward at the nodes along the circumference of the pole at the intersection of the cone primitives. Load was applied until the experimental failure load. The loading pattern used in the model was the same asymmetric unequal distribution used in the actual testing.

For the verification of the force in four-point bending, the specimen converged to within 5% of the expected normal stress using standard beam calculations. There were greater than expected shear stresses in the xy, yz plane and normal stresses in other directions for orthotropic materials. This effect was magnified when knots or holes were near the load point, causing excessive deformation and stress. For this reason, a submodel was developed, but not used, that would be most effective in cantilever bending, where the load was far away from the region of interest.

Other loading methods investigated included displacement boundary conditions and a plate bearing downwards. These methods were not validated due to excessive displacements of nodes, and excessive stresses at the contact surface. Using a distributed force over an area was also examined, but not used because it created a larger area with spurious stresses at the edges.

Material Properties

The elastic relationships and strength parameters were obtained from the Wood Handbook for

12% Coastal Douglas fir (Tables 4-1 and 4-2). The material properties were transversely

isotropic, a common assumption although wood is orthotropic. Material direction was defined

by a global cylindrical coordinate system, and the effects of grain angle were ignored. Table 4-1

used elastic ratios for the determination of parameters based on a longitudinal modulus

determined in testing. Table 4-2 includes an estimated shear perpendicular to grain, and the

MOR instead of tension parallel to grain, which is an assumption used in modeling of bending

specimens. A discussion on implementing non-linear behavior is included in Appendix 1.

Table 4-1: Material Properties for Douglas-fir for elastic relationships

E_Z (psi)	E_R & E_T (psi)	G_{RT} (psi)	G_{TL} & G_{RL} (psi)	M_{XY}	μ_{YZ} / μ_{XZ}
E_Z	0.07* E_Z	0.007*E_Z	0.07* E_Z	0.374	0.0325

Table 4-2: Strength Properties for Wood Used in Finite Element Modeling

Tension Perp(psi)	Compression Perp	Tension Para	Compression Para	Shear TL,RL	Shear RT
300	800	13600	7230	3000	1130

Failure Criteria

A common method for determining the mode of failure is to use a failure criterion. The goal of implementing the failure criteria is to perform load stepping while processing and to check the failure state of the material. The model stops when the material reaches the failure criteria, and the dominating stress, location and failing load are recorded. In a further developed model, the load would continue to increase after the initial failure. The Hoffman criteria is a material theory that differentiates between tension and compression and is used for anisotropic materials. The Hoffman failure criteria can be reduced to equation 3 below, when σ_{1-3} represents the stresses in three directions, independent of tension or compression.

These criteria are an extension of the Tsai-Hill failure theory and are similar to the Tsai-Wu theory. The differences between the two theories are the sigma[1] terms and the biaxial terms. The Sigma[1] terms represent the difference between tension and compression, which are less accurate for highly anisotropic materials. The Hoffman theory has been shown to be a more accurate strength predictor than the Tsai-Wu theory(Guindos 2014), although it has the same number of parameters. For this reason, the study used the Hoffman criteria, to determine failure.

$$f = \frac{\sigma_1^2}{X_T X_C} + \frac{\sigma_2^2}{Y_T Y_C} + \frac{\sigma_3^2}{Z_T Z_C} + \frac{\tau_1^2}{S_{XY}^2} + \frac{\tau_2^2}{S_{XY}^2} + \frac{\tau_3^2}{S_{XY}^2} - F_{12}\sigma_1\sigma_2 - F_{23}\sigma_2\sigma_3 - F_{13}\sigma_1\sigma_3 + \frac{\sigma_1}{X_T X_C}$$

$$+ \frac{\sigma_2}{Y_T Y_C} + \frac{\sigma_3}{Z_T Z_C} \quad (3)$$

$$F_{13} = \frac{1}{X_T X_C} + \frac{1}{Y_T Y_C} - \frac{1}{Z_T Z_C}$$

$$F_{23} = -\frac{1}{X_T X_C} + \frac{1}{Y_T Y_C} + \frac{1}{Z_T Z_C}$$

$$F_{12} = \frac{1}{X_T X_C} - \frac{1}{Y_T Y_C} + \frac{1}{Z_T Z_C}$$

Multiple values for the biaxial criteria were considered for the Hoffman criteria. The testing to perform these tests is difficult and there are varied values for different species, with disagreements among researchers. To ensure a closed yield surface, possible values ranged from $-1 < F_{12} < 1$. Previous studies have used values ranging from zero (Patton Mallory 1997, Liu 1984), 0.08 (Eberhasteiner 2002), 0.5 (Tsai 1992). In lieu of tests, the value used was 0.25, which offered greater convergence than zero and 0.5, but was not determined experimentally. Experimental testing would be recommended to find the biaxial coefficient in the three directions.

Traditional stress concentrations are not representative of conditions in wood without consideration of size effects since they occur over an area smaller than the fracture area. For this reason, the mean stress method was implemented to determine stresses over an area. The mean stress method calculates stress over a small volume using dimensions of 20 mm along grain and 4 mm in the radial direction (Thelandersson 2012); however, the volume is typically experimentally determined from elastic moduli and toughness values. Mean stress was calculated with a weighted average based on element volume. The mean stresses were used in the above failure criteria to find the most likely locations of failure and the dominating failure modes.

The mean stress method was implemented using APDL code in the post processing. Results were exported to Excel for calculating the failure criteria, location, and direction.

Parameterization

Models were parameterized to determine relationships between different factors. The following

inputs, geometry, loading conditions, size, and material were parameterized in multiple models.

Parameterized outputs include stress, strain, deformation, failure location, and dominant failure

mode. Additional models were run within a range of parameters and ANSYS created a response

surface to fit these points. The response surface included measurements for the goodness of fit,

and can include verification points. This response surface was created using a second order

polynomial, which provided a good fit if the predicted trend was linear or quadratic.

Chapter 5 - Results and Discussion

Flexural Properties

Edge Distance

The poles were grouped by hole treatment (Table 5-1).The mean values and standard deviations are presented graphically in Figure 5-2. A T-test was first used to compare the means of two groups. The mean MOR for different edge distances were not significantly different from each other ($\alpha = 0.05$). but there was a trend of decreasing strength with decreasing edge distance with the three-inch group similar to the control.

The variation (COV) in each group was similar. This differs from the results reported by Elkins (2005), who found that the control group had the greatest variation and that variation decreased in groups with smaller holes. She cited the defense hole theory as the reason for this trend as the holes should alleviate stresses by redirecting the stress field. Elkins (2005) used the full Merz (1959) pattern for drilling, and the additional holes could have redistributed stress differently.

Table 5-1: Effect of hole edge distance on average MOR of Douglas-fir poles subjected to flexural tests.[1]

Hole edge distance (inches)	Average MOR (psi)		Coefficient of variation (%)	Percent decrease from control (%)
Control	6228.5	(999.0)	16.0	
1	5831.0	(1163.1)	19.9	6.4%
2	5894.6	(1198.9)	20.3	5.4%
3	6301.5	(1275.9)	20.2	-1.2%

[1] Values represent means of 12 poles per drilling group and 11 in the control. One pole was excluded from the control group due to a testing error. Parentheses represent one standard deviation.
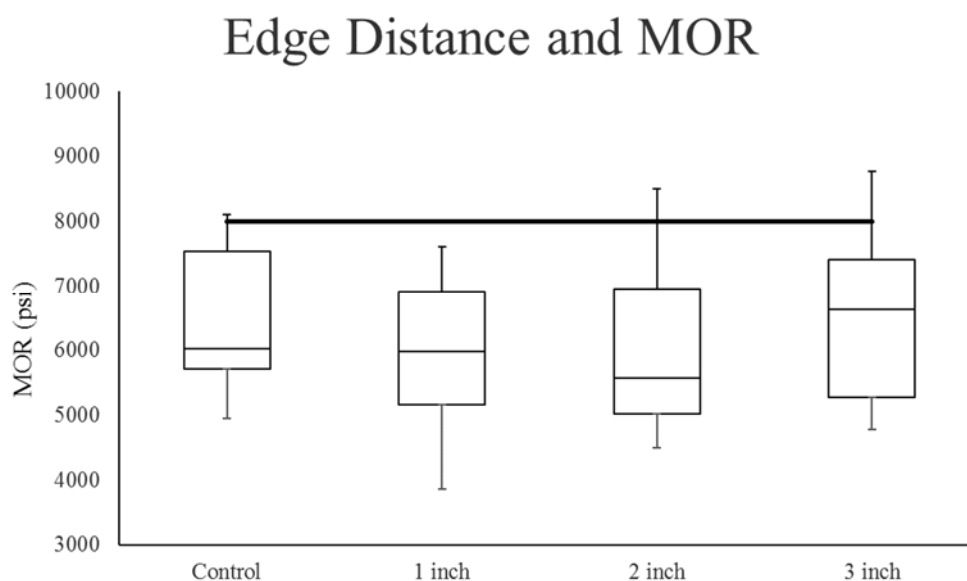
Figure 5-1: Box and whisker plot showing the distribution of MOR for the three edge distances and the control group. The middle line in each group represents the median. The black line represents the ANSI 05.1 fiber stress standard of 8000 psi for Douglas-fir poles (ANSI 2017).

The average MOR for the poles was 6060 psi for all specimens (Figure 5-2). This value is below the ANSI specification of 8000 psi for green poles. Elkins (2005) used the same bending apparatus and found the mean MOR of green poles to be 7350 psi for the poles without through boring, and 6860 psi for the poles with 0.5-inch diameter through-bored holes. Elkins (2005) used an edge distance of 2 inches. Her results for this edge distance were significantly greater than the results for the 2-inch edge group tested here. Morrell et al. (2011) found the mean MOR to be 5750 psi for 0.5-inch diameter through-bored poles at an edge distance of 2 inches.

Although not statistically significant, the difference in strength between poles without holes and those with 0.5-inch diameter holes was 5.5% for the 2-inch edge distance, compared with 6.5% for Elkins (2005). This reduction was also noted in poles with a 1-inch edge distance. Elkins

(2005) found no significant differences in strength between poles with 0.5-inch through-bored holes and the control group (α =.05).

Kiln Cycle

The poles were grouped by kiln cycle (Table 5-2). There were significant differences in moisture content (α = 0.05) between poles from different kiln cycles. However, MC was poorly correlated to MOR (R^2 = 0.05) as expected and varied by only a few percent. Despite differences in MC from poles in the third charge, mean MOR did not differ significantly, although poles from the first charge had a higher MOR. This effect may be due to pole size, as the first charge contained significantly smaller poles than the other charges.

Table 5-2: Effect of kiln charge on MOR of Douglas-fir poles with edge distance groups equally distributed to each.

Kiln cycle	Average MOR (psi)		Coefficient of variance (%)	Moisture content (%)
1	6588.4	(935.3)	14.2	14.6
2	5998.7	(1224.6)	20.4	14.8
3	6014.4	(1228.2)	20.4	16.2

MOE

MOE has generally been well correlated with MOR (R^2 = 0.45-0.72) in previous pole tests using the same test method (Elkins 2005, Clauson et al. 2017). R^2 values for the current set of data were around 0.4. One possible reason for the lower correlations was the high frequency of end shear. MOR is a measure of bending strength, and the presence of shear failures obscures the effects of bending strength. The R^2 values improve to 0.67 when the end-shear specimens are

removed from the data. It is unclear why end-shear was more prevalent in the current test

although the presence of deep checks on some poles may have facilitated this failure mode.

Effect of Pole Circumference

Although not typically correlated with MOR, pole size seemed to be a factor in the current study.

Previous tests showed poor correlations ($R^2 = 0.08$-0.15) between diameter and MOR (Elkins

2005, Clauson et al. 2017). MOR in the current study was negatively correlated with pole

circumference (Figure 5-3).
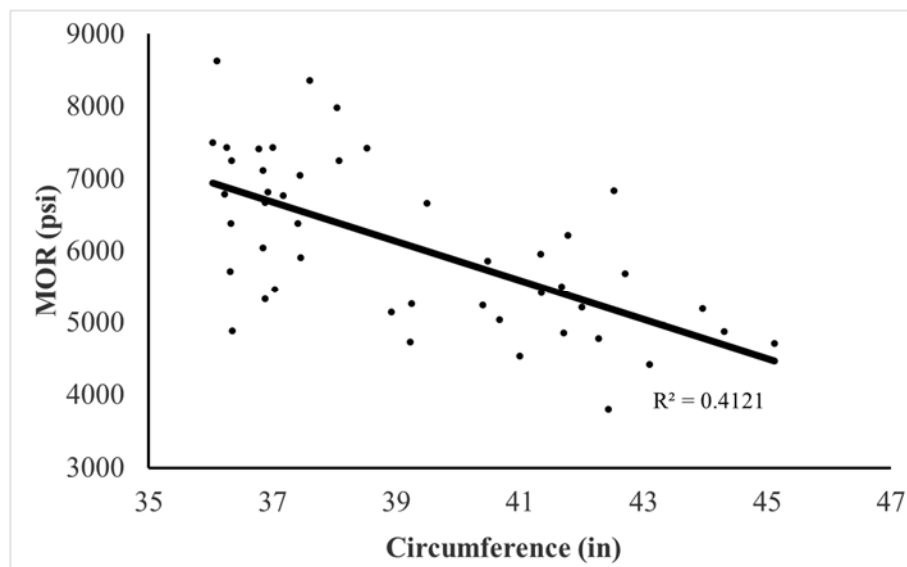
Figure 5-2: Relationship between pole circumference and MOR of Douglas-fir poles with and without through boring.

The size dependency of MOR differed between groups. Figure 5-4 below displays the

normalized edge distance (c/e) and MOR: for the 1-inch edge distance ($R^2 = 0.34$), for the 2-inch

edge distance ($R^2 = 0.27$) and for the 3-inch edge distance ($R^2 = 0.75$) (Figure 5-4). Although not

displayed, the $R^2 = 0.41$ for the controls.

Stress concentration theory predicts that a smaller c/e ratio causes increased stress. Following

that prediction, an initial hypothesis for the current study was that c/e would affect MOR.

However c/e and MOR were poorly correlated for all through-bored holes ($R^2 = 0.08$).

Therefore, c/e and, consequently, edge distance did not affect MOR in the current study.
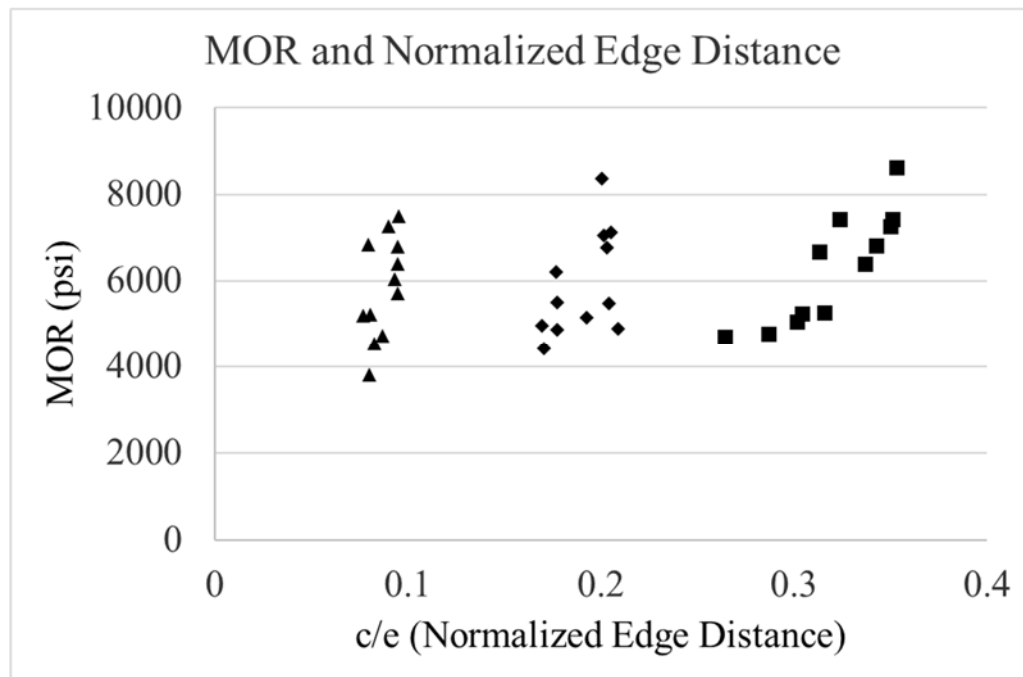
Figure 5-4: Normalized edge distance (c/e) and MOR, where c is the edge distance and e is diameter minus the edge distance. Normalizing edge distance is a method of graphically separating groups. Three distinct groups, representing: 1-inch, 2-inch and 3-inch drilling distances are shown from left to right.

Poles from the first kiln charge (Table 4-1) had a larger mean strength than those from the other

two charges, while the diameter was significantly smaller (p = .003) than poles in the other two

charges. Smaller diameter poles could have lost less strength from kiln drying, likely due to

different drying patterns.

Statistical Analysis Of Above Variables

T-tests confirmed that neither edge distance nor kiln cycle affected pole properties significantly. The data was subjected to an analysis of covariance (ANCOVA), ANCOVA was preferred over an analysis of variance (ANOVA) because it allowed the pole diameter and MOE to be included, which were both covariates. Assumptions of an ANCOVA test are homogeneity of variance, parallel regression slopes for each independent variable, and normality. Homogeneity in variance was tested by using Levene's test, which showed no difference in variance between groups. The MOR appeared to be binormal (Figure5-5), which would violate the assumptions used in the Student's t-test and ANCOVA. A Shapiro- Wilk normality test did not detect departures of normality (p =.185). The regression slopes for each group were roughly parallel.

The ANCOVA used a linear model, with the factors of kiln cycle and edge distance, and the covariates of diameter and MOE. No significant differences were found for kiln cycle or edge distance (p = 0.54), but diameter and MOE had a significant effect (p = 0.001). A Kruskal-Wallace test assesses whether a non-normal distribution would change the significance of any factors (Ramsey and Schafer 2012). The Kruskal-Wallace test did not reveal any variables with a significant effect on the MOR.

An experimental assumption was that the COV would be approximately 13% and differences between groups would be 15%. The variance in groups ranged from 14% to 20%. The sources of variance were kiln-drying and testing below the fiber saturation point. The greater-than-expected variance showed that the power of the statistical tests performed was lower than expected.

Histogram of MOR
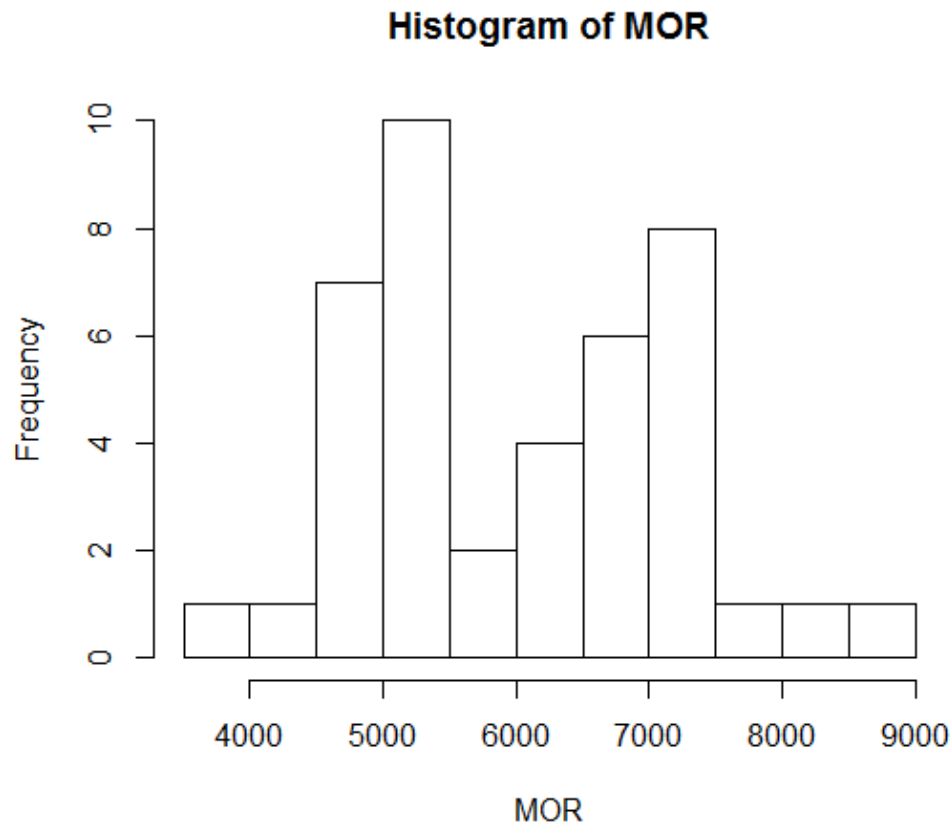
Figure 5-4: Distribution of MOR values in Douglas-fir poles with and without through-bored holes

Physical Properties of Test Poles

Moisture Content

The moisture content (MC) of the kiln-dried poles was 8% to 16% in the outer inch, as measured

with a Delmhorst RDM-3 resistance-type moisture meter. The MC measurement after testing,

using the oven-dry method showed an averaged MC of 15.2% and a range of 11% to 19% (Table

5-1). Moisture content of poles from the third charge differed significantly from that of poles in

the first and second charges ($p = 0.003$ and $p = 0.047$ respectfully). The second and third kiln

charges ended when the outer inch reached 15% MC, while the first was subjected to a drier

cycle due to human error. Although the second and third charges underwent the same drying cycle, the second charge was not removed from the dry kiln immediately, allowing the residual heat in the dry kiln to continue to dry the wood. This would tend to make moisture levels near the surface more similar to that of the first group. The potential effects of kiln charge on flexural properties were minimized by equally distributing poles from each charge to each edge distance group.

Weight and Specific Gravity

The average pole weight was 518 lb, with a range of 388 to 694 lb. The wide range reflects the fact that pole diameter varied by 3 inches. The specific gravity of the measured poles averaged 0.51, which is consistent with the reported value for oven-dried Douglas-fir of 0.5 (USDA 2010).

Circumference

The poles were a mixture of Class 4, 40-foot, Class 2, 35-foot, and Class 1, 40-foot. The average circumference of the poles was 40.8 inches at the butt and 35.3 inches at the tip. The average circumference at the groundline was 39.22 inches. The pole circumferences were not normally distributed (Figure 5-1). The supplier chose poles that had a circumference greater than 36 inches; and three different classes of poles were present. Previous pole studies have not shown strength differences between classes for distribution poles. The poles were sorted so that average diameter was equal for each edge distance group, in order to limit possible size effects. The poles were then visually assessed for knot checks, knots, and other defects to ensure that they met the ANSI 05.1 requirements.
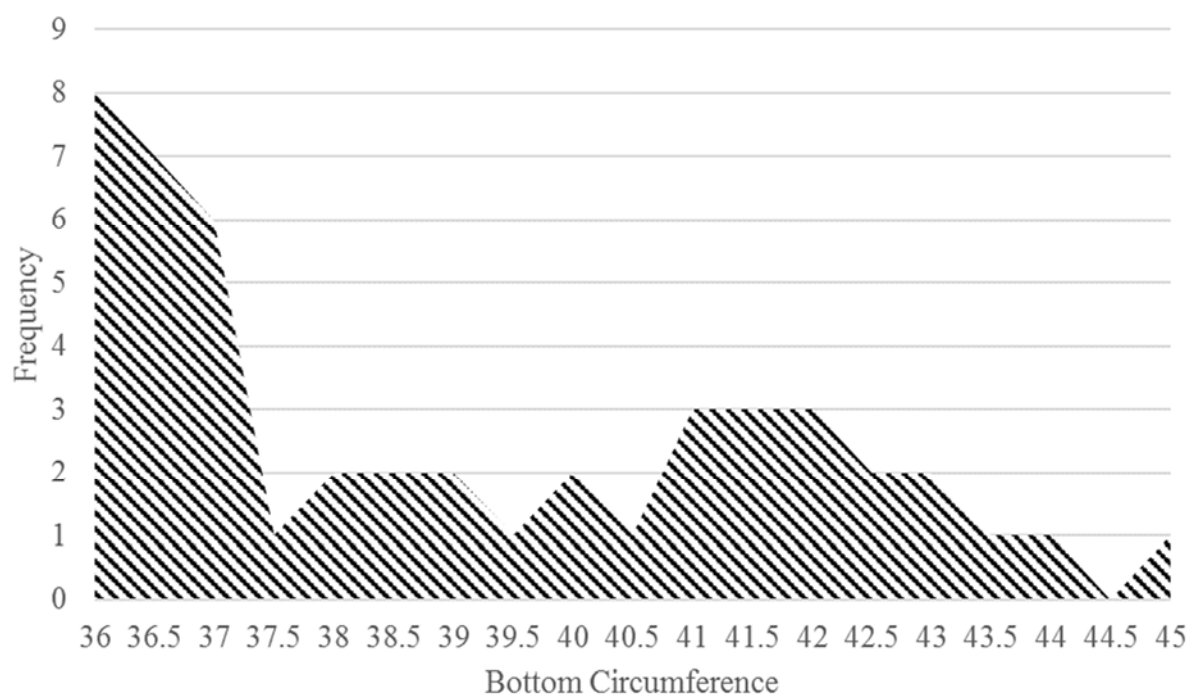
Figure 5-5: Distribution of circumferences of 48 Douglas-fir poles.

Ring Count

The average age of the poles was 45 years, with a range of 23 to 77 years. The number of growth rings in the outer 2 inches averaged 19, with a minimum of 10 rings. All poles met the ANSI requirement for a minimum of 5 rings per inch in the outer 2 inches (Appendix 3)

Failure Types

Ultimate failures were separated into three groups: tensile (Figure 5-6), end shear (Figure 5-7), and compression (Figure 5-8). Most tensile failures occurred around a knot or hole. Some tensile failures were attributable to slope of grain. End shear is a shear failure at the end of the pole. Compression failures occurred near the top of knots and holes, but were not the ultimate cause of failure.

Figure 5-6: Tensile failures caused by failure at a knot and rupture of fibers.

Figure 5-7: Two end shear failure at the pole end, marked by separation of the areas above and below the center of the pole.

Figure 5-8: Compression failure marked by buckling of wood fibers around the hole.

Most failures occurred at knot clusters, the same result observed by Elkins (2005). This observation suggests that the largest stress concentrations remain at knots. The weakest failed modes failed under compression and end shear. Only three specimens failed in compression, making statistical comparisons impossible. End shear strength was lower (Table 5-3), but not significantly lower. End shear caused the ultimate failure in 35% of all poles, but was present in 68.8% of poles (Figure 5-9). Penultimate end shear failures release energy and change material properties such as MOE. The unexpected presence of end shear and its implications will be discussed below.
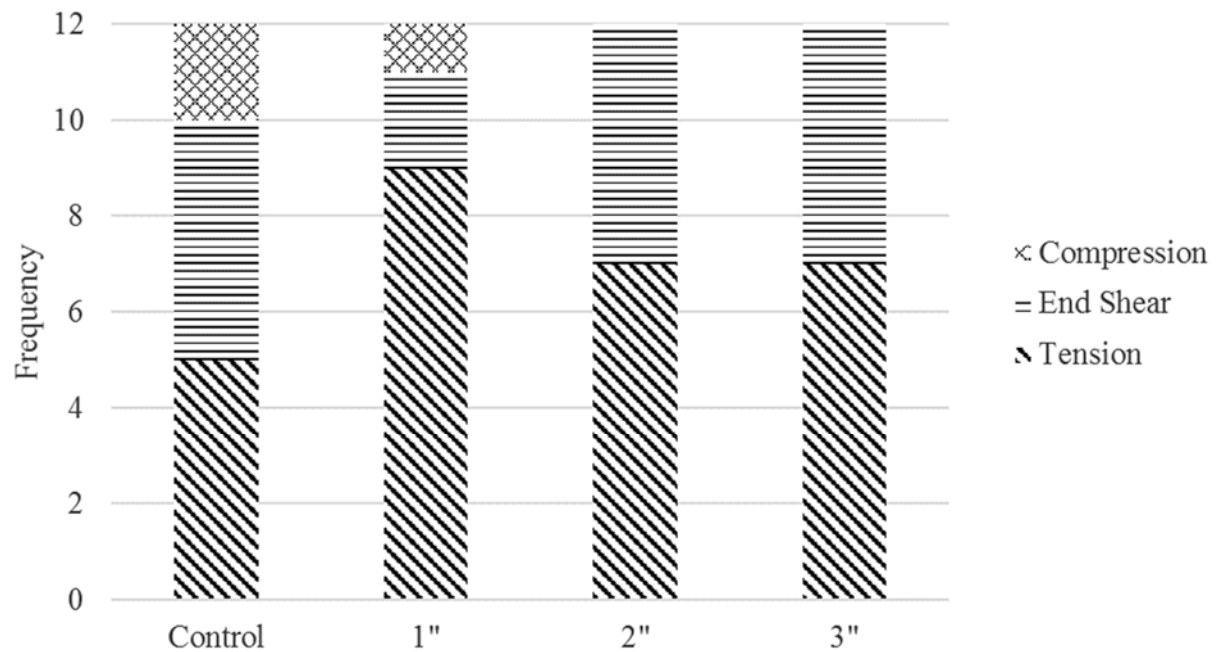
Figure 5-9: Frequency of ultimate failure modes for each edge distance group.

Many failures in the control group were end shear or compression, suggesting that holes cause more tensile failures to occur. As the highest average MOR is tensile failures, it is beneficial to force the pole to break in tension. The majority of failures in the one inch group were tensile failures, whereas the failure modes in the two and three inch group were a mix. Drilling holes closer to the edge causes more tensile failures, but may also reduce the poles strength as seen in Table 5-1. Although the failure patterns in the two and three-inch group are similar the three inch group is stronger (Table 5-1). This is due to some holes in the two-inch group causing failure compared to none in the three –inch group. Drilling at a two or three inch group seems to be optimal, with a three-inch group causing no strength loss.

Table 5-3: MOR of each failure mode.

	Average MOR	Standard Deviation	Coefficient of Variance
Tension	6252.9	1282.6	0.205
End shear	5867.0	881.6	0.150
Compression	5423.9	374.5	0.069

One load deflection curve was accidentally deleted after testing; however, the maximum load and deflection were still recorded. In another test, the cylinder reached the maximum load limit that could be recorded. The cylinder continued to deflect downward, while the load remained constant, before the test stopped. The pole was tested again, but previous plastic deformations reduced the maximum load. For this reason, this data point was not included in the above data set.

Comparison to Previous Data

The average MOR for all poles was 6060 psi for all specimens. This value is below the ANSI specification of 8000 psi for green poles. Elkins (2005) found the mean MOR of green poles to be 7350 psi for poles with no through boring, and 6860 psi for poles with 0.5-inch diameter through-bored holes drilled at a 2-inch edge distance. Morrell et al. (2011) found the mean MOR to be 5750 psi for poles with 0.5-inch diameter through-bored holes drilled at a 2-inch edge distance . Bodig et al. (1986) found the mean MOR for green Douglas-fir poles to be 6630 psi. Elkins (2005) and Morrell et al. (2011) used the same test set-up as in the current study, although they tested poles in the green condition; class and age were similar, however, and poles were also obtained from stands in western Oregon or Washington.

The average MOR found in the current study fell between the MOR for poles in the green condition, as reported by Elkins (2005) and Morrell et al. (2011). However, drying increased the

strength of poles in this study. Philips et al. (1985) found that air-drying Douglas-fir poles increased MOR by 8%, compared to green poles. For this study, poles arrived in an air-seasoned condition, and then were kiln-dried to reduce moisture variability. ANSI 05.1 suggests using a 0.9 strength reduction for kiln-dried poles.

Decreases from kiln drying and increases from air-drying seem to be conflicting, and these effects will be addressed shortly. The presence of a size effect and end shear were not seen previously, and causes for these will be discussed below as well.

Effect of Kiln Drying

In the current study, many poles were pith checked and lost shear resistance due to kiln drying. In another study, steamed southern pine poles developed pith checks and lost 20% strength (Wood et al. 1960), compared to the predicted 15% loss (ANSI 2017). The strength reduction of 0.9 found previously is an accurate representation of strength loss (Eggleston 1952, Thompson 1969, Bodig et al. 1986), although greater reductions can occur. The internal checking reported by Graham and Womack (1972) caused by differential shrinkage may change for different sizes of poles and could explain lower stresses in larger poles. Moisture content of poles in some studies was above the fiber saturation point (Thompson 1969), which would result in no strength increases due to drying, but little checking. Douglas-fir poles are usually not kiln-dried below the fiber saturation point, therefore larger and more frequent cracks appeared in the poles in this study compared to the industry.

Effect of Air seasoning

Bodig et al. (1986) also showed an increase of 1% to 10% in strength properties of air-dried poles, with MOR significantly greater. The poles in this study had been air seasoned previously, and kiln drying opened existing checks and created new ones. Although the poles gained strength from drying, the increased magnitude of defects controlled the failures. Madsen (1975) found that that strength of weaker material does not change with moisture content due to stress concentrations causing a different mode of failure.

Effect of Check Formation

The poles checked heavily after kiln drying, with many checks pith centered and extended for multiple feet, discontinuously. Wood et al. (1960) recognized that checks affect the shear area, and that shear stress in bending is typically low. They also stated that the strength of treated Douglas-fir decreases radially inward. Decreased core strength would explain the presence of end shear in the current study.

Additionally, multiple checks opened at the pole ends. It was not possible to avoid placing checks horizontally and creating a shearing plane. There were also honeycomb-like checks in some of the larger poles. These checks would have rapidly decreased the pole's shear resistance.

Cause of Diameter Effect

A linear relationship of decreasing strength with increasing size was observed. A diameter effect has not been seen previously in utility poles (Bodig et al. 1986, Wood et al. 1960). This is not due to a material effect, rather an artifact of kiln drying. This effect was clearly seen in the first charge. The MOR of the first charge was larger but not significantly larger than that of the other

charges, but the diameter was significantly smaller. The strength increase was not due to MC; correlations between MC and size ($R^2 = 0.03$) and MC and MOR ($R^2 = 0.06$) were poor. The first charge was likely stronger due to the smaller size of the poles. Larger poles developed checks that failed in shear through higher drying stresses.

Stress concentration theory predicts decreasing strength with decreasing size. This did not occur in the current study, as the effect was present in the control poles too. Instead, knots controlled the majority of tension failures, and the strength of poles remained the same between groups. Failures at holes did occur at holes in the 1-inch sample, but this edge distance is impractical to drill.

One difference between poles in this study and previous tests was size. Diameter in previous testing was not related to MOR ($R^2 = 0.08$). Average pole diameter in the current study was 1.5 inches larger than in previous tests. In previous tests, end shear was rare. Shear increases less than other properties when dried. The distance between the center of the loading head and support in the test apparatus was small, 2.0 to 2.5 times as large as the pole diameter. ASTM D198 suggests that ratios of 2.5 and under cause frequent shear failures. This ratio is for symmetric four-point bending, but indicates that test geometry influences the frequency of shear failures, and that these reasons explain the high frequency. End shear was not seen previously, due to smaller diameters, lack of end checking, and material properties.

The R^2 correlations between diameter and MOR jumped to 0.75 when end shear was not included in the data. Consequently, end shear failures did not cause the size effect; rather, kiln drying affected larger poles more. Kiln drying seems to be the cause of the diameter effect

Chapter 6- Finite Results and Discussion

Verification

As a part of the verification process, the physics in the model must be validated against theoretical results. Aspects of the model that can be compared against theoretical calculations are stress and deflection in the four-point bending of a tapered beam and the stress concentrations around holes. Aspects of the model that can be implicitly verified are stress concentrations at knots and the mean stress method.

Four-point bending stress and deflection

The bending pole model was loaded to a total of one kip distributed asymmetrically. Stress and deflection were compared to theoretical results. Table 6-1 shows the difference theoretical and modeling values are low, less than 10%. The model is conservative compared to the experimental and theoretical values. Theoretical deflection calculations are for an isotropic material, whereas the finite element uses an orthotropic material.

Table 6-1: Deflection and stresses using theoretical, element, and experimental methods of a 20 ft. utility pole.

	Hand Calculation	Finite Element	Experimental
Deflection (inch)	1.65	1.81	1.62
Maximum Normal Stress(psi)	2800	3000	2800

Stress Concentration around Hole

An initial model was created to examine how the finite element software can handle the

prediction of stress concentrations for an orthotropic and cylindrical material. A rectangular

cantilever beam with a ½ in hole at varying edge distances was placed into bending. The

maximum stresses at the hole were divided by nominal stresses to find stress concentrations. A

finely meshed model is able to predict the theoretical stress concentration (Figure 6-1) for an

isotropic rectangle with a high degree of precision. A coarser mesh is still close to the theoretical

and finely meshed SCFs (Figure 6-1). For the validation of an orthotropic rectangle, the derived

orthotropic factor was multiplied by the theoretical calculation (Appendix X). Figure 6-2 shows

that the multiplier is conservative. This is not surprising; the orthotropic factor was previously

inaccurate within 15% (Smith 1944). For a more detailed look at the modeling, look at Appendix

X. This method is accurate although a derivation in three dimensions may produce a result closer

to the method used in the finite analysis.
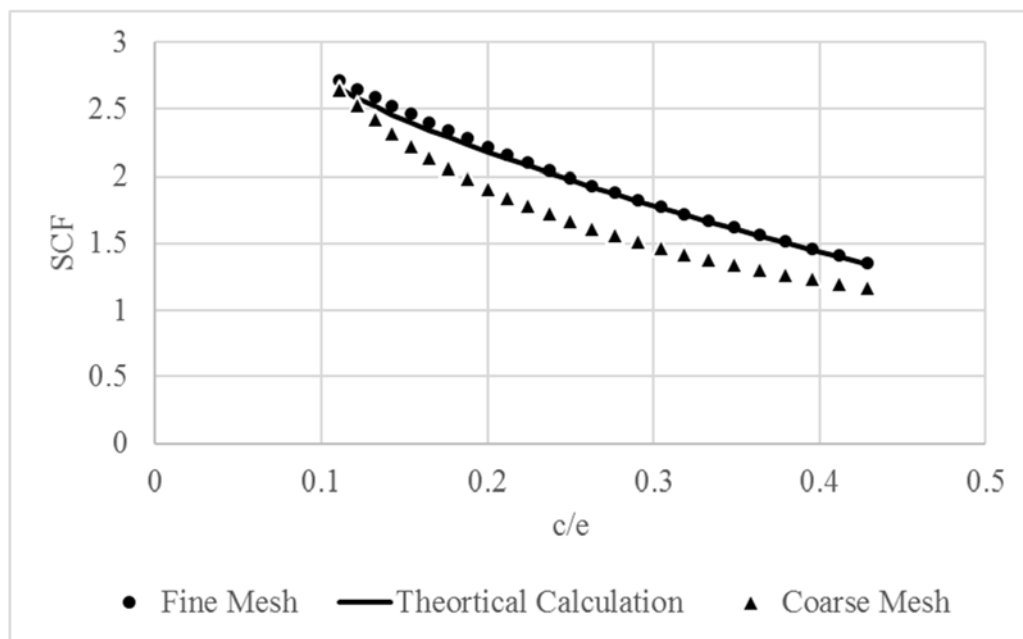
Figure 6-1: Two meshes were used to create the above curves along with theoretical calculations for the stress concentration in an isotropic rectangle.
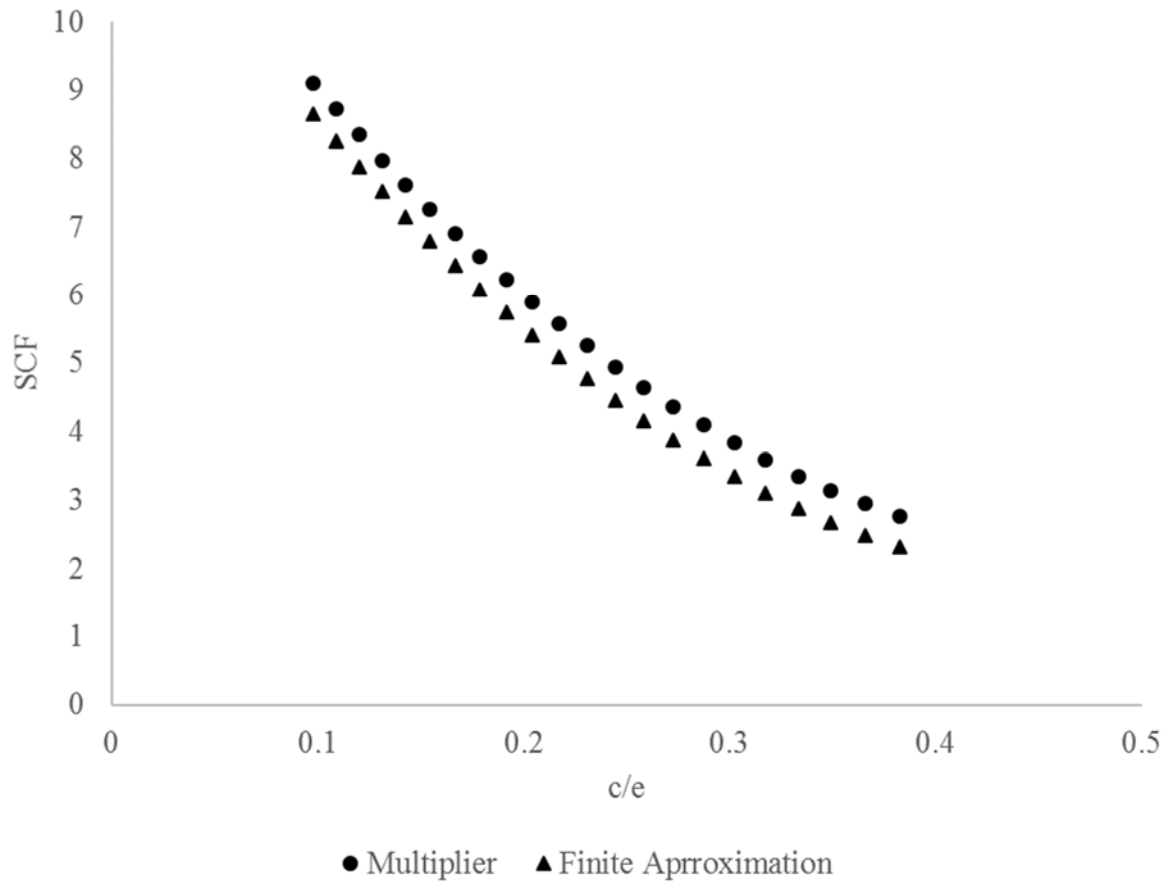
Figure 6-2: Normal stresses for an orthotropic cylinder. The multiplier curve uses the orthotropic multiplier found in Appendix 1.

Saint Venant's Principle

One aspect of the model that could not be verified was placing a hole near the load. Stresses are higher closer to the loading point as predicted by St. Venant's Principle as seen in Table 6-2. This is not seen for all directions of stress, but is most evident in tension perpendicular to grain and shear perpendicular to grain. The higher stress cause inaccurate failure criteria predictions.

For this reason, stresses near the loading point were ignored. For this reason, further modeling in future experiments could be done in cantilever bending, to limit distance effects.

Table 6-2: Stresses at a hole near and far from hole. Near and far are defined as 1 and 10 inches respectively.

	Near Loading Point	Far From Loading Point
Maximum Normal Stress Z (psi)	24950	24700
Maximum Normal Stress Y (psi)	2360	860
Maximum Shear Stress XY (psi)	3775	1750
Maximum Shear Stress YZ (psi)	2130	2230

Linear Assumption

An assumption of the model is a linear relationship between deflection and load, whereas the true relationship is nonlinear. The load-deflection curve in Figure 6-3 shows the convergence of experimental and finite element behavior; however, beyond the elastic region there is a difference between the two curves. The average difference between linear predictions and experimental deflections at maximum load is 20%. However, the relationship between MOE and MOR will remain the same. The MOE is dependent on the linear portion of the graph, while the MOR is dependent on the applied force.
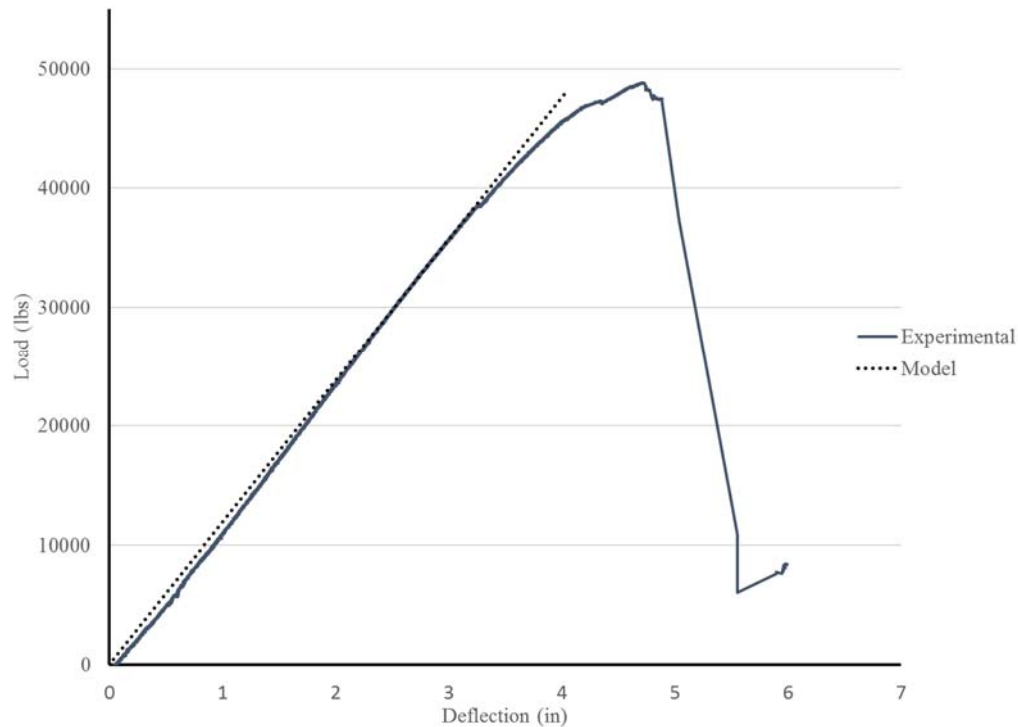
Figure 6-3: Experimental and linear predicted load-deflection curves of Pole 554

Comparison of Knot and Hole Concentrations

A set of models were created to compare the stresses created by knots and through-bored holes. This is important, as the largest stress concentrations can dictate the failure location and failure mode for the pole. This was seen in this set of experiments and previous experiments. Modeling knots is important as most poles failed at knot clusters in previous testing (Elkins 2005). It may also mean that hole edge distance can be increased until the knot SCF is reached at which point the failure mode may shift. In any one pole, the size and location of knots are randomly determined. By generating a population of knot characteristics and their associated stress

concentrations, manifested stress concentrations from holes can be determined. The probability of failure due to holes at different edge distance can then be found.

Models with knots and through-bored holes were compared (Figure 6-5 and 6-6), to examine the difference between stresses and failure modes. The through-boring pattern was 9" spacing, 2" edge distance and ½" diameter holes. The applied load was 1kip. The stresses at the knots in each directions were normalized against through-boring stresses, and presented in Table 6-3. In addition, the knot cluster is rotated 90° to compare how the stresses can change.
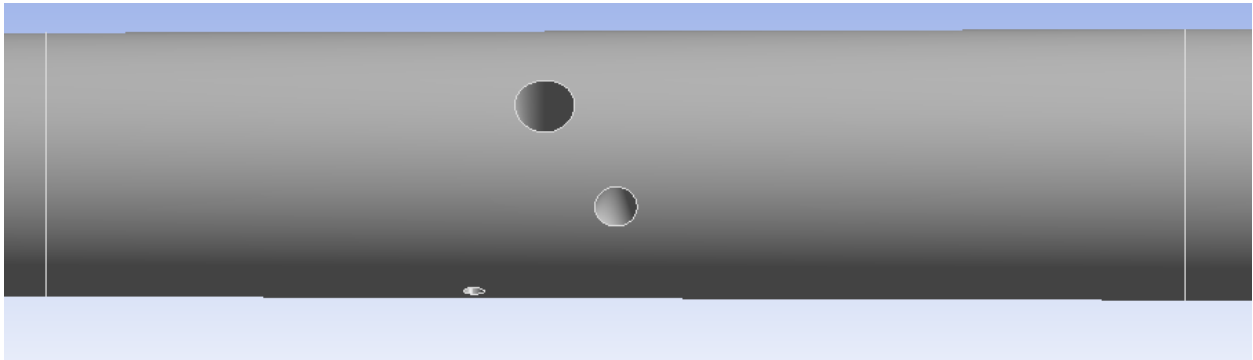
Figure 6-4: Example of a Knot Cluster
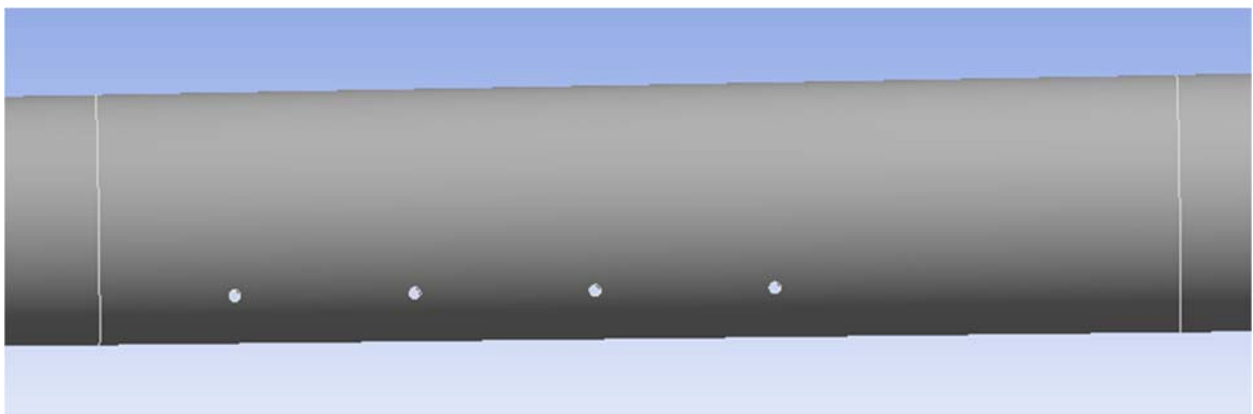
Figure 6-5: Example of Through Borne Section

Table 6-3: Knot and Through-bored stress ratios

	Knot/Through bored	Knot/Through bored 90
+σ L (psi)	1.018	1.035
-σ L (psi)	1.61	2.51
τTL	1.32	1.65
τRL	0.42	.4236
+σ T (psi)	0.659	1.0162

This particular knot cluster was the cause of failure in a previous test. This is not representative

of all knot conditions and edge distances, but shows that knots can dominate the failure of a pole.

Due to knot's influence in failure modes, this model was expanded upon.

Validation using test data

Pole strength was investigated by their stress concentrations using the above methods. Knot

maps, modulus of elasticity, and geometry were inputted for every pole. The model was initially

validated by comparing the experimental and model deflections at a load in the elastic region.

The deflections matched within 5% in all cases. Based on this initial validation the model was

loaded to the ultimate load. At this point, the mean stress macro ran and collected this data into a

text file. The text file was imported into Excel and analyzed to find the maximum Failure

Criteria. A failure criterion greater than one indicates the model over predicts strength, under one

indicates under prediction of stress.

The Hoffman criteria and was used for failure analysis. The nine necessary parameters are

reduced to six, as there are equal strength parameters for the tangential and radial directions.

These strength parameters are listed in Table 4-2. The most likely failure locations in term of

failure criteria were collected for each pole. One artifact of the model is increased stresses at the

loading points. As per St. Venant's principle, stresses near the load are highly magnified and are

inaccurate. There was always a hole near the loading point in the experiment. Points nearest the load were ignored for this reason.

Only tensile failures were considered, not compressive or end shear failures. A failure criterion beyond one in compression is not an ultimate failure. Rather, compressive failures change the neutral axis location and decrease the apparent moduli of elasticity. As nonlinear effects were not considered in this model, no compressive failures were considered in the ultimate analysis. End shear failures were caused by checks in the butt end. As checks were not modeled, poles that failed by end shear were not considered.

Experimental Data

The most likely failure locations for all poles are shown below in Table 6-4. The model correctly predicted the average failure criteria within 25%. However, the model correctly predicted the strength at the failure location within 8% accuracy; however, the coefficient of variance is 43%. The model correctly predicted the failure location in 36% of the models, but predicted the location within the first three most likely locations. The MOR/failure criteria column contains erroneous results, containing MOR well above the ANSI fiber stress of 8000 psi (ANSI 2017) and the Wood Handbook MOR of 12400 psi (USDA 2010). The failure mode for each pole is noted too, and is dictated by tensile parallel to grain. Tensile parallel to grain is present in all holes and knots, and tensile perpendicular to grain is dominant in 42% of the poles. While tensile perpendicular to grain can be the ultimate cause of failure, parallel to grain is always nearly equal in terms of failure criteria. Shear is present in locations closest to the load. The percent difference between the 1st and actual failure averages 45% when ignoring poles where the location was correctly predicted and 29% when those poles are included. Three FEM failure

criteria are twice as large as the failure criteria at the location due to large knots at those

locations. Large knots oriented in the tension face cause the largest SCs but smaller downward

oriented knots can still control failures.

Table 6-4: The Failure Criteria and Location of Modeled Sections, the experimental failure

location and its associated failure criteria.[2]

Pole #	FEM Predicted Location (in)	Failure Criteria	Actual Failure Location (in)	Failure Criteria	MOR/Failure Criteria
1	91.5	1.71	91.5	1.71	5045
2	78	0.65	78	0.65	5848
540	63	1.19	63	1.19	4324
554	44.25	0.945	75.5	0.92	7250
568	69	1.8	69	1.8	3769
707	60	1.27	51	0.92	6937
715	39.9	0.75	126	0.57	9221
727	87.1	0.8	78	0.66	7898
822	94	1.93	94	1.93	3760
997	64.5	1.57	53	1.45	5110
4248	68.9	1.45	87	0.888	4199
4771	52	1.1	52	1.1	4506
4774	51.1	0.75	63	0.454	9983
4789	94.5	1.57	52.3	0.818	7596
4850	87	1.27	87	1.27	3482
4853	78	1.95	60	1.78	3839
4855	88.7	0.933	60.25	0.57	13993

---

[2] Pole 4988 does not have an MOR due to a testing error.

4897	89.4	0.89	60.4	0.82	6605
4899	72.9	1.04	36	0.45	10463
4926	87	1.09	48	0.999	6778
4963	70	1.41	70	1.41	5268
4966	87	1.65	78	1.503	5561
4977	98	0.717	76	0.399	17249
4988	74.5	1.32	74.5	1.32	
4993	66	1.5	79	1.21	5825
4995	87	1.87	78	1.68	4459
4996	83	0.92	61	0.37	18432
5218	60	1.38	60	1.38	5119

The model correctly predicts average strength within 10%, however there is a high degree of variance. MOE and MOR are well correlated *with an $R^2=0.42$*, ranging from $R^2=0.4$-0.65 in other tests (Elkins 2006, Clauson et al. 2015). The correlations between the failure criteria and MOR are $R^2=0.334$. This suggests that stress concentrations caused by knots and holes can predict the MOR, however MOE remains a better indicator of MOR.

The model may be able to predict strength more accurately at different edge distances, diameters, or types of failure. By predicting trends in through-boring patterns or boring geometries, designs could be optimized with less testing.

A failure criterion near one means that for that population of poles, the failure criteria is near the breaking strength. For an individual pole, that ratio can be off, but averages to near one. The average failure criteria being above 1 indicates the model is conservative.

In Table 6-5, the two-inch edge distance and control show the least variance in the failure criteria. An ANOVA test shows that there is not a significant difference of load until failure for the four groups. There was no significant difference in strength between groups in the experimental analysis either.

Table 6-5: Average failure criteria for each edge distance. The fourth column is the averaged load for failure criteria to equal unity for each pole. The failure criteria is the FEM predicted FC.

	Average FC	Standard Deviation	COV	Load/FC (kips)
Control	1.016	0.363	0.357	48.8
1 inch	1.103	0.558	0.506	39.9
2 inch	1.181	0.233	0.198	37.4
3 inch	1.078	0.685	0.636	44.0

The variance in both the one-inch and three-inch groups need to be addressed. The COV of MOR in the experimental breaking data is 14-20%. The dominant cause of failure in the finite one-inch group is due to holes and tension parallel to grain. Many of the experimental one-inch samples failed at the holes, but holes were not the ultimate cause of failure. Reasons for this are twofold; drilling at angle due to the highly curved at the edge, and wood fibers beyond the hole remained intact after failure at the hole. For the three-inch group the majority of failures occurred at knots, but there does not seem to be an explanation for the variation. The two-inch group performed well and failed at knots. The difference between these groups is there seems to be less premature failures from cracks. This is likely a random occurrence as the poles were sorted

beforehand to limit size and kiln cycle, but not crack length. However, due to the small sample size of each group any statistical power is limited.

Validation with Past Data

Further modeling was done on a previous set of through-boring poles (Elkins 2005). Additionally the data may be better suited to see observable trends in the model; there are higher correlations between MOE and MOR in the control poles (R^2=0.67 vs 0.4), and there are significant differences in strength between groups. If the finite model is able to predict significant differences between groups, it will be better validated. The data set has the following limitations; no photographs of failure zones to compare to handwritten notes and no load deflection curves.

Five poles were selected from the control, ½ in, ¾ in and 1-inch groups (Elkins 2005). The model correctly predicted the failure location in 40% of tests and overpredicted the average failure criteria by 23% (Appendix 1, Figure 3). The average FC in the control group and ½ in are near unity (Table 6-7). An ANOVA test does show a significant difference (p=0.00668) between the groups for the load at a failure criteria of one, but not a significant difference between average failure criteria. This is expected as Elkins reported a difference in strength between the ¾ and one-inch groups and the control (Elkins 2005). However, the model did not reveal a difference in strength in the ¾-inch group, but concurred with Elkins (2005) in the one inch holes. Holes have previously increased the average strength of poles (Elkins 2005), a trend seen below (Table 6-6) but not seen in this study (Table 6-5). The trend may be due to comparable size knots in a smaller pole (Elkins) compared to larger knots controlling failure in this study. Additionally, the load until failure in Table 6-5 and 6-6 are not directly comparable as the poles are sized differently.

Table 6-6: Average failure criteria for three sizes of holes in the Elkin's data set. The fourth

column is the averaged load for failure criteria to equal unity for each pole. The failure criteria is

the FEM predicted FC.

	Average FC	Standard Deviation	COV	Load/FC (kips)	
Control	1.07	0.33	0.309	32.4	(6.52)
1/2 inch	1.01	0.246	0.242	40.4	(9.33)
3/4 inch	1.13	0.289	0.255	28.2	(6.34)
1 inch	1.31	0.336	0.256	23.6	(3.94)

Predictive Behavior

 The model does have predictive behavior and can predict differences in strength between

parameters. The user must input several characteristics and be mindful of several pitfalls. First

the user has to input the modulus of elasticity, the knot map, and hole pattern. The user would

find the dynamic modulus of elasticity using an NDE device. R^2 correlations between the

dynamic and static moduli are near 0.80 (Elkins 2005). The user then must input the knot map

and hole geometry into ANSYS's geometry modeler. Any force can be inputted and the user can

solve for the failure load after finding the failure criterion. This can be done easily by

multiplying or dividing the stresses by the square root of the failure criteria.

The associated load and failure criteria has a strong correlation with MOR. Load multiplied by

failure criteria have correlations of 0.30 for this study and 0.49 for past data. This improves upon

a relationship with applied load and MOR with correlations of 0.10 and 0.37 respectively. MOE

and MOR correlations are 0.60 and 0.45. Failure criteria and MOE are similarly correlated to strength and could be used to sort weaker poles from a population. The model is not accurate enough to predict a single poles strength, nor is it efficient to model a single poles strength, but could be used to examine differences between groups

Due to the difficulty of correctly measuring all defects and coupled with woods natural heterogeneity, the largest stress concentration may not necessarily cause the ultimate failure as seen in Table 6-5. For this reason, it is important to note the range of failure criteria in different locations. Users should be aware of locations near the loading point, where there are excessive deformations and overlook these locations. By instead modeling cantilever bending instead of four-point bending, excessive St Venant deformations can be avoided.

When looking at the optimization of through-boring or other drilling patterns, the efficacy of the patterns can be determined if the failure mode changes. If the failure location is occurring at knots, there is minimal loss of strength. If the failure location changes to holes, the pole is losing strength.

Determining the efficacy of a pattern based off one knot map and modulus of elasticity is not enough. There have been hundreds of knot maps for Class 4 poles collected in this and previous studies. Performing a statistical study to determine any detrimental effects can be done with this data.

Improvements to the model

Nonlinearity

Nonlinearity could be approached in two methods in ANSYS; the Newton-Raphson Method and Element Birth and Death. The Newton-Raphson method is a numerical method used to change the stiffness matrix to achieve convergence as the material yields. This method will use the tangential material properties. In Element Death, the program multiplies the stiffness matrix for a particular elements by a small number as the element yields, simulating decreased stiffness but maintaining symmetry. Both methods require many iterations for the model to converge correctly. A similar technique has been used by previous researchers (Cramer 1986, Williams et al. 2000, Ghan 2009). This method is also similar to damage mechanics method, which expresses a crack as a damaged zone, and the area around the crack can be investigated.

One difficulty with this approach is gathering post processed data and inputting it into the solver. The mean stress method used an exported text file inputted to excel to find the maximum failure criteria. Using the mean stresses in a nonlinear procedure would require significant coding in APDL to solve.

Differentiation of Knots and Holes

The representation of knots can be improved for three reasons; the coordinate system, distinction between knots and holes, and material differences in tension and compression. The current model's coordinate system is cylindrical, oriented in the radial, tangential and longitudinal directions. The idealized cylindrical coordinate system represents the grain direction in a homogeneous substance, but the flow of grain is not truly cylindrical. Knots redirect the flow of

grain, and spiral grain can be present as well. Guindos and Guaita (2012) modeled the flow of grain in dimensional lumber in ABAQUS using a fluid flow simulator and coupled the results to a structural solver. A similar method can be used to model grain direction and redirection around knots. Applying the results of the coordinate system to each element, holes can then be introduced and the model can run normally.

Additionally the current model does not distinguish between knots and holes, although their behavior is different. Holes interrupt the flow of grain, whereas knots redirect it. Another method would be to introduce a local coordinate system at each knot. The result of this is that some perpendicular to grain stresses would be converted to parallel to grain. Creating the coordinate system could be done with a macro.

Knots were modeled as holes, whereas behavior is different in tension and compression. Knots can be modeled as holes in tension (Baño et al. 2011, Pellicane et al. 1994). Material behavior of knots must be included for compression to be correctly modeled. As compression failures were not considered as ultimate failures in the finite model, all knots were considered as holes to save processing time.

Chapter 7-Conclusions

Through boring and other pretreatment methods have improved preservative penetration and extended the service life of utility poles. Through boring has been proven to have minimal effects on strength. A single pattern for through boring has been developed through rigorous testing; however, testing of new patterns is expensive and time consuming. Additionally, a single pattern is recommended for all pole sizes. The goal of this thesis was to create a finite-element model to optimize through-boring and other drilling patterns for other pole classes.

The model was validated by determining the differences in strength between different edge distances of through-bored holes. There is one standard edge distance currently used for all poles classes. However, stress concentration theory predicts that maximum stress will change for different pole classes. In order to test the effect of through boring at different edge distances, 48 poles were tested in a four-point bending setup.

The average MOR of both the through-bored and control poles was lower than the ANSI standard, but comparable to previous research. Variations were greater in this population than in previous tests. An ANCOVA test showed that there were no significant differences in strength between poles drilled at different edge distances. The lack of significant differences suggested that knots, rather than holes, created the greatest stress concentrations and initiated failure; the experimental results of this study confirmed this finding. However, the ANCOVA also showed that diameter had a significant effect on strength. This was likely not due to edge distance, as was hypothesized, but due to checks created through kiln drying. A large number of end-shear failures also occurred, possibly due to the combination of kiln drying and distance between the loading head and supports.

The presence of drying defects, end-shear failures, and low MOE, but high diameter correlation imply a high amount of experimental error. Additional testing of smaller sizes with no 1-inch distance and with testing at or above the FSP would reduce variance. These improvements to the experiment would increase the likelihood of recognizing significant differences between groups.

Finite element analysis results were nearly uniform for all groups, but had high variance. The model found the point of failure accurately in 36% of tests. Moreover, the actual failure occurred within the first three predicted locations. The largest knot was often not the cause of failure;

rather, failure tended to occur at knots oriented perpendicular to the load direction. Holes were the predominant cause of failure in the group with holes drilled at a distance of 1 inch inward from the pole edge.

As with the experimental data, differences between groups were insignificant. A data set from a previous through-boring test was also simulated by the model, and resulted in less variance and more accurate predictions of strength (Elkins 2005). The model was able to correctly find differences in strength for different hole sizes.

The model developed in the study could be used in the future to predict stresses in cantilever bending. Additional studies can use this population of pole characteristics, including MOE, failure mode, knot maps, and diameter to investigate other through-boring patterns. Future studies should test changes in failure modes, stress, and locations as through-boring characteristics change. This model would also have to be validated for species other than Douglas-fir, as fracture volume, dependence on knot concentrations, and size could change.

References

American National Standards Institute (ANSI). 2017. American National Standard for Wood Poles - Specifications and Dimensions. ANSI, New York, NY. 52 pp.

ANSYS. Vers. 17.0. Cecil Township: ANSYS, 2017. Program documentation.

Baño, V., Arriaga, F., Soilán, A., Guaita, M. "Prediction of bending load capacity of timber beams using a finite element method simulation of knots and grain deviation." *Biosystems Engineering* 109.4 (2011): 241-249.

Baño, V, Arriaga, F., and Guaita, M. "Determination of the influence of size and position of knots on load capacity and stress distribution in timber beams of Pinus sylvestris using finite element model." *Biosystems Engineering* 114.3 (2013): 214-222.

Bodig, J., and Goodman, J.R. "Prediction of elastic parameters for wood." *Wood Science* 5.4 (1973): 249-264. Web.

Bodig, J., Goodman, J.R., Philips, G.E., and Fagan, G.B. "Douglas fir data." *Wood Pole Properties* 2 (1986).

Bodig, J., Goodman, J.R. and Brooks, R.T. "Western redcedar data and size effect." *Wood Pole Properties* 3 (1986).

Boresi, A. P., and Schmidt, R.J. *Advanced mechanics of materials* New York: Wiley, 2003. Print.

Brown, D. L., and Davidson, D.F. "Field tests of relative strength of incised fir poles." Portland General Electric Co., Portland, Oregon (1961).

Cabrero, J. M., Blanco, C., and Gebemedhin, K.G. "Assessment of phenomenological failure criteria for wood." European Journal of Wood and Wood Products 70.6 (2012): 871-882.

Chiang, C, R. "Stress concentration factors of edge-notched orthotropic plates." The Journal of Strain Analysis for Engineering Design 33.5 (1998): 395-398.

Clauson, M, Morrell, J., Romanaggi, B., and Sinha, A. "Nondestructive bending tests on Douglas-fir utility poles as a potential tool for pole sorting and for prediction of their behavior in service." Holzforschung., 71.5 (2017): 397-403.

Cornish, R. "Statistics: An introduction to sample size calculations." Mathematics Learning Support Centre. Loughborough University, June 2006. Web.

Cramer, S. M., and Goodman, J.R. "Model for stress analysis and strength prediction of lumber." *Wood and Fiber Science* 15.4 (1983): 338-349.

Cramer, S. M., and Goodman, J.R. "Failure modeling: a basis for strength prediction of lumber."

Wood and Fiber Science 18.3 (1985): 446-459.

Crews, K., Boughton, G. and Falck, D. "Determination of characteristic stresses and residual life expectance of preservative treated hardwood and softwood poles." *Australian Government. Forest and Wood Products Res. and Development Corporation. Victoria, Australia* (2004).

Danielsson, H. The strength of glulam beams with holes: a probabilistic fracture mechanics method and experimental tests. Thesis. Lic. avh. Lund: Lunds universitet, 2009. N.p.: n.p., n.d. Print.

Davis, P.M., Gupta, R.and Sinha, A. "Revisiting the neutral axis in wood beams." Holzforschung 66.4 (2012): 497-503.

Eberhardsteiner, J. "Mechanisches Verhalten von Fichtenholz [mechanical behavior of spruce wood]." *Wien: Springer-Verlag* (2002).

Eggleston, R. C. "Pole Strength Tests." *Forest Products Research Society* 2 (1952): 2-24. Print.

Elkins, Lori A. Establishing a through-boring pattern and method of test for utility poles. Thesis. 2005. N.p.: n.p., n.d. Print.

Erickson, P. E., and Riley, W.F. "Minimizing stress concentrations around circular holes in uniaxially loaded plates." *Experimental Mechanics* 18.3 (1978): 97-100.

Falk, R. H., DeVisser, D., Plume, G.R., and Fridley, K.J. "Effect of drilled holes on the bending strength of large dimension Douglas-fir lumber." *Forest Products Journal* 53.5 (2001): 55-60. Web.

Forest Products Laboratory. Wood Handbook—Wood as an Engineering Material. General Technical Report FPL-GTR-190. Madison, WI: U.S. Department of Agriculture, Forest Service, Forest Products Laboratory. (2010). 508 p.

Guan, Z. W., and Zhu, E.C. "Nonlinear finite element modeling of crack behavior in oriented strand board webbed wood I-beams with openings." *Journal of Structural Engineering* 130.10 (2004): 1562-1569.

Graham, R. D., and Womack, R.J. "Kiln-and Boulton-drying Douglas-fir pole sections at 220 to 290 F." *Forest Prod J* 22.10 (1972): 50-55.

Graham, R. D., D. J. Miller, and R. H. Kunesh. "Pressure Treatments and Strength of Deeply Perforated Pacific Coast Douglas Fir Poles." *Proceedings from American Wood Preservers Association* 65 (1969): 234-41. Print.

Guindos, P., and Guaita. M. "A three-dimensional wood material model to simulate the behavior of wood with any type of knot at the macro-scale." *Wood Science and Technology* 47.3 (2013): 585-599.

Guindos, P, and Guaita, M. "The analytical influence of all types of knots on bending." *Wood Science and Technology* 48.3 (2014): 533-552.

Gustafsson, P. J., Petersson, H. and Stefansson, F. "Fracture analysis of wooden beams with holes and notches." *Proceedings of the International Wood Engineering Conference*. Vol. 4. 1996.

Heywood, R. B. *Designing by photoelasticity*. Chapman & Hall, 1952.

Hill, R. "A theory of the yielding and plastic flow of anisotropic metals." *Proceedings of the Royal Society of London A: Mathematical, Physical and Engineering Sciences*. Vol. 193. No. 1033. The Royal Society, 1948.

Kent, S. "Structural calculations to estimate the effect of ground line holes in wood poles". Report to USDA Forest Service. (2003). Unpublished. 22 pp.

Kozlik, C. J. "Kiln-drying Douglas-fir pole sections: effects on strength and checking." *Forest Products Journal* 32.6 (1982):24-30

Landelius, J. Finite Area Method. Rep. no. TSVM-5043. Lund University, Sweden: Division of Structural Mechanics, 1989. Print.

Madsen, B. "Moisture content–strength relationship for lumber subjected to bending." *Canadian Journal of Civil Engineering* 2.4 (1975): 466-473.

Mankowski, M., Hansen, E., and Morrell, J.J. "Wood pole purchasing, inspection, and maintenance: A survey of utility practices." *Forest products journal* 52.11/12 (2002): 43.

Masuda, M., and Ryuusuke H. "Theoretical analysis on bending of lumber containing knots by using finite element method." *Journal of the Japan Wood Research Society (Japan)* (1994).

Meguid, S. A. "Finite element analysis of defense hole systems for the reduction of stress concentration in a uniaxially-loaded plate with two coaxial holes." *Engineering Fracture Mechanics* 25.4 (1986): 403-413.

Merz, G. K. "Merz method for heartwood treatment of ground line area of poles." *Unpublished report. Portland General Electric Co., Portland, Oregon* (1959).

Morrell, J. J., Love, C., and Clauson, M. "Effect of through boring, radial drilling and deep incising on flexural properties of Douglas-fir poles." *American Wood Protection Association Proceedings*(2011): 99-103.

Morrell, J. J. Utility Pole Research Cooperative Report. College of Forestry. Oregon State University. Corvallis. OR. 1993., pp. 45-57

Morrell J. J. Utility Poles Research Cooperative Report. College of Forestry. Oregon State University. Corvallis. OR. 2002, pp. 55-61

Morrell, J. J., and Norton, J. "Potential for using through-boring to improve groundline treatment of Australian wood species: A preliminary study." *Forest Products Journal* 59.9 (2009): 61.

Morrell, J.J. and Schneider, P.F. "Through boring of poles for improving treatment: Distribution of preservative and effect on performance." *In.* Proc. American Wood-Preservers' Assoc., Granbury, TX. 90(1994):317-324.

Moses, D. M., and Prion, H.G.L. "Anisotropic plasticity and failure prediction in wood composites." *University Of British Columbia, Vancouver, British Columbia, Canada* (2002).

Moses, D. M., and Prion, H.G.L. "Stress and failure analysis of wood composites: a new model." *Composites Part B: Engineering* 35.3 (2004): 251-261.

National design specification for wood construction. Leesburg,VA: American Wood Council, 2015. Print.

Newbill, M. "Bonneville Power Administration's wood pole management program." *Transmission and Distribution Construction and Live Line Maintenance, 1993. Proceedings from ESMO-93., Sixth International Conference on.* IEEE, 1993.

Newbill, M. A., James, R., Asgharian, D., and Morrell, J. J. "Full-length through-boring: Effect on pentachlorophenol penetration and retention and residual strength of Douglas-fir poles." *Forest Products Journal* 49.1 (1999): 73.

Patton-Mallory, M., Cramer, S. M., Smith, F. W., Pellicane, P. J. "Nonlinear material models for analysis of bolted wood connections." *Journal of structural engineering* 123.8 (1997): 1063-1070.

Pellicane, P.J. and Franco, N. "Modeling wood pole failure. Part 1. Finite element stress analysis." *Wood Science and Technology*. 28.3(1994): 219-228.

Pellicane, P.J. and Franco, N. "Modeling wood pole failure. Part 2. Material and geometric considerations." *Wood Science and Technology*. 28.4 (1994): 261-274.

Phillips, G. E., Bodig, J. and Goodman, J.R. "Background and southern pine data." *Wood Pole Properties* 1 (1985).

Pilkey, W. D., and Pilkey, D.F. *Peterson's stress concentration factors*. John Wiley & Sons, 2008.

Ramsey, F., and Schafer, D.W. *The statistical sleuth: a course in methods of data analysis.* 3rd ed. Boston: Cengage Learning, 2013. Print.

Roark, R. J., and Young, W.C. "Formulas for Stress and Strain, 8th." *McGraw-Hill* (2011).

Shih, C. F., and Lee, D. "Further developments in anisotropic plasticity." *Journal of*

Engineering Materials and Technology 100.3 (1978): 294-302.

Smith, C. B. "Effect of Elliptic or Circular Holes on the Stress Distribution in Plates of Wood or Plywood Considered as Orthotropic materials". No. FPL-1510. Forest Products Lab, Madison, WI. 1944.

Tabiei, A, and Wu, J. . "Three-dimensional nonlinear orthotropic finite element material model for wood." *Composite Structures* 50.2 (2000): 143-149.

Thelandersson, S, and Larsen, H. J., eds. *Timber Engineering*. John Wiley & Sons, 2003.

Tsai S.W. Theory of composites design. Think Composites, Dayton (1992)

Thompson, W. S. "Effect of Steaming and Kiln Drying On the Properties of Southern Pine Poles." Forest Products Journal 19.1 (1969): 21-28. Print.

Valliappan, S., Boonlaulohr, P. and Lee, I.K. "Non-linear analysis for anisotropic materials." *International Journal for Numerical Methods in Engineering* 10 (1976): 597-606.

Wang, Y., and Bodig, J. "Knot interaction in wood poles." *Wood Science and Technology* 25.1 (1991): 47-56.

Williams, J. M., Fridley, K., Cofer, W.F., and Falk, R.H. "Failure modeling of sawn lumber with a fastener hole." *Finite Elements in Analysis and Design* 36.1 (2000): 83-98.

Wood, L. E., Erickson, E.C.O, and Dohr, A.W. "Strength and related properties of wood poles." American Society for Testing Materials, 1960.

Wu, H, and Mu, B. "On stress concentrations for isotropic/orthotropic plates and cylinders with a circular hole." *Composites Part B: Engineering* 34.2 (2003): 127-134.

Zandbergs, J. G., and Smith, F.W. "Finite element fracture prediction for wood with knots and cross grain." *Wood and Fiber Science* 20.1 (1988): 97-106.

Appendices

Appendix 1: Additional Finite Element Modeling

True Material Behavior

The linearly elastic models run below used the elastic parameters found in Table 4-1 (USDA 2010). Multiple material procedures were examined for nonlinear behavior. The first method was only for compression parallel and perpendicular to grain. Patton-Mallory (1997) derived a trilinear stress strain curve for Douglas-fir, but was not verified for small clear specimens due to experimental error. In addition, two components of the shear modulus and the Poisson's ratio would be modified to maintain stiffness matrix symmetry. This option was briefly modeled but was not used. This is due to the shear stress and the normal direction in the tangential and radial direction were modeled incorrectly (Moses and Prion 2002).

Table 4-1: Material Properties for Douglas-fir (USDA 2010)

E_Z (psi)	E_R & E_T (psi)	G_{RT} (psi)	G_{TL} & G_{RL} (psi)	M_{XY}	μ_{YZ} / μ_{XZ}
1.78e6	1.05E5	12.46E4	1.264E5	0.374	0.0325

Figure 1 shows the ideal load-displacement curve for curve. This behavior was implemented successfully for bolted Douglas-fir connections (Moses Prion 2003) using the ANISO command. Yield parameters in Table 1 and tangent moduli in Table 4-3 were initially used (Moses and Prion 2003). The ANISO command can be used to account for the differences in yield strengths in directions. This command is based off the generalized Hill Theory, and accounts for strength

differences between tension and compression (Shih 1978), and anisotropic work hardening

(Valliappan et al. 1976). However, there is a requirement for incompressibility, which is shown

in Equation 4. In order for equation 4 to be satisfied, tangent moduli, tensile and compressive

yield stresses must remain nearly equal. ANSYS is not able to run successfully when that

requirement is not met. Figure 2 shows behavior of the ANISO command, which is dissimilar to

Figure 1. Moses and Prion solved this problem by only using the command in compression. One

solution that was not fully developed is identifying the stress state of the material with a test

load. The material properties can then be switched depending on if it's in tension or

compression. By identifying material behavior in compression or tension from a test load, the

appropriate tangent moduli, yield strength can then be chosen, and the ANISO command will

then model more accurate behavior.

Table 1: Anisotropic Tangent Material Properties (Moses Prion)

Etx	Ety	Etz	Gtxy	Gtyz	Gtxz
580	580	20300	7.25	667	667
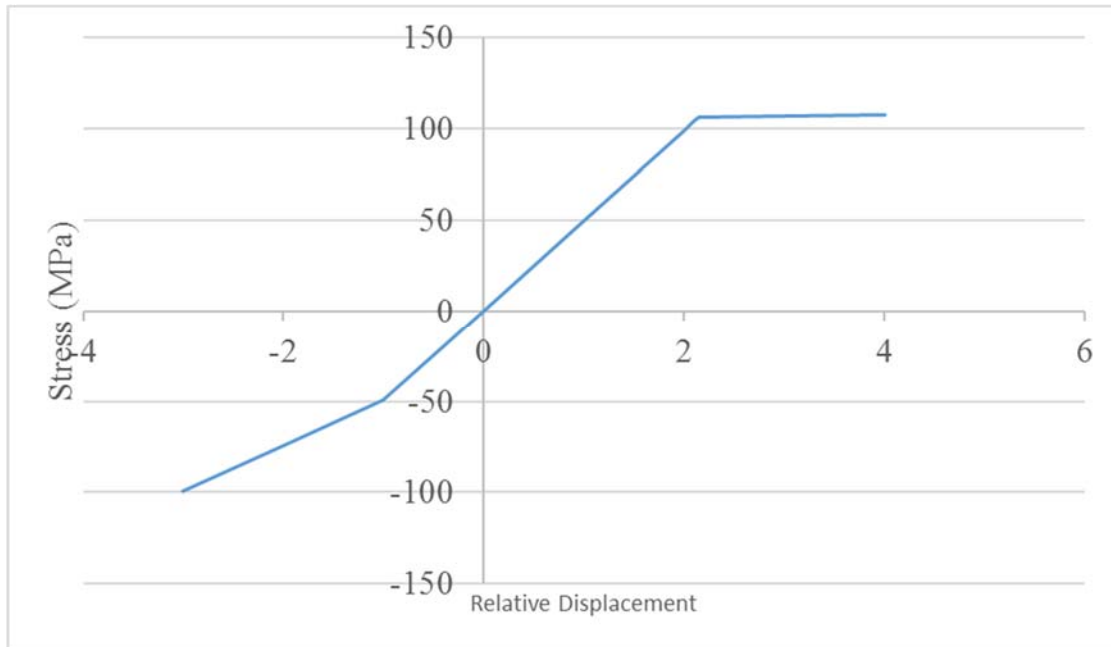
Figure 1: The Ideal Load-Displacement Curve for Tension and Compression in the Longitudinal

Direction. The yield strength is different for tension and compression. Additionally the tangent

moduli after yielding is different, representing both the ductile and brittle behavior of wood.
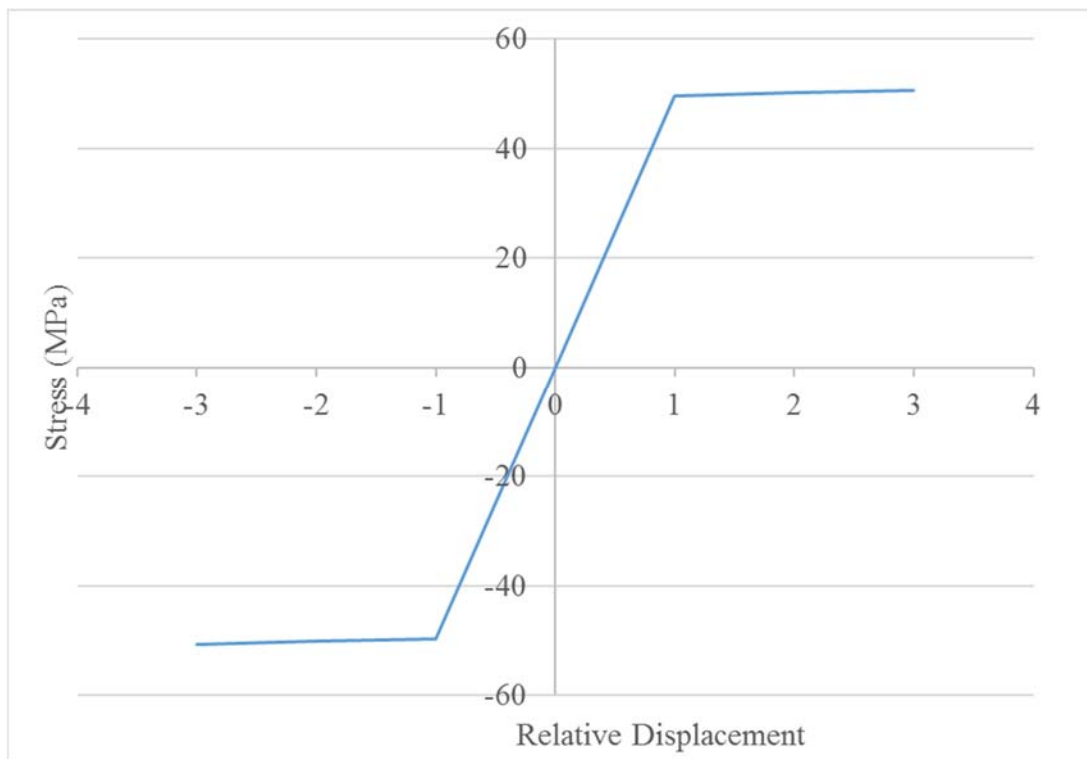
Figure 2: The Load-Displacement Curve in the Longitudinal Direction as inputted into ANSYS. Yield strength and tangent moduli have to be nearly equal in tension and compression.

$$\frac{\sigma_x + \sigma_{-x}}{\sigma_x * \sigma_{-x}} + \frac{\sigma_y + \sigma_{-y}}{\sigma_y * \sigma_{-y}} + \frac{\sigma_z + \sigma_{-z}}{\sigma_z * \sigma_{-z}} = 0 \ (4)$$

Maximum Stress Location for Cantilever Bending

Mechanics can predict the location of greatest stress in a tapered cantilever beam. The maximum stress occurs at the support at a prismatic cantilever beam, where the greatest moment occurs. The section modulus reduces along the section in a tapered section, and the maximum stress will occur elsewhere depending on the reduction.

Equation 5 shows the theoretical location of failure is dependent on the ratio between the top and bottom diameters (McCutcheon 1983). This is significant for longer poles where the ratios will be greater than 1.5. A pole under cantilever loading was modeled, with a 1-kip load at the tip, and the location of greatest stress recorded in finite. The tip and butt diameter were calculated using the ANSI05.1 minimum bottom and top diameters for a Class 2 Douglas fir pole. Figure 3 shows a good fit between finite and theoretical failure locations for longer poles. For shorter poles, the theoretical failure location is assumed to equal zero, and quickly begins to approach zero.

$$x = \frac{1}{2(r-1)} \ for \ r > 1.5 \ (5)$$

$$r = \frac{bottom \ diameter}{top \ diameter}$$

The majority of through-boring tests have been conducted on Class 4-40 foot long poles. A few tests have been conducted on Class 2, 60 foot long poles (Newbill et al. 1999). The authors found no relationship between stress and failure location. Additionally, through-boring did not appear to change the theoretical failure location. However, no knots were measured in the study. Additionally, it is impossible to know the failure location in identical non through-bored poles. Knots may still control the failure location, but through boring could change the failure location to the groundline in some instances. A practicality of the developed model is to investigate changes in the theoretical failure location.
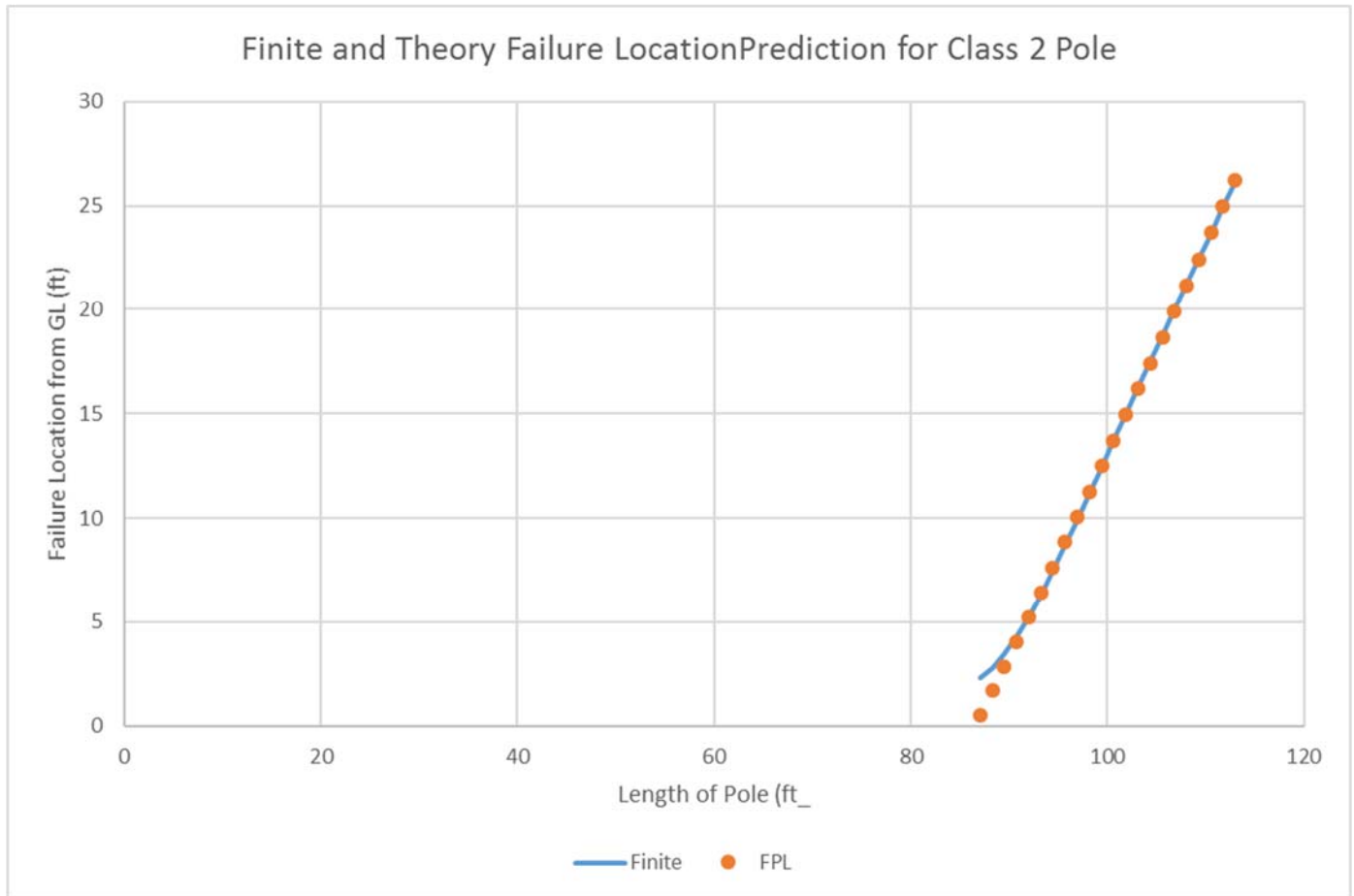
Figure 3: Position of greatest stress for a Class 2 Pole

Sweep Difference Stiffness

Sweep was parameterized to investigates how it affects pole stiffness. A previous study showed

that there is a significant difference in stiffness as the pole rotates (Clauson et al. 2017). This

model was developed to characterize the rotational stiffness of a pole and investigate if sweep

was the cause of differences. A full-length pole 20 ft. long was modeled with a 2" defect similar

to Figure 4 below (ANSI 05.1 2015). The ANSI 05.1 standards allows for a maximum sweep of

1" per 10 ft. The pole was rotated 90 ° and tested every 22.5° to investigate the change in stiffness. There was no difference in stiffness at this standard sweep.
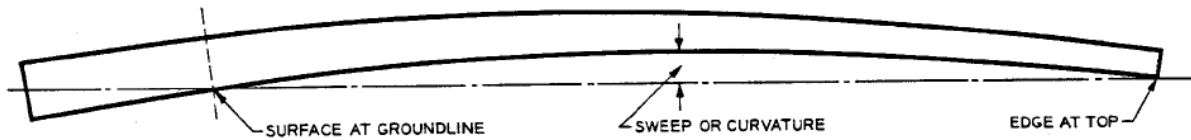
Figure 4: ANSI 05.1 and measurement of single sweep.

Submodel

Submodeling is typically used to create a finer mesh at an area of interest. By only modeling a small area, it can reduce the number of nodes and reduce runtime. Submodeling is achieved in ANSYS workbench by first running a coarse model. The coarse model provides accurate deformations but inaccurate stresses. The submodel is then ran using the displacements from the full model at the cut boundaries. One particular aspect is the cut boundaries need to be far from any stress raisers.

A full-scale model was created using the cones described above, with knots added as well. The model was loaded until the maximum load from testing was reached. A submodel was created, of the through-bored section plus 12" on either side. The 12" provides more locations for knots and failure locations. The submodel also needs to include any surface loads at the body.

To validate the submodel, the maximum stresses of the submodel and full model were compared. The maximum stresses in the submodel with load are within 10% of the full model except for compression parallel to grain.

Running the submodel without the load was an attempt to reduce shear caused at the load point when a knot or hole is nearby. The stresses in the submodel are under predicted without the load as seen in Table 2. With inaccurate stresses, this submodel was not included either. Submodeling would be more useful where stresses are further away from the boundaries, such as cantilever bending.

Table 2: Maximum stresses in full model and submodel

	Full Model With Knots and Holes		Submodel With Load		Submodel Without Load	
	T	C	T	C	T	C
σz	179.3	-381.0	176.6	-450.9	163.2	-436.1
σy	14.7	-29.8	13.1	-23.5	7.2	-16.1
σx	31.9	-46.6	29.7	-43.4	5.8	-8.9
τxy	18.6	-17.6	14.6	-16.1	2.3	-4.6
τxz	26.3	-24.8	25.3	-24.4	24.3	-23.8
τyz	32.7	-35.2	32.8	-31.9	19.8	-22.2

Although the submodel with the load was nearly validated, creation of it does not save many elements. In addition, both the submodel and the full model overpredict shear at the loading point when a hole is placed there. For this reason, results of the full model at the loading points were cautiously looked at and stresses ignored if a hole was placed directly at the loading point.

Edge Distance Calculations

Through boring is typically done using the Merz Pattern, which provides complete preservative treatment over the ground line. Previous works investigated the spacing used in the Merz pattern, and briefly looked at the edge distance. A set of models were created to estimate the stress concentrations at varying edge distances.

The effect of edge distance was first investigated using an isotropic rectangular member. A rectangular isotropic member in bending was first chosen to compare the accuracy of finite modeling to existing work. The SCFs were compared to derivations from photoelastic experiments (Isida 1952). There are no existing models to estimate stress concentration factors for cylindrical members in bending, or for orthotropic members with a hole, although there are methods to estimate both. For each edge distance referred to as c, the secondary edge distance from the other edge to the hole was taken as e (Figure 5). The nominal stress at the edge of the member was calculated using standard stress calculations based on moment, distance from the neutral axis, and moment of inertia. The maximum stress at the hole was calculated using a stress probe that finds the maximum σZ at the hole. σZ was used, as it represents the bending moment in this model. Rectangular models were created at 108 by 2 in and either 8,10,12,14 in wide. The hole has a diameter of ½". The hole is located above the fixed boundary and not at the bottom of the model to reduce meshing errors causing a large stress increase. Edge distances, c were 1, 1.5, 2, 2.5, and 3 in. The secondary edge distance, e was calculated for each member.
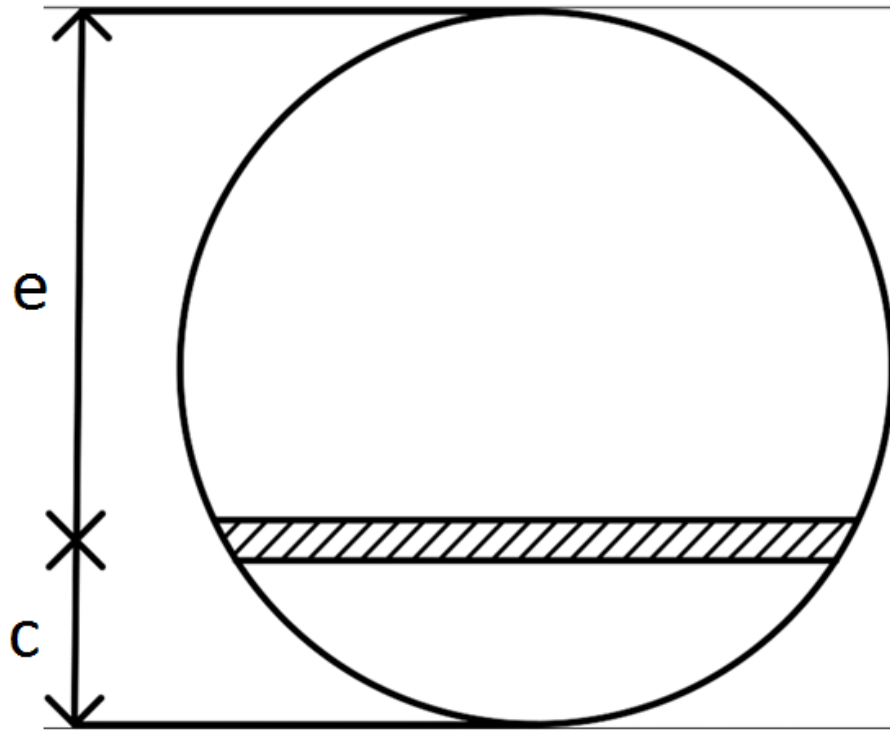
Figure 5: c and e ratio for a cylindrical member. This ratio was also used for rectangle as well.

The models were meshed, with a default mesh, and then converged to find the correct mesh size. By converging the mesh, the response surface follows the theoretical curve within 1% error for an isotropic material, as shown in Figures 7 for the four rectangles. By this measure, finite elements can produce correct stress concentration factors, and then stress concentration factors for both cylindrical and orthotropic models can be calculated using the mesh. In figure 8 the rectangles are plotted on the same graph, which shows that different sized members can have the same SCF with different edge distances. An orthotropic rectangle and its associated SCFs are shown in Figure 9; again, there is good convergence between each size. This suggests that in practice, there is a different optimal edge distance for each member size. Stress concentration factors are calculated using Formula 6, where Sigma max is the maximum model stress, and Sigma nominal the calculated stress using beam theory.

$$SCF = \frac{\sigma_{max}}{\sigma_{nom}} \ (6)$$
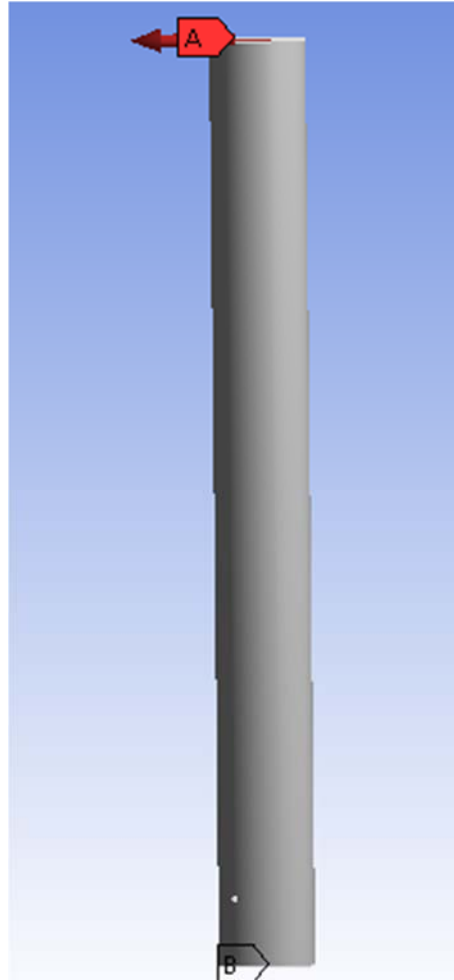
Figure 6: Reference Section for Determination of Cylindrical Stresses
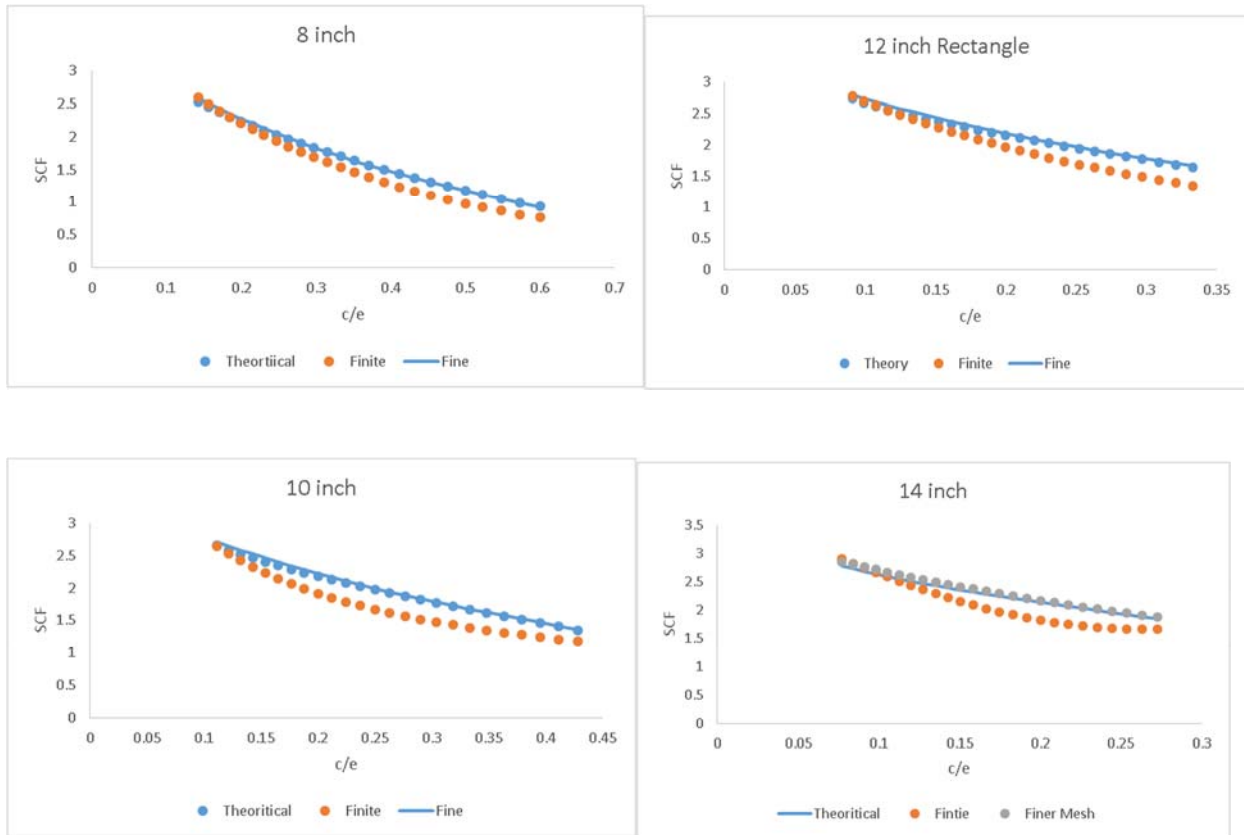
Figure 7: Theoretical stresses for rectangular sections with a ½ in hole. The curve for converged

and non-converged meshes are shown as fine and finite respectively.
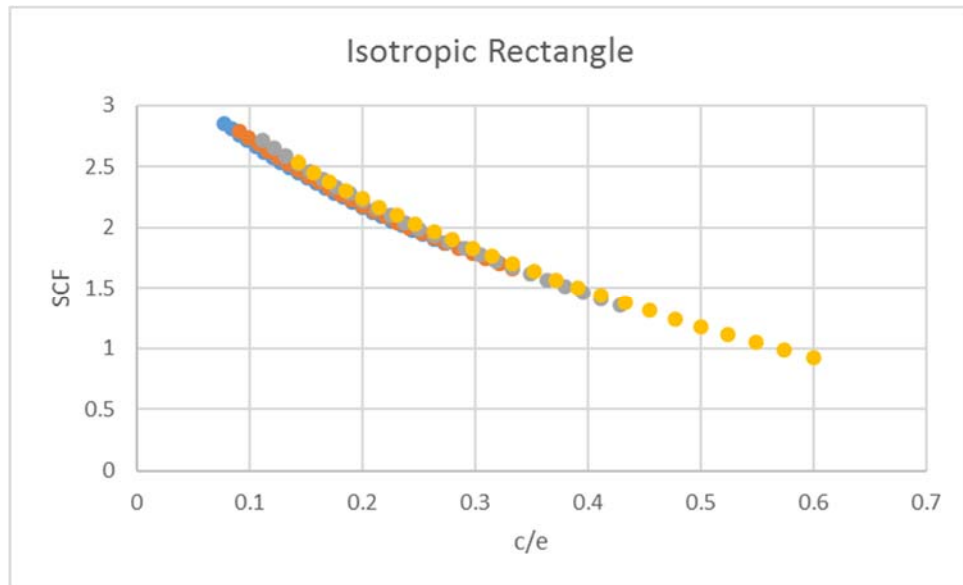
Figure 8: Isotropic Rectangle for the graphs above
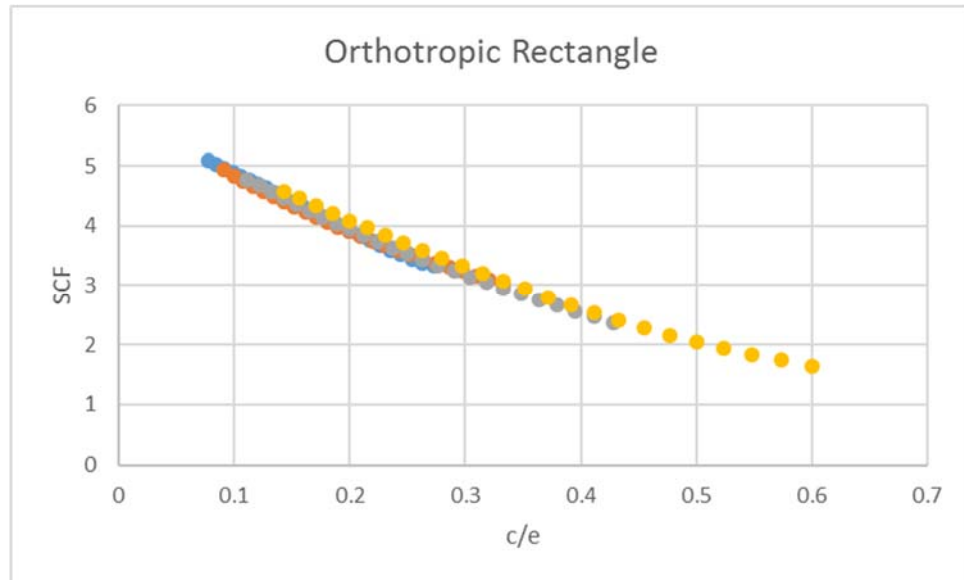
Figure 9: Orthotropic Rectangle and associated SCF

The isotropic and orthotropic cylinder SCFs are shown in Figures 10 and 11. Figure 10 shows

divergence for each cylinder. The cylinders had a radius of 4, 5.6, 6.92, and 7.64 in, and had a

range of edge distances ranging from 1 to 3 inches. In the figures, the stress concentrations still

follow the same c/e curves regardless of the size. For a homogenous material of different sizes,

exist different edge distances necessary to reduce the stress concentrations below a threshold.

Compared to the isotropic rectangular stress concentrations, the SCFs increase dramatically for a

cylinder and for an orthotropic material.
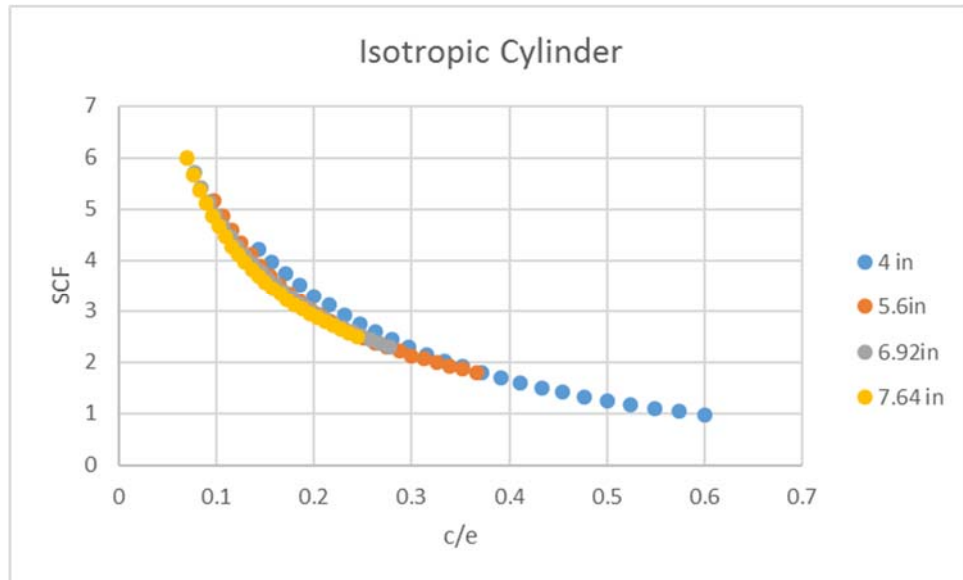
Figure 10: SCF for an isotropic Cylinder of different radii
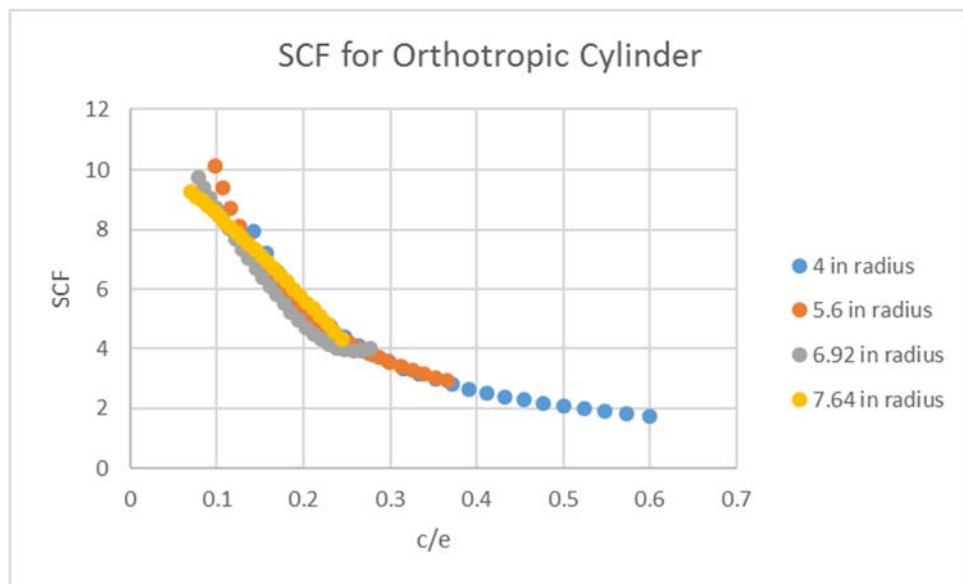
Figure 11: SCFs for an orthotropic cylinder of different radii

The predicted SCFs for an orthotropic cylinder may be predicted by the ratios of orthotropic/isotropic material and cylinder/square SCFs. Wu (2003) used this method to predict stress concentrations in orthotropic cylinders in tension. In order to predict cylindrical stress

concentrations, the first method used was with a central hole in a cylinder in bending, the values

of the stress concentrations were generated by Eqn. 7, an empirically derived equation (Pilkey

1997). d/D is a ratio between the hole and cylinder diameter. An orthotropic SCF was

determined by Eqn. 8, developed by Smith for the plane bending of plywood (1944). Eqn. 8 uses

the moduli of elasticity in the x and y direction, and μ_{XY} is the moduli of rigidity in the xy plane.

This is idealized only in the xy directions, a true orthotropic concentration would be in all three

directions. For the purposes of finding an initial value for the orthotropic increase, it should be

effective. The orthotropic\isotropic ratio ends up equaling 1.9 (5.7/3).

$$K_{tg} = 3 + .427\left(\frac{d}{D}\right) + 11.357 * \left(\frac{d}{D}\right)^2 \quad (7)$$

$$S(\alpha * \epsilon + \beta * \epsilon + 1) \; where \; (8)$$

$$\epsilon = \sqrt[4]{\frac{E_X}{E_Y}}$$

$$\alpha = e^{\phi/2}, \beta = e^{-\phi/2}, \phi = \cosh^{-1} k$$

$$\kappa = \frac{\sqrt{E_X E_Y}}{2} * \left(\frac{1}{\mu_{xy}} - \frac{2\,\sigma_{xy}}{E_X}\right)$$

Using just the initial stress concentrations is not accurate. Figure 12, shows how the finite

approximation and the theoretical product calculations do not match. The primary reason for this

occurring is the cylinder is located in the center and does not account for curvature of the

cylinder. Whereas in the finite approximation as the hole moves to the edge, the length of the

hole gets smaller, and stress increases. A cylinder and square in bending behave nearly

identically when a hole approaches the center of specimen with a SCF of one as seen in Figures 8

and 10 at larger c/e ratios.
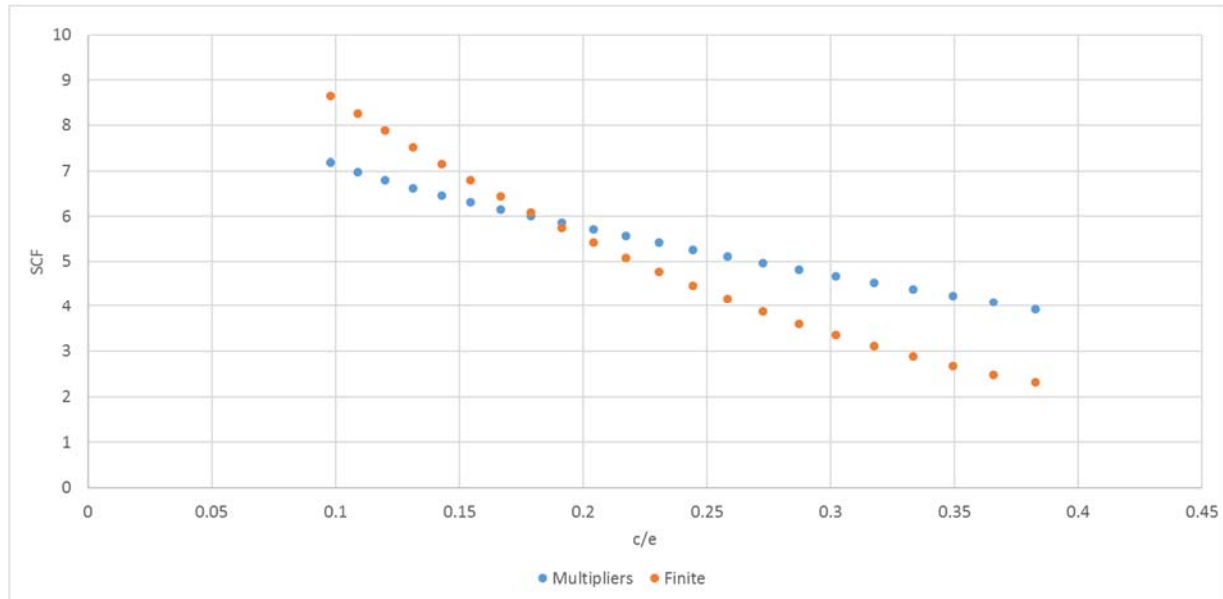
Figure 12: Finite Approximation and theoretical product calculations

In Figure 13 below the multiplier factor was found at different c/e ratios by dividing the

cylindrical to rectangular stress concentrations. This cylindrical factor was then multiplied by the

orthotropic and rectangular concentrations. The difference between Figure 12 and Figure 13 is

that the cylindrical factor is not a constant, as it is dependent on the edge distance. In figure 13

below, the quotient between the two lines are nearly constant, showing that the orthotropic

concentration is not dependent on edge distance, but is dependent on material parameters. The

orthotropic method developed previously for a plate in bending is close to the factor used in the

model. Equations 8 represents an orthotropic concentration for a plate, whereas an equation for

orthotropic behavior will contain three directions. Smith (1944) saw differences between

experimental and mechanical predictions between 15%, so it may be expected for stresses to differ.
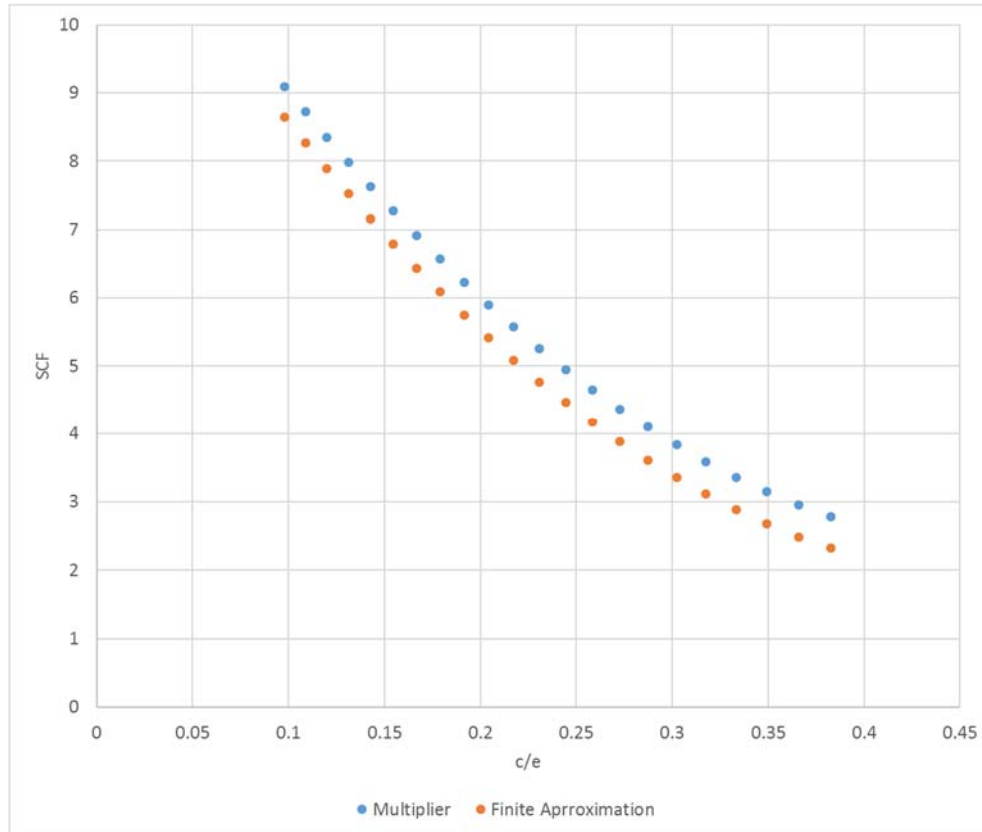
Figure 13: Stress Curves using Finite Multipliers.

Elkins Data Run

Table 3: The Failure Criteria and Location of Modeled Sections, the experimental failure location and its associated failure criteria. Boxes are blank due to correct location prediction. Group e is the control, group d is 1-inch holes, group c is ¾-inch holes and group b is ½ inch holes.

Pole #	FEM Predicted Location (in)	Failure Criteria	Actual Failure Location (in)	Failure Criteria	MOR/FC
5e	67.8	0.95	67.8	0.95	5835
10e	84.2	1.4	96	1.33	6026
15e	84	1.35	68.5	0.783	10342
20e	93.5	1.49	93.5	1.49	5260
25e	48	1.02	88.9	0.78	9024
4D	50.8	1.48	75.2	0.978	6190
9D	80.7	1.68	80.7	1.68	3950
14D	81	1.38	81	1.38	4703
19D	81.5	1.17	48	0.947	4504
24D	81	1.35	81	1.35	4219
8C	81	1.38	94	0.978	6508
18C	68	1.29	68	1.29	5510
28C	70	1.45	70	1.45	4496
33C	70.4	1.24	70.4	1.24	5114
43C	81	0.856	87.4	0.715	8372
2B	69.1	0.585	69.1	0.585	9308
12B	66	1.06	86	1.06	7230
17B	65.95	1.15	81	1.13	6312
22B	81	1.02	81	1.02	6374
27B	70.5	1.018	97.1	0.961	5915
32B	44	1.42	71	1.33	5918

Appendix 2: APDL Code

```
!This is in mm
rangez = 9.906
rangexy = 2.032
!nsel,s,node,,max
```

```
SET,LAST
*dim,results1,array,2000,1
*dim,resultsx,array,2000,1              !Dimension results array for all stress directions
*dim,resultsy,array,2000,1
*dim,resultsz,array,2000,1
*dim,resultsxy,array,2000,1            !
*dim,resultsyz,array,2000,1
*dim,resultsxz,array,2000,1
*dim,resultszloc,array,2000,1

RSYS,12
!*vfill,results1(1),ramp,1,1

ETABLE,estrx,S,X                        !Create Stress Tables for x,y,x
ETABLE,estry,S,Y
ETABLE,estrz,S,Z
ETABLE,estrxy,S,XY                      !Create Stress Tables for x,y,x
ETABLE,estryz,S,YZ
ETABLE,estrxz,S,XZ

*do,i,1,2000
/GOPR
*Del,SMASK
*dim,SMASK,array,1
NSEL,ALL
!nsel,s,node,,i,i+1                     ! Select the ith node
!*vget,SMASK(1),Node,1,nsel             !Puts a 1 for all selected nodes

CSYS,0                                  !Go into Global Cooridinates

xloc = NX(i)                            !x,y,z cooridinates
yloc = NY(i)
zloc = NZ(i)
my_x=xloc
my_y=yloc
My_Z=zloc
resultszloc(i)=my_z
!nsel,s,loc,x,xloc-rangexy,xloc+rangexy  !Select Nodes Within a x,y,z range of the
maximum
!nsel,r,loc,y,yloc-rangexy,yloc+rangexy
!nsel,r,loc,z,zloc-rangez,zloc+rangez

esel,s,cent,x,xloc-rangexy,xloc+rangexy
esel,r,cent,y,yloc-rangexy,yloc+rangexy
esel,r,cent,z,zloc-rangez,zloc+rangez

*get,n_nodes,node,0,count              !Get the number of nodes
!*get,n_nodes,node,,s,z
my_n=n_nodes                           !The number of nodes
ESLN,r,0,ALL
NSLE,r,CORNER


*DEL,E_stressx
*DEL,E_stressy
*DEL,E_stressz
*DEL,E_stressxy
*DEL,E_stressyz
*DEL,E_stressxz
*DEL,E_vol
*DEL,NMASK
*DEL,wts_x
*DEL,wts_y
*DEL,wts_z
*DEL,wts_xy
```

```
*DEL,wts_yz
*DEL,wts_xz
*DEL,Ele_Id

*GET,numNd,Elem,0,NUM,MAX
*dim,NMASK,array,numNd
RSYS,12
*DIM,E_stressx,Array,numNd                 !Create Array for Average Stress X Elements
*DIM,E_stressy,Array,numNd
*DIM,E_stressz,Array,numNd
*DIM,E_stressxy,Array,numNd
*DIM,E_stressyz,Array,numNd
*DIM,E_stressxz,Array,numNd

*DIM,E_vol,Array,numNd                      !Array For Volumes

!*Dim,Ele_Id,Array,numNd

*DIM,wts_x,Array,numNd                      !Array for Weighted Stresses
*DIM,wts_y,Array,numNd
*DIM,wts_z,Array,numNd
*DIM,wts_xy,Array,numNd                     !Array for Weighted Stresses
*DIM,wts_yz,Array,numNd
*DIM,wts_xz,Array,numNd


*vget,NMASK(1),ELEM,1,esel               !Puts a 1 for all selected nodes
*vmask,NMASK(1)                          !Mask All Unselected Elements
*Vget,E_stressx(1),Elem,1,ETAB,estrx     !Get Masked Sx Array

*vmask,NMASK(1)
*Vget,E_stressy(1),Elem,1,ETAB,estry
*vmask,NMASK(1)
*Vabs, 1
*vmask,NMASK(1)
*Vget, E_vol(1), Elem, ,Geom
*vmask,NMASK(1)
*Vget,E_stressz(1),Elem,1,ETAB,estrz
*vmask,NMASK(1)
*Vget,E_stressxz(1),Elem,1,ETAB,estrxz
*vmask,NMASK(1)
*Vget,E_stressxy(1),Elem,1,ETAB,estrxy
*vmask,NMASK(1)
*Vget,E_stressyz(1),Elem,1,ETAB,estryz

!*vfill,Ele_Id(1),ramp,1,1                !Fill Array with 1:NumNd


*VOPER, Wts_x(1), E_stressx(1), MULT, E_vol(1)          !Multiply Volumes and Stress to
Create Weights
*VOPER, Wts_y(1), E_stressy(1), MULT, E_vol(1)
*VOPER, Wts_z(1), E_stressz(1), MULT, E_vol(1)
*VOPER, Wts_xy(1), E_stressxy(1), MULT, E_vol(1)
*VOPER, Wts_yz(1), E_stressyz(1), MULT, E_vol(1)
*VOPER, Wts_xz(1), E_stressxz(1), MULT, E_vol(1)

*VSCFUN, Num_x, SUM, Wts_x(1)
*VSCFUN, NUM_y, SUM, Wts_y(1)
*VSCFUN, NUM_z, SUM, Wts_z(1)
*VSCFUN, Num_xy, SUM, Wts_xy(1)
*VSCFUN, NUM_yz, SUM, Wts_yz(1)
*VSCFUN, NUM_xz, SUM, Wts_xz(1)


*VSCFUN, Den, SUM, E_vol(1)

*If,Den,eq,0,then
```

```
Den=.001
*EndIf

Avg_Stress_x = Num_x / Den
Avg_Stress_y = Num_y / Den
Avg_Stress_z = Num_z / Den
Avg_Stress_xz = Num_xz / Den
Avg_Stress_yz = Num_yz / Den
Avg_Stress_xy = Num_xy / Den


results1(i)=i
resultsx(i)=Avg_Stress_x
resultsy(i)=Avg_Stress_y
resultsz(i)=Avg_Stress_z
resultsxz(i)=Avg_Stress_xz
resultsyz(i)=Avg_Stress_yz
resultsxy(i)=Avg_Stress_xy

!*DEL,single
!*Dim,single,array,,1,4
!*vmask,SMASK(1)

!*Vget,results1(1)=i
!*Vget,results1(2)=Avg_Stress_x
!*Vget,results1(3)=Avg_Stress_y
!*Vget,results1(4)=Avg_Stress_z
/GOPR
*enddo

*CFOPEN,results1,txt                !Opens a File
*vwrite ! Write header information
('NODE',18x,,'Z Loc',18x,'Sx',18x,'Sy',18x,'Sz',18x,'Sxy',18x,'Syz',18x,'Sxz',18x)
!*vmask,NMASK(1)                     !Masks so only 1 will be written
*VWRITE,results1(1),resultszloc(1),resultsx(1),resultsy(1),resultsz(1),resultsxy(1),results
yz(1),resultsxz(1)
(F18.8,F18.8,F18.8,F18.8,F18.8,F18.8,F18.8,F18.8)
*CFCLOS
```

Appendix 3: Knot Maps

Pole # __1__ Date Tested __4/8/17__

P Max __52,320__ Deflection Max __4.2__

Measurements

    Circumference

    Butt: __37.375__ Weight: __484__

    Load 1: __37.25__ MC: __13.7__

    Load 2: __36.5__ Length: __241.5__

    Tip: __33.125__

Edge Distance

    Compression Hole __1 -3.25 -3__ Hole __6 -3.25 -2.7-__

    Tension Hole __1 -2.75 -2.55__ Hole __4 -2.85 2.95-__

Disk

    Distance from butt end _____

    Weight: Wet __3.3445 lb__

         Dry __2.9965__

    Volume __?__

    Specific Gravity __R. .519__

    Total # of rings __40__

    Total # of rings in outer 2" __21__

    Heartwood Diameter __8.25__

All sher very close to Top of hole. Also Continued Tensile Failure to hole 6, from Knot, Then Shearing @ The Top of The hole

Defects: _____

Looks like It could Compress Before TB from split fibers, lots of nonlinearity. Far Rings lifting above LOUD! Tensile, Knot 16, along existing check, Opening To Hole 4, Then Shearing Through All Holes

	Time	Load	Cause	Location				Type				
			Knot		KC	Hole	Other	Ten	Comp	Shear	Brash	Oth
Initial												
Second												
Second												
Ultimate												

Knot Map

Knot #	Diameter	Position (in)	Arc Distance (in)	Knot #	Diameter	Position (in)	Arc (in)
1	.2	0-13	-1-0	14	0.9	90	7.5
2	.35-.55	22-86	0 -1	15	0.8	89.5	-2.5
3	.17-.3	79-105	84-0	16	1	91	17
4	.15	0-38	-6	17	0.7	89	-12
5	.1	0-24	14	18			
6	.65	33	0	19			
7	.7	34	5.5	20			
8	.9	35	16	21			
9	.8	33.5	-11.5	22			
10	.9	63	-5.5	23			
11	.75	64	4	24			
12	.8	64.5	-13	25			
13	1.0	62	10	26			

Pole # __2__   Date Tested __4/6__

P Max __38071__   Deflection Max __3.9"__

Measurements

Circumference

Butt: __44"__   Weight: __584__

Load 1: __43__ ↑ Planed   MC: __15.4__

Load 2: __42.25__ ↓   Length: __240__

Tip: __38.75__

Edge Distance

Compression Hole __6 - 1.1 - .95__   Hole __3 - 1.15 - 1__

Tension Hole __6 - 1.1 - 1.0__   Hole __3 - .45 - 1 -__

Disk

Distance from butt end _____

Weight: Wet __1.169   4.41__

Dry __1.025   3.91__

Volume _____

Specific Gravity __.52__

Total # of rings __55__

Total # of rings in outer 2" __18__

Heartwood Diameter __8.8__

Defects:

Shear at 28,000 lbs. Shear at 32,000 lbs. At Butt. Tensile failure Hole 3 @ 34,000. Shear Failure 38,000 through holes @ 1 @ 3,4,5 through Preexisting Check Running Through Hole

	Time	Load	Cause	Location				Type				
			Knot		KC	Hole	Other	Ten	Comp	Shear	Brash	Oth
Initial												
Second												
Second												
Ultimate												

Knot Map

Knot #	Diameter	Position (in)	Arc Distance (in)	Knot #	Diameter	Position (in)	Arc (in)
1	1.5	46	-1	14	.35	0-52	18
2	1.8	49	47.5	15			
3	.75	48	15	16			
4	.7	61	-5.5	17			
5	1.7	77	0	18			
6	1.7	76	-7.5	19			
7	1.2	60	10	20			
8	.5	72	6	21			
9	1.15	77	12.5	22			
10	1.5	91	4.5	23			
11	1	93	16.0	24			
12	1.8	93	-4.5	25			
13	.3	55-77	16	26			

Pole #__540__
P Max __M.9 K__ *
Date Tested __3/29/17__
Deflection Max __2.68__

Measurements

    Circumference

    Butt: __40.5__
    Load 1: __41__
    Load 2: __39__
    Tip: __35.25__

    Weight: __526__
    MC: __13__
    Length: __241__

Edge Distance

    Max Compression Face _____ Min Compression Face _____
    Max Tension Face _____ Min Tension Face _____

$\frac{1}{2.03}$ $\frac{5}{1.5}$
2.03   1.95

$\frac{1}{1.6}$ $\frac{6}{1.6}$
1.85   2.0

Disk

    Distance from butt end _____
    Diameter in _____
    Thickness _____
    Weight: Wet __2248 2.2__
           Dry __1950__
    Total # of rings __29__
    Total # of rings in outer 2" __14__
    Heartwood Diameter _____

Defects: _____

Short Through   Bottom Holes/Crack @ 17 k, opened a bit. Sheared Through Butt at

	Time	Load	Cause	Location				Type				
			Knot		KC	Hole	Other	Ten	Comp	Shear	Brash	Oth
Initial						X				✓		
Second				Butt						X		
Second												
Ultimate												

Knot Map

Knot #	Diameter	Position (in)	Arc Distance (in)	Knot #	Diameter	Position (in)	Arc (in)
1	.25	0-39	11	14	.5	80	-12
2	.5	55-75	0	15	.75	84	-6
3	.56	72-92	-1	16	1	84	-11.5
4	.45	92-105	-1	17	1.25	60	-7
5	.65	93-128	0-1	18	2	90	-13
6	.1	31-123	5.5	19	.5	24	1
7	.1	48-64	15	20	.6	25	10.5
8	.1	38-85	-15	21	.6	26	6
9	.1	75-100	-5	22	2.25	63	18
10	1	25.5	-2.5	23	.8	90	1
11	1.25	25.5	-9	24	.7	90	10
12	1.75	25.5	-14	25	1.25	92	17
13	.95	48	-10	26			

6 Running Through and Near Holes

7

Pole #____554____   Date Tested__3/27/17____

P Max__48843____   Deflection Max __4"____

<u>Measurements</u>

    <u>Circumference</u>

    Butt:____40____   Weight:__462____

    Load 1:__38.5____   MC:__11____

    Load 2:__37____   Length:__24'____

    Tip:__33.375____

Edge Distance

    Max Compression Face __N/A____   Min Compression Face__N/A____

    Max Tension Face____N/A____   Min Tension Face__N/A____

Disk
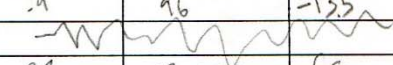
    Distance from butt end _____

    Diameter in_____

    Thickness_____

    Weight: Wet__1749.62____

        Dry__1520____

    Total # of rings __69____

    Total # of rings in outer 2"__24____

    Heartwood Diameter__7.5____

Defects:_____

Adrupt. Tension. Possibly Knot at 99". Or check, Tension face @ 79", Splintery.

	Time	Load	Cause	Location				Type				
			Knot		KC	Hole	Other	Ten	Comp	Shear	Brash	Oth
Initial												
Second												
Second												
Ultimate												

Knot Map

Knot #	Diameter	Position (in)	Arc Distance (in)	Knot #	Diameter	Position (in)	Arc (in)
1	.5	36	2.5	14	.8	79	-12.5
2	1	35	13	15	1	86	-1
3	.65	44	16	16	.5	87	-10.5
4	.9	52	14.5	17	.9	91	-1
5	.9	85	11	18	.9	96	-13.5
6	1.25	99	13	19			
7	1	97	1	20	2.8	80-100	65
8	.9	74	3.5	21			
9	.9	38	-4	22			
10	.5	46	-13.5	23			
11	.8	55	-1	24			
12	.5	63	-11	25			
13	.75	74	-9	26			

Pole #: 568 Date Tested: 3/30/17

P Max: 42.3 Deflection Max: _____

Measurements

    Circumference

    Butt: 37.5 Weight: 520

    Load 1: 37.5 MC: 14.3

    Load 2: 37.25 Length: 242

    Tip: 33.25

	2	5
	.6	.5
	1.25	1.3

Edge Distance

    Max Compression Face _____ Min Compression Face _____

    Max Tension Face _____ Min Tension Face _____

	6	2
	.95	.9
	1	.5

Disk

    Distance from butt end _____

    Diameter in _____

    Thickness _____

    Weight: Wet 2254.5

          Dry 1970

    Total # of rings 36

    Total # of rings in outer 2" 18

    Heartwood Diameter _____

Defects: Egg Shaped. Check 16 Near Choles. Crackin Butt got longer.
Initial tensile failure @ 4,5. Splintered. Sheared Through Rest of Holes. Final Shear @ Butt.

	Time	Load	Cause	Location				Type				
			Knot		KC	Hole	Other	Ten	Comp	Shear	Brash	Oth
Initial		41.3		4,5		X		X		X		
Second		42.3		4,5	X			X		X		
Second		40.5		Butt						X		
Ultimate												

Knot Map

Knot #	Diameter	Position (in)	Arc Distance (in)	Knot #	Diameter	Position (in)	Arc (in)
1	.4	0-24	1	14	1	96	1
2	.2	28-63	-2 - -5	15	.7	94	8.5
3	.2	42-80	2 - 0	16	.2-.25	57-108	16.5
4	.5	48	-11	17			
5	.85	53	-5.5	18			
6	.9	79	0	19			
7	1	79	-11	20			
8	1.1	95	-7.5	21			
9	1	96	-18	22			
10	1	51	7.5	23			
11	.85	51	16	24			
12	1.05	79	14	25			
13	1.05	81	4	26			

Pole #_____707_____   Date Tested___3/30/17_____

P Max____40.1_____   Deflection Max _____

Measurements

    Circumference

    Butt: 37.75 _____   Weight:___418_____

    Load 1: 37.25 _____   MC:_____10.2_____

    Load 2: 36.25 _____   Length:___241_____

    Tip: 33 _____

Edge Distance

    Max Compression Face _____ Min Compression Face_____

    Max Tension Face_____ Min Tension Face_____

$$\frac{5}{.4} \quad \frac{1}{.6}$$
$$1.45 \quad 1.4$$

Disk

    Distance from butt end _____

    Diameter in_____

    Thickness_____

    Weight: Wet_246, 348, 422.2_____

          Dry_212.9, 307.4, 369.1_____

$$\frac{5}{1.2} \quad \frac{1}{.7}$$
$$.9 \quad .7$$

    Total # of rings ___34_____

    Total # of rings in outer 2" _17____

    Heartwood Diameter_8.7"____

Defects:_____ But not actual failure _____ Knot nearby, but not cause of fail

Cracking Below C-Holes @ 34.5K, 35.5K, Hole 2 Broke Tension, continues to propagate shr along T face. from

Load continued until 40.1k. While holding, C fail @ Z and knot.

	Time	Load	Cause	Location				Type					
			Knot		KC	Hole	Other	Ten	Comp	Shear	Brash	Oth
Initial		34.5					Check					
Second		35.5	x			X		X				
Second		40.1				X		X				
Ultimate		38	X	Hole 2		X				x		

Knot Map

Knot #	Diameter	Position (in)	Arc Distance (in)	Knot #	Diameter	Position (in)	Arc (in)
1	.675	46	8.5	14	.95	92	-12.5
2	1.25	53	1.5	15	.2-.35	0-62	1 - -1
3	1.3	54	6.5	16	-.1-.2	46-91	-3 - -5
4	1.1	82	3	17			
5	1	84	15	18			
6	1.15	87	10.5	19			
7	1.35	89	6	20			
8	1.25	96	-18	21			
9	.75	54.5	-2.5	22			
10	.8	54	-15	23			
11	1.2	91	-17.5	24			
12	.5	86	-10	25			
13	.55	89	-4.5	26			

Pole #____715____
P Max____20844____ *

Date Tested____3/28/17____
Deflection Max____3.8____

Measurements

Circumference
Butt:____41.55____
Load 1:____40____
Load 2:____38.75____
Tip:____34____

Weight:____464____
MC:____11.2____
Length:____24____

Edge Distance

Max Compression Face____3.25____   Min Compression Face____2.75____
Max Tension Face____3.____   Min Tension Face____3.1____

Disk

Distance from butt end _____
Diameter in_____
Thickness_____
Weight: Wet____628, 409.1, 661.8____
Dry____548, 356.6, 566.9____
Total # of rings ____23____
Total # of rings in outer 2"____10____
Heartwood Diameter____9.3"____

Defects:_____   Shear at

Knots 126" @ 15, 18", 1.5", .5". Initial Knot/Hole at 80", Ran along Bottom Check to 126"

	Time	Load	Cause	Location				Type					
			Knot		KC	Hole	Other	Ten	Comp	Shear	Brash	Oth	
Initial		20844	x	80		X		X					
Second			x	126			Check			X			
Second													
Ultimate													

Knot Map

Knot #	Diameter	Position (in)	Arc Distance (in)	Knot #	Diameter	Position (in)	Arc (in)	
1	.5	31	12	14	.4	38	-12	
2	1.25	40	7	15	1.25	40	-7.5	
3	1.75	42.5	3.5	16	.9	72	-10.5	
4	1.25	40	12	17	.7	79	-8	
5	.5	38	15	18	1.1	81	-14.5	
6	.5	61	15	19	1.25	83	-4	
7	.625	A	6	20	1	89	-10	
8	1.5	81	3.5	21	.66	37	-1	
9	.5	83	4.5	22	.4	0-60	0 - -5	Discontin
10	1.5	84.5	7.5	23		17 max		
11	1	81	11	24	.25	36-103	-14 - -16	
12	1.25	37	-1	25				
13	.6	32	-14	26				

Pole #__727____   Date gmTested 4/15/17_____

P Max__50.6____   Deflection Max 3.4_____

Measurements

    Circumference

    Butt: 43.5_____   Weight: 536_____

    Load 1: 42.5 *_____   MC:_____

    Load 2: 41.5 *_____   Length: 241_____

    Tip: 38.5_____

Edge Distance

    Compression Hole 5 -.65 - 1.2____   Hole 2 -1 - 1.2 -_____

    Tension Hole 1 - 1 -.7 -____   Hole 5 - 1. 05-.95_____

Disk

    Distance from butt end _____

    Weight: Wet__5.2645_____

         Dry__4.4865_____

    Volume_____

    Specific Gravity_____

    Total # of rings ___29___

    Total # of rings in outer 2" 13____

    Heartwood Diameter 9.75_____

Defects:_____/ ∩/50 knot 3____

Shearing@ 1 Holes(4,5) 41K. T Fail @ 6 45 K. C above Hole 5. Holes 2,3 @ 50K, Shear @ Butt. 50 ?
and shear @ Butt @ 50K for ultimate, little sliver   caused by cheeks

	Time	Load	Cause	Location					Type				
			Knot		KC	Hole	Other		Ten	Comp	Shear	Brash	Oth
Initial		41				x					x		
Second		45				x			x				
Second		50											
Ultimate		50.6											

Knot Map   56   Check

Knot #	Diameter	Position (in)	Arc Distance (in)	Knot #	Diameter	Position (in)	Arc (in)
1	.5	49	-3	14			
2	.72	78.5	-4	15			
3	.9	78	-11	16			
4	1	48	t 8	17			
5	1.2	48	16.5	18			
6	.8	76	2.25	19			
7	2	78	7.5	20			
8	.25	22-58	14	21			
9	.3	60-82	11.5	22			
10	.2	0-23	0	23			
11				24			
12				25			
13				26			

Pole #__728__ Date Tested__3/27/17__
P Max__35470__ Deflection Max __2.5__
Measurements   35074

   Circumference
   Butt: 11.75 ____ 38 Weight: 478 ____
Butt Load 1: 12.2 ____ 38.5 MC: __
Tip Load 2: 12.0 ____ 38 Length: 241"
   Tip: 10.75 ____ 34.25

Edge Distance
   Max Compression Face N/A   Min Compression Face N/A
   Max Tension Face N/A   Min Tension Face N/A

Disk
   Distance from butt end ____
   Diameter in____
   Thickness____
   Weight: Wet 1186, 943 ____
   Dry 1036, 817 ____
   Total # of rings __71__
   Total # of rings in outer 2" __39__
   Heartwood Diameter __9.6__
Defects: Initial Cracks Originating From Butt, Shear Failure
Check Butt.

	Time	Load	Cause Knot	Location	KC	Hole	Other	Type Ten	Comp	Shear	Brash	Oth
Initial		35000								X		
Second												
Second												
Ultimate												

Knot Map   CW

Knot #	Diameter	Position (in)	Arc Distance (in)	Knot #	Diameter	Position (in)	Arc (in)
1	.5	72	19.5	14	.33	80-96	8.5
2	.75	77	16	15	.30	101-115	8.5
3	.25	102	12	16	.15	23-37	19.5
4				17	.1	40-43	14
5				18			
6		51		19			
7		57		20			
8		62		21			
9				22			
10	.185	23-42	16.5	23			
11	.36	42-57	11	24			
12	.37	57-71	11	25			
13	.35	72-82	10	26			

Width

Pole #_____739_____ Date Tested___4/10/17_____
P Max___36.4_____ Deflection Max ___4.0___

Measurements

    Circumference
    Butt:___38.125_____   Weight:___510_____
    Load 1:___37.5_____   MC:_____
    Load 2:___36.875_____   Length:___241.5_____
    Tip:___34.5_____

Edge Distance

    Compression Hole 4 -2.15 -1.75   Hole 3 -2.05-1.7 -_____
    Tension Hole 3 1.95 - 1.9   Hole 4 -1.9 -1.8 -___ 5-2.05-1.95

Disk

    Distance from butt end _____
    Weight: Wet___1.336 , 2.2915_____
            Dry___1.1685 , 1.9935_____
    Volume_____
    Specific Gravity___.55_____
    Total # of rings ___70_____
    Total # of rings in outer 2" 16_____
    Heartwood Diameter 8.25_____

Defects:_____
Cracking at Butt @ 29k and 31.6k. More Failures @ Butt until 36.4 K and 4in, some cracks extending until & TB Zone. No HOLES!

	Time	Load	Cause	Location				Type				
			Knot		KC	Hole	Other	Ten	Comp	Shear	Brash	Oth
Initial		29,31.6		Ⓞ			Crack			X		
Second		35		σ						X		
Second		36.4		Ⓞ						X		
Ultimate												

Knot Map

Knot #	Diameter	Position (in)	Arc Distance (in)	Knot #	Diameter	Position (in)	Arc (in)
1	.3	0-65	3-0	14			
2	.55	46	12.5	15			
3	.7	31	-18	16			
4	.7	42	-19	17			
5	.5	60	<3	18			
6	.9	61	13.5	19			
7	.5	75	7	20			
8	.9	80	16	21			
9	.9	101	12	22			
10	.6	98	16.5	23			
11	.6	101	-5	24			
12				25			
13				26			

Pole # __755__ Date Tested __4/8/17__
P Max __45358__ Deflection Max __2.5__

Measurements

Circumference
Butt: __42.5__ Weight: __432__
Load 1: __41.0__ MC: __13.7__
Load 2: __39.5__ Length: __240.5__
Tip: __35.5__

Edge Distance
Compression Hole __2 -2.8 -2.7__ Hole __4 -2.9 2.85__
Tension Hole __2 -3.05 -2.85__ Hole __4 -3.1 -2.9__

Disk
Distance from butt end _____
Weight: Wet __3.6575__
Dry __3.2135__
Volume _____
Specific Gravity __.446__
Total # of rings __31__
Total # of rings in outer 2" __15__
Heartwood Diameter __8.875__

Defects: __Egg Shaped. Vol- 15" Hd- 12"__
__Shear 45,000 Psi, Check opened into throughborne zone Center, through pre-existing small checks__

	Time	Load	Cause	Location				Type				
			Knot		KC	Hole	Other	Ten	Comp	Shear	Brash	Oth
Initial												
Second												
Second												
Ultimate												

Knot Map

Knot #	Diameter	Position (in)	Arc Distance (in)	Knot #	Diameter	Position (in)	Arc (in)
1	.45	44	5.5	14			
2	1.4	46.5	13.5	15			
3	1.9	44	16.0	16			
4	1.0	44	-14	17			
5	.75	47	-8.5	18			
6	1.7	46.5	-17.5	19			
7	2.1	86	17	20			
8	0.5	84	4.5	21			
9	1.15	85.5	-10.5	22			
10	1.50	75.5	-16.5	23			
11	.15	64-117	8- 4	24			
12				25			
13				26			

DC

Pole #_____8622_____   Date Tested____5/30/11 T_____
P Max__45.7k_____   Deflection Max __3.75_____

Measurements
  Circumference
  Butt:___38.625_____   Weight:___428_____
  Load 1:__38.25_____   MC:____10.5_____
  Load 2:__36.5_____   Length:____241____
  Tip:____31.0_____

                                                    $\frac{2}{3.0}$ $\frac{5}{2.65}$
                                                    3.1   3.15

Edge Distance
  Max Compression Face _____ Min Compression Face_____
  Max Tension Face_____ Min Tension Face_____ $\frac{3}{3.1}$ $\frac{6}{3.2}$
                                                                        2.7   2.9
Disk
  Distance from butt end _____
  Diameter in_____
  Thickness_____
  Weight: Wet___2000.14_____
       Dry___1750_____
  Total # of rings _____44_____
  Total # of rings in outer 2"__19____
  Heartwood Diameter___8.6"_____

Defects:_____
43, lots of noise, butts opened but still going, Small tensile failure below hole X@ 43. Catastrophic failure there @ 45, b
caused by knot @ 94, splintery extended to all T holes. or knot @ Hole 4. Prob Hole 4.

	Time	Load	Cause	Location				Type					
			Knot		KC	Hole	Other	Ten	Comp	Shear	Brash	Oth
Initial		43	X	74				X				
Second		45	X	74, 95.5		\						
Second		45								X		
Ultimate												

Knot Map

Knot #	Diameter	Position (in)	Arc Distance (in)	Knot #	Diameter	Position (in)	Arc (in)
1	3-.4	0-94	0--2	14			
2	1.15	47.5	-9.5	15			
3	1.4	47.5	-12.5	16			
4	1.25	75	-8.5	17			
5	1.4	74	-17	18			
6	1.4	94	-11	19			
7	.5	95.5	-2	20			
8	.8	25	8	21			
9	1.15	47	12	22			
10	.6	73	4	23			
11	1.15	72.5	12.5	24			
12	1.55	94	-17	25			
13	1.2	95.5	-10	26			

* Hit Butt sensor @ .5in, does not seem to be working, however

Pole #: 997 Date Tested: 3/31/17
P Max: 48.3 Deflection Max: 3.75

Measurements

Circumference
Butt: 38.5 Weight: 478
Load 1: 38.25 MC: 11.8
Load 2: 37.0 Length: 241.5
Tip: 32.75

Edge Distance
Max Compression Face: N/A   Min Compression Face: N/A
Max Tension Face: N/A   Min Tension Face: N/A

Disk
Distance from butt end: _____
Diameter in: _____
Thickness: _____
Weight: Wet: 1873.41
   Dry: 1650
Total # of rings: 30
Total # of rings in outer 2": 13
Heartwood Diameter: 7.8

Defects: Tensile failure beginning at Knot 4, propagating through other Dow Tension Knots @ 48.3k

	Time	Load	Cause	Location				Type				
			Knot		KC	Hole	Other	Ten	Comp	Shear	Brash	Oth
Initial		38	X									
Second												
Second												
Ultimate												

Knot Map

Knot #	Diameter	Position (in)	Arc Distance (in)	Knot #	Diameter	Position (in)	Arc (in)
1	.1-.3	0-97	-2-1	14			
2	.7	28	-5.5	15			
3	.75	48	-6.5	16			
4	.85	52	10.5	17			
5	1.3	53	16	18			
6	.55	85	10	19			
7	1	93	14	20			
8	1.8	64.5	-16.5	21			
9	1.3	89	-8.5	22			
10	.85	94	-4.5	23			
11				24			
12				25			
13				26			

Pole #__4248__ Date Tested__3/30/17__

P Max__39.6__ Deflection Max __3.25 in__

Measurements

Circumference

Butt:__38.5__ Weight:__445__

Load 1:__38.6__ MC:__10.9__

Load 2:__37.25__ Length: __242__

Tip:__33__

Edge Distance

Max Compression Face _____ Min Compression Face_____

$\frac{5}{1.3}$ $\frac{2}{1.5}$

.45 .5

Max Tension Face_____ Min Tension Face_____

$\frac{6}{.72}$ $\frac{3}{1.05}$

.7 .85

Disk

Distance from butt end _____

Diameter in_____

Thickness_____

Weight: Wet__1668.42__

Dry__1460__

Total # of rings __26__

Total # of rings in outer 2" __13__

Heartwood Diameter __8.2"__

Defects:_____

Tension Failure Hole 6, 37 k. Ultimate Failure 39.7k, same place, Propagated toward tip in shear and to hole 5.

	Time	Load	Cause	Location				Type					
			Knot		KC	Hole	Other	Ten	Comp	Shear	Brash	Oth	
Initial		37	X			X		X					
Second		39.7	X			X		X		X			
Second													
Ultimate													

Knot Map

Knot #	Diameter	Position (in)	Arc Distance (in)	Knot #	Diameter	Position (in)	Arc (in)
1	.4 - .5	59-12a	-1 - -5	14			
2	.25-.4	0-58	-11 - -13	15			
3	1.1	31.5	-1	16			
4	.6	29	-16	17			
5	.5	38	-15	18			
6	.55	76	-6	19			
7	.8	85.5	-7.5	20			
8	1.3	38	4.5	21			
9	.6	78	4	22			
10	1.75	84.5	11	23			
11	1.25	86.5	4.5	24			
12	1	78	12.5	25			
13	1.4	88	18	26			

Pole #_____4771_____ Date Tested_____4/13/17_____

P Max__5286__ Deflection Max 4.3

Measurements

Circumference

Butt:__45.5__ Weight:__664_____

Load 1:__43.125__ MC:_____✗_____

Load 2:__42__ Length:__240.5_____

Tip:__38.25__

Edge Distance

Compression Hole 4 - 2.25 1.75 Hole 3 - 2.2 1.8_____

Tension Hole 2 - 1.9 - 1.8 - Hole 3 - 1.9 - 1.95

Disk

Distance from butt end _____

Weight: Wet 1.5985_____

Dry 1.382_____

Volume_____

Specific Gravity____.558_____

Total # of rings _____31_____

Total # of rings in outer 2" __14__

Heartwood Diameter_____8_____

T @ K5.0 52.8, then s
Thrugh holes, then droppe
to 46K to u ultmately (237)

Defects:_____

Shear @ Butt 42K, 46 S. Creaking @ knot. b the sh't failed 153 in, K D. C @ 40kS (little bit) F @ '

	Time	Load	Cause	Location				Type				
			Knot		KC	Hole	Other	Ten	Comp	Shear	Brash	Oth
Initial												
Second												
Second												
Ultimate												

Knot Map

Knot #	Diameter	Position (in)	Arc Distance (in)	Knot #	Diameter	Position (in)	Arc (in)
1		0-36	-2	14			
2		23-85	-2 - -4	15			
3	1.9	27	3.5	16			
4	2.7	52.5	9	17			
5	1.65	53	19.5	18			
6	1.6	82.5	0	19			
7	1.9	82	12.5	20			
8	1.65	82	20.5	21			
9	1.2	26	-7.5	22			
10	1.4	52.5	~4	23			
11	1.25	54	-9	24			
12	1.55	82	-15	25			
13				26			

Pole #__4773__   Date Tested__4/13/17__
P Max__35.8__   Deflection Max 3__

Measurements

    Circumference
    Butt:__38.06__   Weight:__514__
    Load 1:__37.625__   MC:__✗__
    Load 2:__36.875__   Length:__241__
    Tip:__32.25__

Edge Distance

    Compression Hole 5 - 1.4 -.8   Hole 3 -.75 -1.25
    Tension Hole 3 - 1.1 -.95   Hole 4 -1.25 1 -

Disk

    Distance from butt end _____
    Weight: Wet __3.8235, 2.4805__ 3.057, 1.88
        Dry __2.688, 1.645__
    Volume_____
    Specific Gravity__.48__
    Total # of rings __56__
    Total # of rings in outer 2" __26__
    Heartwood Diameter__7.4__

Defects:_____ ✓Not Sure

P6? Failure @ 35.8 K. Ultimate Failure @ 35k 3in. C Failure @ B Hole 2. Also caused by 2 preexisting checks above and below. @ Top.

	Time	Load	Cause	Location				Type				
			Knot		KC	Hole	Other	Ten	Comp	Shear	Brash	Oth
Initial		35.8										
Second		35.0	-X			✗	Check					
Second												
Ultimate												

Knot Map

Knot #	Diameter	Position (in)	Arc Distance (in)	Knot #	Diameter	Position (in)	Arc (in)
1	.6	36	1.5	14	.75	100	18.5
2	.65	37	18	15	.5	65	-7.5
3	.5	36	-8.75	16	.9	95	-2.25
4	.5	53	-4.5	17	.2	0-73	4 - -1
5	1.2	52	-13	18			
6	.8	51	1.5	19			
7	1	65	1	20			
8	.7	61.5	8.5	21			
9	.6	52	15	22			
10	.5	64	13	23			
11	.6	71	14	24			
12	.9	80	3.5	25			
13	1.2	101	5	26			

Pole #: 4774   Date Tested: 4/15/17
P Max: 40-97   Deflection Max: 3.75

Measurements

    Circumference
    Butt: 43.25   Weight: 558
    Load 1: 41.5*   MC: 8.7
    Load 2: 40.5   Length: 24
    Tip: 35.75

Edge Distance

    Compression Hole 2 -.85 -1.2   Hole 6 -1.3 -.95 -
    Tension Hole 5- 1-1.1 -   Hole 4 -1.15- 1.15

Disk

    Distance from butt end _____
    Weight: Wet 5.4350
            Dry 4.716
    Volume _____
    Specific Gravity — .482
    Total # of rings 34
    Total # of rings in outer 2" 16
    Heartwood Diameter 10.125

Defects:
37K?, prob shear Butt. 39? T beyond load Z, partially caused by knot 40.9, continuing along grain @ H6. Steadily decreasing

	Time	Load	Cause	Location				Type				
			Knot		KC	Hole	Other	Ten	Comp	Shear	Brash	Oth
Initial												
Second												
Second												
Ultimate												

Knot Map

Knot #	Diameter	Position (in)	Arc Distance (in)	Knot #	Diameter	Position (in)	Arc (in)
1	1	27	-3	14			
2	.8	65.5	-2.5	15			
3	1.4	63	-18	16			
4	1.1	27.5	8.5	17			
5	1.0	64.5	9	18			
6	1.2	92	18	19			
7				20			
8				21			
9				22			
10				23			
11				24			
12				25			
13				26			

Pole # 4779

P Max 46.2

Date Tested 4/10/17

Deflection Max 2.3

Measurements

Circumference

Butt: 44

Load 1: 43

Load 2: 41.5

Tip: 36.375

Weight: 591

MC: 12.7

Length: 240

Edge Distance

Compression Hole 3 1.5 -1.9

Tension Hole 3 -2.3 -1.75

Hole 5 -1.8 -2.05-

Hole 4 -2.1 -2.05-

Disk

Distance from butt end _____

Weight: Wet 6.29955

Dry 5.549

Volume _____

Specific Gravity .515

Total # of rings 41

Total # of rings in outer 2" 19

Heartwood Diameter 11

Defects: _____

Failed in Shear at 46.2K, along existing and new checks.

	Time	Load	Cause Knot	Location				Type Ten	Comp	Shear	Brash	Oth
					KC	Hole	Other					
Initial												
Second												
Second												
Ultimate												

Knot Map

Knot #	Diameter	Position (in)	Arc Distance (in)	Knot #	Diameter	Position (in)	Arc (in)
1	1.1	58	-9	14			
2	1.1	59	0	15			
3	.9	56	8	16			
4	.8	54	14	17			
5	1.2	94	0	18			
6	1.1	95.5	8	19			
7	.95	95	-7	20			
8	.8	93.5	-11	21			
9	1.0	97	-20	22			
10	0.2	0-60	-2	23			
11				24			
12				25			
13				26			

Pole #__4789__ Date Tested __4/17/18__

P Max __59.4__ Deflection Max __3.5 in__

Measurements

Circumference

Butt: __43.5__ Weight: __618__

Load 1: __43 k__ MC: __×__

Load 2: __42__ Length: __241__

Tip: __37.75__

Edge Distance

Compression Hole __3 -1 -2.2__ Hole __5 -1.3 -3.3 -__

Tension Hole __5-1.8-2.15__ Hole __- 1.8-2.0 -__

Disk

Distance from butt end _____

Weight: Wet __5.9745__

Dry __2.8915__ , __2.5420__

Volume _____

Specific Gravity __.472__

Total # of rings __65__

Total # of rings in outer 2" __25__

Heartwood Diameter __9.25__

Defects: _____

Shear @ 42,000, @ 2in, 55K continued shear. 59.4k, Tensile @ 44k, 50in, near Knot 4, hole 1, Shear @ Hole 2

	Time	Load	Cause	Location				Type				
			Knot		KC	Hole	Other	Ten	Comp	Shear	Brash	Oth
Initial												
Second												
Second												
Ultimate												

Knot Map

Knot #	Diameter	Position (in)	Arc Distance (in)	Knot #	Diameter	Position (in)	Arc (in)
1	.75	36	8	14			
2	1.05	37	19	15			
3	.6	51.5	5	16			
4	1.1	52	21	17			
5	1.1	72	19	18			
6	.85	95	8.5	19			
7	.75	34	-9.5	20			
8	1.15	54	-9	21			
9	1.45	73	-12	22			
10	1.5	95	-20	23			
11	.8	96	-9	24			
12				25			
13				26			

Pole # 4797   Date Tested 4/15/17
P Max 47.3   Deflection Max 3.2

Measurements

Circumference
Butt: 44   Weight: 556
Load 1: 41.75*   MC: 9.6
Load 2: 42*   Length: 241
Tip: 38.25

Edge Distance
Compression Hole 3 -2.55 3.1   Hole 4 -2.7.5 -2.9
Tension Hole 5 -2.85 -3.05   Hole 4 -2.9-2.9-

Disk
Distance from butt end _____
Weight: Wet 3.9540, 1.311√
         Dry 3.477 1.153
Volume _____
Specific Gravity _____
Total # of rings   80
Total # of rings in outer 2" 27
Heartwood Diameter 8.875

Checks...@42"

Defects:

Shearing @ Butt without loss strength. @ 47.3k, no observable cause then slope of grain small existing checks there

	Time	Load	Cause	Location				Type				
			Knot		KC	Hole	Other	Ten	Comp	Shear	Brash	Oth
Initial												
Second												
Second												
Ultimate												

Knot Map

Knot #	Diameter	Position (in)	Arc Distance (in)	Knot #	Diameter	Position (in)	Arc (in)
1	1.7	101	2	14			
2	1.9	24	5	15			
3	1.8	91	12	16			
4				17			
5				18			
6				19			
7				20			
8				21			
9				22			
10				23			
11				24			
12				25			
13				26			

Pole #__4849_____   Date Tested__7/1/11_____

P Max__40.8_____   Deflection Max __2.78_____

Measurements

Circumference

Butt:__37.0 38.5__   Weight:__522_____

Load 1:__39.0_____   MC:__15.5_____

Load 2:__37.75_____   Length:__242_____

Tip:__35.0_____

Edge Distance

Compression Hole __-N/A-_____   Hole__-__-N/A-_____

Tension Hole ____-N/A-_____   Hole__-__-N/A-_____

Disk

Distance from butt end _____

Weight: Wet__4.325_____

Dry__3.725_____

Volume_____

Specific Gravity__.47_____

Total # of rings __40_____

Total # of rings in outer 2"__22_____

Heartwood Diameter__9.4_____

Defects:__Large Butt Checks_____
(@ 32,000, Shear @ 33,000 @ But. C Break continuing. @Load 2 T @ 40.8 near load 1 Shear @ 40.7

	Time	Load	Cause	Location				Type				
			Knot		KC	Hole	Other	Ten	Comp	Shear	Brash	Oth
Initial												
Second												
Second												
Ultimate												

Knot Map

Knot #	Diameter	Position (in)	Arc Distance (in)	Knot #	Diameter	Position (in)	Arc (in)
1	.5	0-74 31	-1	14			
2	.4	24-49	-2	15			
3	.3	43-75	-4	16			
4	1.1	31	-5.5	17			
5	1	43.5	-2	18			
6	.85	30	-13	19			
7	1.25	31	15	20			
8	1.1	34	-17	21			
9	.75	78.5	0	22			
10	1.25	76	-5.5	23			
11	1.0	76	-18.5	24			
12	1.15	105	-5	25			
13				26			

Pole #   4850
P Max   46.4

Date Tested   7/6/11
Deflection Max   3.1

<u>Measurements</u>

   <u>Circumference</u>

   Butt: 45.5

   Load 1:   44.5

   Load 2:   43.5

   Tip: 32.5

Weight: 568
MC: 18.0
Length: 241.5

<u>Edge Distance</u>

   Compression Hole 6 -2.35 2 1.25   Hole   - 2.5 - 1.4 -

   Tension Hole 3   2.05 - 1.7   Hole 6 - 1.8 - 2.5 -   5 - 1.9 - 1.7

<u>Disk</u>

   Distance from butt end _____

   Weight: Wet 7.2445

         Dry 6.3995

   Volume_____

   Specific Gravity   .42

   Total # of rings   50

   Total # of rings in outer 2"   6

   Heartwood Diameter   10

Defects:

Shear @ Butt 41.3 K. 46.4 K. Tensile failure @ Knot 16. Sheared Through Hole 6.
Around Knot 9 and Knot 8. Shear from knot 8 to 100".

	Time	Load	Cause	Location				Type				
			Knot		KC	Hole	Other	Ten	Comp	Shear	Brash	Oth
Initial												
Second												
Second												
Ultimate												

Knot Map

Knot #	Diameter	Position (in)	Arc Distance (in)	Knot #	Diameter	Position (in)	Arc (in)
1	1.25	38	13	14	.95	87	-2
2	1.7	25	12.5	15	1.7	86	-13
3	1.3	24	-4.5	16	1.4	86	-21
4	1.6	25	-14	17	1.9	103	-10
5	1.3	40	-17	18	.27"	0-45	1 - -4
6	2	54	20	19	.24	86-110	0- -2
7	1.7	85	7	20			
8	1.7	86	14	21			
9	2.4	85	18	22			
10	1.1	105	3	23			
11	1	54	-3	24			
12	1.75	53	-14	25			
13	1	84	-5.5	26			

Pole #___4853___ Date Tested___4/6/17___
P Max___68900___ Deflection Max___3.4"___

Measurements

Circumference
Butt:___44.25___ Weight:___680___
Load 1:___43.5___ MC:___17%___
Load 2:___42.5___ Length:___244___
Tip:___38.5___

Edge Distance
Compression Hole 2 - .6 - 1.1 Hole 5 - 1.1 - 1.2 -___
Tension Hole 1 - 1.05 - 1.1 Hole 4 - .6 - .9 -___ 6 - .9 - 1. 05.5 Not present

Disk
Distance from butt end ___———___
Weight: Wet___4.6635___
Dry___3.9570___
Volume___———___
Specific Gravity___.496___
Total # of rings ___63___
Total # of rings in outer 2"___8.25 21___
Heartwood Diameter___8.25___

Defects:_____

Crack in Butt has Opened 3/4" Wide Without Breaking. Tension @ 69K @ Hole 3. Sheared Through 2,4 Above 5, Through 6.

	Time	Load	Cause	Location				Type				
			Knot		KC	Hole	Other	Ten	Comp	Shear	Brash	Oth
Initial												
Second												
Second												
Ultimate												

Knot Map

Knot #	Diameter	Position (in)	Arc Distance (in)	Knot #	Diameter	Position (in)	Arc (in)
1	.8	35.5	9	14			
2	.5	66	16	15			
3	1.2	95	11	16			
4	.75	86	-13	17			
5	1.15	94	-10	18			
6		25-72	-1- 0	19			
7		71-113	-6	20			
8				21			
9				22			
10				23			
11				24			
12				25			
13				26			

Pole #___4854___ Date Tested___4/9/17___

P Max___57.773 K___ Deflection Max___5 2.57___

Measurements

Circumference

Butt:___45.75___ Weight:___694___

Load 1:___43.75___ MC:___X___

Load 2:___42.50___ Shaved Length:___24___

Tip:___39.75___

Edge Distance

Compression Hole _2 - .45 - 1.05_ Hole _6 - .5 - 1.1 -_

Tension Hole _2 - .9 - .55 -_ Hole _5 - .6 - .65 -_

Disk

Distance from butt end _____

Weight: Wet___4.336_____

Dry___3.881_____

Volume___X_____

Specific Gravity___.542___

Total # of rings ___49___

Total # of rings in outer 2" _20___

Heartwood Diameter _10.25___   K10

Defects:___

Cracks in Butt growing throughout. Cabac Hole, 4,5, Shary 57 @ K at Butt.

	Time	Load	Cause	Location				Type				
			Knot		KC	Hole	Other	Ten	Comp	Shear	Brash	Oth
Initial												
Second												
Second												
Ultimate												

Knot Map

Knot #	Diameter	Position (in)	Arc Distance (in)	Knot #	Diameter	Position (in)	Arc (in)
1	.6	0-41	*2- 20	14	.85	89	14
2	.6	41-72	-2-3	15	.95	87	26
3	.45	63-98	0-2	16	1	90	.4
4	.3	90-122	-1 - -3	17	1.35	87.5	-7.5
5	.8	29	-13.5	18	1.15	89.0	-13.5
6	1.25	28 1/2	-10	19			
7	1	29	-16.5	20			
8	.7	59.5	0	21			
9	.55	58	5.75	22			
10	1.2	60	20	23			
11	.85	58.5	-11	24			
12	.75	57	-17	25			
13	.65	88	6	26			

Pole # 4855   Date Tested 4/14

P Max 57.6   Deflection Max 4.18

Measurements   *Butt ∆ is off

    Circumference

    Butt: 40.25   Weight: 484

    Load 1: 39.5   MC: 8

    Load 2: 38   Length: 241

    Tip: 32.875

Edge Distance

    Compression Hole N/A -   Hole -   -   -

    Tension Hole   -   Hole -   -   -

Disk

    Distance from butt end _____

    Weight: Wet 4.4865

        Dry 3.7795

    Volume _____

    Specific Gravity .547

    Total # of rings 33   Sheared Thru K3

    Total # of rings in outer 2" 8.25 10

    Heartwood Diameter 8.25

Defects: Tensile @ 54.5K, Ultimate @ 57.6K, with a series of tensile failures along the grain rings, part. No knots @ Tface @ 60in. Some preexisting checks too. Lots of Splintering @ 90in Too.

	Time	Load	Cause	Location				Type				
			Knot		KC	Hole	Other	Ten	Comp	Shear	Brash	Oth
Initial		54.5		60				X				
Second		57.6		60				X				
Second		52.5								X		
Ultimate												

Knot Map

Knot #	Diameter	Position (in)	Arc Distance (in)	Knot #	Diameter	Position (in)	Arc (in)
1		12-87	0	14			
2	1.65	34.5	10	15			
3	2	59	6	16			
4	.85	61	13	17			
5	.67	35.5	-1	18			
6	1.6	89.5	6	19			
7				20			
8				21			
9				22			
10				23			
11				24			
12				25			
13				26			

Pole #__4856____   Date Tested__4/10/17____
P Max__54.7____   Deflection Max __2.95__
Measurements 55.2   __3.52__
    Circumference
    Butt:__42.875____   Weight:__628____
    Load 1:__41.0____   MC:__✕____
    Load 2:__40.0____   Length:__246.5____
    Tip:__37.75____

Edge Distance
    Compression Hole __-N/A -____   Hole__- N/A -____
    Tension Hole __N/A -____   Hole__- N/A- -____

Disk
    Distance from butt end _____
    Weight: Wet__5.5605____
         Dry__4.928____
    Volume_____
    Specific Gravity__.56____
    Total # of rings __77____
    Total # of rings in outer 2"__25____
    Heartwood Diameter__9.5____

Defects:_____
Shaving Bet 54.2k, and 54.5k, Shear Cracks extend to 24" max
and 55

	Time	Load	Cause	Location				Type					
			Knot		KC	Hole	Other	Ten	Comp	Shear	Brash	Oth	
Initial													
Second													
Second													
Ultimate													

Knot Map
w/knots

Knot #	Diameter	Position (in)	Arc Distance (in)	Knot #	Diameter	Position (in)	Arc (in)
1		49	4.5	14			
2		49	-9	15			
3		59	1.5	16			
4		72	6	17			
5		86.5	8	18			
6		61	-5.75	19			
7		73	-6.25	20			
8		88	-2.5	21			
9		45-94	-7.5 -11	22			
10				23			
11				24			
12				25			
13				26			

Pole #__4875____   Date Tested__4/16/17____

P Max__52.5____   Deflection Max __3.5____

Measurements Forgot to open PartofFile...

Circumference

Butt: __39.5____   Weight: 2 548_____

Load 1: __39.5____   MC: __9.6_____

Load 2: __38.25____   Length: __241.5_____

Tip: __34.75____

Edge Distance

Compression Hole 2 -1.5 -.5____   Hole 6 -1.25 -.75 -____

Tension Hole 5-1-1.3 -____   Hole 4 - 1 - 1.1 -____

Disk

Distance from butt end _____

Weight: Wet __3.04____ __1.041____

Dry __2.635____ __.895____

Volume_____

Specific Gravity__.55____

Total # of rings __47____

Total # of rings in outer 2" __26____

Heartwood Diameter __8.75____

Defects:_____

48.9K some shearing @ Butt and continued shearing. Ultimate was t @ K11, then shear Through H4,3,2,1 K10

	Time	Load	Cause	Location				Type				
			Knot		KC	Hole	Other	Ten	Comp	Shear	Brash	Oth
Initial				Butt						✓		
Second		50	X	77				X		X		
Second					X					x		
Ultimate												

Knot Map

Knot #	Diameter	Position (in)	Arc Distance (in)	Knot #	Diameter	Position (in)	Arc (in)
1	.8	38	8	14			
2	1.6	41	3.5	15			
3	.95	38	17	16			
4	1.15	44	13	17			
5	1.0	73	2.5	18			
6	1.25	73	10.5	19			
7	1.35	73	16	20			
8	1.0	40	-8.5	21			
9	1.1	39	-15	22			
10	1.3	77	-18	23			
11	.4	0-64	0 -2	24			
12				25			
13				26			

Pole #__4880____ Date Tested__4/13/17____

P Max__55.5____ Deflection Max _____

Measurements

    Circumference

    Butt: 46.25____ Weight: 421_____

    Load 1: 43.75*____ MC: 10.5_____

    Load 2: 42.75*____ Length: 241_____

    Tip: 39.75____

Edge Distance

    Compression Hole ___- N/A____ Hole__-___-___-____

    Tension Hole _____-____ Hole__-___-___-____

Disk

    Distance from butt end _____

    Weight: Wet__4.8525_____

    Dry___4.1645_____

    Volume_____

    Specific Gravity____.51_____

    Total # of rings ___46_____

    Total # of rings in outer 2" 20____

    Heartwood Diameter___9_____

Defects:_____

52K or small Shear @ Butt from existing check, check continue to open up @ 55.5. Compression @ 2 Checks @ 16 in.

	Time	Load	Cause	Location				Type				
			Knot		KC	Hole	Other	Ten	Comp	Shear	Brash	Oth
Initial												
Second												
Second												
Ultimate												

Knot Map

Knot #	Diameter	Position (in)	Arc Distance (in)	Knot #	Diameter	Position (in)	Arc (in)
1	1.4	23	5.5	14			
2	1.65	50.5	0	15			
3	1.2	51	10.5	16			
4	1.25	68	16	17			
5	1.4	80	12	18			
6	1.1	51	-9.5	19			
7	1.65	52	-21	20			
8		78	-12.5	21			
9	1.63	104	-7.5	22			
10	.24 - .25	55-110	-4- -8	23			
11	1.66	109	0	24			
12				25			
13				26			

Pole # 4886
P Max 52.2
Date Tested 4/16/17
Deflection Max 3.35

Measurements

Circumference
Butt: 43.25
Load 1: 42.25 *
Load 2: 42.0 *
Tip: 38.0

Weight: 610
MC: 9.5
Length: 240.9

Edge Distance
Compression Hole 2 -1.75-2.25
Tension Hole 4- 1.95-2.05
Hole 5 -2.3 -1.7 -
Hole 5 -1.95-2.05

Disk
Distance from butt end
Weight: Wet 3.3235, 2.4809
Dry 2.8045 , 2.132
Volume
Specific Gravity .483
Total # of rings 62
Total # of rings in outer 2" 29
Heartwood Diameter 10.25

Defects:
49.7, some shear @ Butt (Small), continued cracking, 52 K shear @ Butt.

	Time	Load	Cause	Location				Type				
			Knot		KC	Hole	Other	Ten	Comp	Shear	Brash	Oth
Initial												
Second												
Second												
Ultimate												

Knot Map

Knot #	Diameter	Position (in)	Arc Distance (in)	Knot #	Diameter	Position (in)	Arc (in)
1	.9	25	8	14			
2	.7	44	6	15			
3	1.35	46	18	16			
4	1.2	68	11.5	17			
5	1.1	87.5	7.5	18			
6	1.05	27	-20	19			
7	.9	46	-5.5	20			
8	1.25	67	-13	21			
9	1.25	68	-21	22			
10	1.4	83	-13.5	23			
11	1.3	84	-18.5	24			
12				25			
13				26			

Pole #___4896___   Date Tested _4/15/17_

P Max___53.9___   Deflection Max 3___

Measurements

    <u>Circumference</u>

    Butt: _40.25_   Weight: _545_

    Load 1: _41.75_ *   MC: _9.8_

    Load 2: _41.5_   Length: _242_

    Tip: _37.75_

Edge Distance

    Compression Hole _3 - 2.45 3.4_   Hole _4 - 1.9 3.1 -_

    Tension Hole _3 - 3-2.8_   Hole _4 - 3.2-2.85_

Disk

    Distance from butt end _____

    Weight: Wet _5.268___

    Dry _4,520___

    Volume_____

    Specific Gravity _.46_

    Total # of rings _58_

    Total # of rings in outer 2" _17_

    Heartwood Diameter _8.875_

Defects:_____

    Shear @ Butt, @ 53.9K, along cheek and growth ring

	Time	Load	Cause	Location				Type				
			Knot		KC	Hole	Other	Ten	Comp	Shear	Brash	Oth
Initial		53.9					Check			X		
Second												
Second												
Ultimate												

Knot Map

Knot #	Diameter	Position (in)	Arc Distance (in)	Knot #	Diameter	Position (in)	Arc (in)
1	.64	40.5	-11	14			
2	.7	42	-16	15			
3	.7	53	-12.5	16			
4	.55	55.5	-3	17			
5	.75	70	-13	18			
6	1	82	-14	19			
7	1	55	^18.5	20			
8	.85	72	19	21			
9	.2	0-15	4 - 2	22			
10	.2	57-83	5 - 3	23			
11				24			
12				25			
13				26			

Pole # 4897

Date Tested 4/16/17

P Max 50.2

Deflection Max 3.6

Measurements

Circumference

Butt: 43.0

Weight: 620

Load 1: 41.5*

MC: 9.2

Load 2: 41.0 *

Length: 241

Tip: 37.5

Edge Distance

Compression Hole ___ - ___ - ___

Hole ___ - ___ - ___

Tension Hole ___ N/A ___ - ___

Hole ___ - ___ - ___

Disk

Distance from butt end _____

Weight: Wet 1.563, 2.35

Dry 1.344, 2.028

Volume _____

Specific Gravity .498

Total # of rings 52

Total # of rings in outer 2" 21

Heartwood Diameter 8.75

Defects: _____

Tensile failure @ K12 @ 50.2K and also K4.

	Time	Load	Cause	Location				Type				
			Knot		KC	Hole	Other	Ten	Comp	Shear	Brash	Oth
Initial												
Second												
Second												
Ultimate												

Knot Map

Knot #	Diameter	Position (in)	Arc Distance (in)	Knot #	Diameter	Position (in)	Arc (in)
1	1.7	38	9.5	14	.7	85.5	-7.5
2	1.6	37	18.5	15	1.2	82.5	-5
3	1.6	59.5	8.5	16			
4	1.5	65	15.0	17			
5	1.7	88	12.0	18			
6	1.8	89	20.5	19			
7	1.5	32.5	6.5	20			
8	1.3	33.5	-3	21			
9	1.3	37.5	-7	22			
10	1.9	34.0	-17	23			
11	1.1	60.5	-5	24			
12	1.8	61.0	-17.5	25			
13	1.3	82	-9.5	26			

Pole # __4898__   Date gmTested __4/14/17__

P Max __49.3__   Deflection Max __3.4__

Measurements

    Circumference

    Butt: __38.5__   Weight: __388__

    Load 1: __38__   MC: __8.1__

    Load 2: __37__   Length: __241__

    Tip: __33.5__

Edge Distance

    Compression Hole __ - N/A -__   Hole __ - - -__

    Tension Hole __ -__   Hole __ - - -__

Disk

    Distance from butt end __/__

    Weight: Wet __4.5340__

    Dry __3.91__

    Volume __/__

    Specific Gravity __.517__

    Total # of rings __34__

    Total # of rings in outer 2" __15__

    Heartwood Diameter __8.625__

Defects: __Crushing @ 51, 0__
__Shear Failure @ Butt 49.3 K. No preexisting Cracks @ Location, along growth ring too__

	Time	Load	Cause	Location				Type				
			Knot		KC	Hole	Other	Ten	Comp	Shear	Brash	Oth
Initial												
Second												
Second												
Ultimate												

Knot Map

Knot #	Diameter	Position (in)	Arc Distance (in)	Knot #	Diameter	Position (in)	Arc (in)
1	.3	0-45	0	14			
2	.34	51-85	-1	15			
3	.4	84-105	-2	16			
4	1.72	25	11.5	17			
5	.7	52.5	-1	18			
6	1.7	57	14.5	19			
7	1.75	90	16	20			
8	1	88	-14	21			
9	.7	57	-10	22			
10				23			
11				24			
12				25			
13				26			

Pole # 4899

Date Tested 4/16/17

P Max 56.7

Deflection Max 3

Measurements

Circumference

Butt: 48*

Load 1: 46* *

Load 2: 44* *

Tip: 38.375

Weight: 658

MC: 11.6

Length: 241

Edge Distance

Compression Hole 4 . 2.9 . 3.05   Hole 5 . 2. 7. 3

Tension Hole 4 - 3.25   2.5   Hole 5 - 3.15 2.75

Disk

Distance from butt end

Weight: Wet 3.954, 1.311 4.8295

Dry 4.0645

Volume _____

Specific Gravity .475

Total # of rings 46

Total # of rings in outer 2" 18

Heartwood Diameter 10.125

✓ near existing shear crack

Defects:

56.7 Shear @ Butt, Then Continued at 56K til ultimate failure. T @ K10 too, along rings

	Time	Load	Cause	Location				Type				
			Knot		KC	Hole	Other	Ten	Comp	Shear	Brash	Oth
Initial		56.7		Butt								
Second		56		Butt								
Second		56	X	36								
Ultimate												

Knot Map

Knot #	Diameter	Position (in)	Arc Distance (in)	Knot #	Diameter	Position (in)	Arc (in)
1	.9	37	-13.5	14			
2	1.8	42	-18.0	15			
3	1.45	69	-19.6	16			
4	2.2	73	-21.0	17			
5	1.6	74.5	-10.0	18			
6	1.3	95.0	-16.0	19			
7	1.25	38.0	9.5	20			
8	1.25	43	1	21			
9	1.6	42	15	22			
10	1.8	36	21	23			
11	1.2	70.5	15	24			
12	1.6	74	3	25			
13	.3	33-91	14	26			

Pole #__4925__   Date Tested__4/7/18__

P Max__37.4__   Deflection Max __2.6__

Measurements

Circumference

Butt:__40.5__   Weight:__598__

Load 1:__41.0__   MC:__14.5__

Load 2:__40.0__   Length:__239.5__

Tip:__36.25__

Edge Distance

Compression Hole 2 - 1.25 .75   Hole 3 - 1.1 - .5 -

Tension Hole 4 - .85 - 1.15   Hole 5 - .8 - .7 -

Disk

Distance from butt end _____

Weight: Wet____4.964____

Dry____4.318____

Volume_____

Specific Gravity____.526____

Total # of rings ____34____

Total # of rings in outer 2" | 5

Heartwood Diameter____| 0.2____

Defects: _May Large Initial Check_
Slight Shear @ 25k @ Butt More Shearing @ Butt Crkt @ 37k and continued to failure

	Time	Load	Cause	Location				Type				
			Knot		KC	Hole	Other	Ten	Comp	Shear	Brash	Oth
Initial												
Second												
Second												
Ultimate												

Knot Map

Knot #	Diameter	Position (in)	Arc Distance (in)	Knot #	Diameter	Position (in)	Arc (in)
1	.3-.54	0-83	1 - -1	14			
2	.5	80-150	-1 - -5	15			
3	1.5	43	-6	16			
4	1.5	48	5	17			
5	1.4	52	-17	18			
6	1.4	76	-4	19			
7	1.5	76	4	20			
8	1	40	3	21			
9	1.2	42	14	22			
10	.9	76	-13	23			
11	1.3	77	-16.5	24			
12	1	97	-4.5	25			
13				26			

Pole # 4926   Date Tested 3/31/17

P Max 45.6   Deflection Max 3.1

Measurements

Circumference

Butt: 38.75   Weight: 457

Load 1: 38.125   MC: 11.7

Load 2: 37.0   Length: 242

Tip: 33.5

	6	2	
	1.55	1.65	
	2.25	2.0	

Edge Distance

Max Compression Face _____ Min Compression Face _____

Max Tension Face _____ Min Tension Face _____

	6	2	3
	2.1	2.2	2.2
	2.0	1.6	1.8

Disk

Distance from butt end _____

Diameter in _____

Thickness _____

Weight: Wet 316, 1665

Dry 277, 1410

Total # of rings 52

Total # of rings in outer 2" 22

Heartwood Diameter 9.2"

Defects: _____

2 Tensile Failure

	Time	Load	Cause	Location				Type					
			Knot		KC	Hole	Other	Ten	Comp	Shear	Brash	Oth
Initial		45.6	X	48				X				
Second		43		Butt			Check			X		
Second												
Ultimate												

Knot Map

Knot #	Diameter	Position (in)	Arc Distance (in)	Knot #	Diameter	Position (in)	Arc (in)
1	.4-.5	0-56	2 - 0	14	1	92	-2.5
2	.2-.4	77 123	1 - -2	15	1.25	93	-13.0
3	1	37	12	16	1	48	-19.0
4	.75	48	4	17			
5	.85	48.5	8.5	18			
6	1	48	15	19			
7	.8	67	1	20			
8	.9	69	9	21			
9	1	92	8.5	22			
10	.85	44	-4	23			
11	.8	46	0	24			
12	.95	49	-8	25			
13	.55	68	-16	26			

Pole #__4960__   Date Tested __4/14/17__

P Max __44.49__   Deflection Max __2.47__

Measurements

Circumference

Butt: __42.25__   Weight: __634__

Load 1: __42.0__   MC: __11.2__

Load 2: __40.5__   Length: __240.5__

Tip: __37.0__

Edge Distance

Compression Hole __3__ -__3.25__ __2.65__   Hole __5__ -__3.25__ __2.65__

Tension Hole __4__ -__2.9__ -__3.05__ -   Hole __5__ -__2.8__ -__3__ -__2__

Disk

Distance from butt end _____

Weight: Wet __3.184__   __3.1125__

Dry __2.83__   __2.73__

Volume _____

Specific Gravity __.57__

Total # of rings __59__

Total # of rings in outer 2" __24__

Heartwood Diameter __7.6__

Defects:

Shear @ Butt. Extended through Existing Crack 3, by other small cracks. Extended to Hole +z ((
By existing and new cracks.

	Time	Load	Cause	Location				Type				
			Knot		KC	Hole	Other	Ten	Comp	Shear	Brash	Oth
Initial												
Second												
Second												
Ultimate												

Knot Map

Knot #	Diameter	Position (in)	Arc Distance (in)	Knot #	Diameter	Position (in)	Arc (in)
1	.65	46	9.5	14			
2	.5	45	18	15			
3	.26	33-104	14	16			
4	1	46	-13	17			
5	1.3	61	14	18			
6				19			
7				20			
8				21			
9				22			
10				23			
11				24			
12				25			
13				26			

DC

TB

Pole #__4961____

P Max__5800__

Date Tested__4/7/17____

Deflection Max __3"__

Measurements

Circumference

Butt:__44.5____

Load 1:__43.0____ *Shaved*

Load 2:__41.75____

Tip:__38.5____

Weight:__584____

MC:__14.1____

Length:__240.5____

Edge Distance

Compression Hole __N/A__ - ____   Hole__ - - - ____

Tension Hole ____N/A__ - ____   Hole__ - - - ____

Disk   *Shaved*

Distance from butt end _____

Weight: Wet____3.13_____

Dry____2.74_____

Volume____/_____

Specific Gravity____.448_____

Total # of rings ____29_____

Total # of rings in outer 2"__12____

Heartwood Diameter____8_____

Defects:_____

58k Compression @ Knot and Check. Buckled at Existing Chek and Split Broke al...

Knot. Continuing

	Time	Load	Cause	Location				Type					
			Knot		KC	Hole	Other	Ten	Comp	Shear	Brash	Oth
Initial			X	125								
Second												
Second												
Ultimate												

Knot Map

Knot #	Diameter	Position (in)	Arc Distance (in)	Knot #	Diameter	Position (in)	Arc (in)
1	.3	0-57	4-0	14			
2	.3	51-103	4-0	15			
3	.8	91	0	16			
4	.4	90	4	17			
5	.4	49	8	18			
6	.4	51	3.5	19			
7	.1	125	0	20			
8	.25	92-120	0--1	21			
9				22			
10				23			
11				24			
12				25			
13				26			

Pole #: 4963

Date Tested: 3/31/17

P Max: 46.5

Deflection Max: 3.75

Measurements

Circumference

Butt: 37.125

Load 1: 37.75

Load 2: 37.5

Tip: 34.25

Weight: 472

MC: 14.7

Length: 241.5

3		6
3.4		3.2
2.8		2.51

Edge Distance

Max Compression Face _____ Min Compression Face _____

Max Tension Face _____ Min Tension Face _____

3	5	6
2.86	2.92	2.85
2.85	3.18	3.05

Disk

Distance from butt end _____

Diameter in _____

Thickness _____

Weight: Wet 458.5, 108.3, 93.7

Dry 380, 94.4, 80.7   .491 SG

Total # of rings: 43

Total # of rings in outer 2": 25

Heartwood Diameter: 9.9

Defects: Noises starting 40 k, indicating nonlinearity. Cracks extending at Hole 2,3 in Shr. C Fail @ 45k @ 46k Knot 11 Hole 4 @ Knot. Tensile failure @ Knot 5 causing catastrophic T/S through holes extending to 6.

	Time	Load	Cause	Location				Type				
			Knot		KC	Hole	Other	Ten	Comp	Shear	Brash	Oth
Initial		46				X	Crack			X		
Second		45										
Second		44										
Ultimate												

Knot Map

Knot #	Diameter	Position (in)	Arc Distance (in)	Knot #	Diameter	Position (in)	Arc (in)
1	.3	27-72	6- 0	14	.65	103.5	-12
2	.75	37	9.5	15	1.5	107	-17
3	1.4	37	19	16			
4	.8	69	7.5	17			
5	1.35	70	17.0	18			
6	.85	107	9.5	19			
7	.9	106	16	20			
8	.65	37	-1	21			
9	.95	38	-10	22			
10	1.25	69	-11.5	23			
11	.8	70	-1	24			
12	.6	106.5	-2	25			
13	.95	108.5	-7	26			

Sheared at Bottom of Holes.

Pole # 4966

P Max 58.86

Date Tested 4/13/17

Deflection Max 4.3

Measurements

Circumference

Butt: 34.25

Load 1: 38.125

Load 2: 36.5

Tip: 33.75

Weight: 522

MC:

Length: 242.5

Edge Distance

Compression Hole 3 -1.15 -1.8   Hole 4 - 1.15 2 -

Tension Hole 3 -1.95 - 1.9   Hole 4 - 1.95 2 -

Disk

Distance from butt end _____

Weight: Wet 4.273

Dry 3.577

Volume _____

Specific Gravity .543

Total # of rings 46

Total # of rings in outer 2" 22

Heartwood Diameter 8.875

T,S,C.
or
C,T,S

Defects: Not many knots

Only sign of nonlinearity. @ 53K is some to bent wood fibers above hole. Beyond Load 2 as well. 58.8K, broke off below Hole 5. Ran Along Grain below H3, sheared Thru H3-5. Tin H6. Comp above Hole 5. 1 in buckled material.

76"

	Time	Load	Cause	Location				Type				
			Knot		KC	Hole	Other	Ten	Comp	Shear	Brash	Oth
Initial		58.8	58.8			x		x				
Second												
Second												
Ultimate												

Knot Map

Knot #	Diameter	Position (in)	Arc Distance (in)	Knot #	Diameter	Position (in)	Arc (in)
1	.35	0-33	-1 - 0	14			
2	.34	32-50	-.5 -1	15			
3	.3	42-63	-1 - -2	16			
4	.45	55-82	-2 - -3	17			
5	.5	57	19	18			
6	.4	34	-8	19			
7				20			
8				21			
9				22			
10				23			
11				24			
12				25			
13				26			

Pole #__4977____ Date Tested__4/10/17____

P Max__43.8 K____ Deflection Max__3.7 in____

Measurements

Circumference

Butt:__38.875____ Weight:__414____

Load 1:__38.5____ MC:_____

Load 2:__37.25____ Length:__241.5____

Tip:__34.0____

Edge Distance

Compression Hole __6 - 2.75 3.25__ Hole __2 .3.3 .265.____

Tension Hole __6- 2.95 - 2.75__ Hole __4 -2.95-2.9 -____

Disk

Distance from butt end _____

Weight: Wet __3.5020____

Dry __3.047____

Volume_____

Specific Gravity__.429____

Total # of rings __24____

Total # of rings in outer 2"__14__

Heartwood Diameter __8.75____

Defects:

_No rep cause__   _compression of knots/Holes on ckhs_

Cracks opening at Butt. Fibers compressing outward in the nonlinear range. Tension NoT at hole o at knot C Though. Some existing cracks, but only surface deep. Then S, T, S, and then ran in shear Through hole 5.

	Time	Load	Cause	Location				Type				
			Knot		KC	Hole	Other	Ten	Comp	Shear	Brash	Oth
Initial				51			X	X				
Second												
Second												
Ultimate												

Knot Map

Knot #	Diameter	Position (in)	Arc Distance (in)	Knot #	Diameter	Position (in)	Arc (in)
1	.5	0-61	0 - -1	14			
2	.13	73-94	-8	15			
3	.11	31-58	9.5	16			
4	.6	44.5	3.5	17			
5	1.3	52	2.5	18			
6	1.25	55	6.5	19			
7	1	57	-5	20			
8	.6	98	-19	21			
9	1.15	92	4.5	22			
10	.85	95	11	23			
11	.00	46-54	14	24			
12				25			
13				26			

Pole #__4986____ Date Tested__4/8/17____
P Max__5,000____ Deflection Max __3.?.1____
Measurements Data Deleted...¨
   Circumference
   Butt: 41.75_____ Weight: 553_____
   Load 1: 41.625____ MC: 12.1_____
   Load 2: 40.75____ Length: 240_____
   Tip: 37.5_____
Edge Distance
   Compression Hole __-N/A-__ Hole_-_-_-___
   Tension Hole ___N/A-___ Hole_-_-_-___
Disk
   Distance from butt end _____
   Weight: Wet 5.7295_____
      Dry 5.643____
   Volume_____
   Specific Gravity .51_____
   Total # of rings 48_____
   Total # of rings in outer 2" 16
   Heartwood Diameter 10.125____
Defects: Large Checks
51266 Shear @ Butt, 48,000 Complete Shearing from Butt to TBZ, a few small existing cracks 13,12

	Time	Load	Cause	Location				Type				
			Knot		KC	Hole	Other	Ten	Comp	Shear	Brash	Oth
Initial												
Second												
Second												
Ultimate												

Knot Map

Knot #	Diameter	Position (in)	Arc Distance (in)	Knot #	Diameter	Position (in)	Arc (in)
1	.35	0-50	1 - -1	14			
2	.4	34-63	4- 2	15			
3	.4-.5	76-133	2- -4	16			
4	x.9	34	5.5	17			
5	1.05	32	-3	18			
6	1.15	62	-2.5	19			
7	1.15	59.5	-11	20			
8	0.6	62.5	7.5	21			
9	1.6	92	-6	22			
10	.1	84-96	8	23			
11	.05	75-100	-8	24			
12	.05	0,12-48	-6 --8	25			
13	.05	0-24	10	26			

DC Shear DC cd DC

Pole #___4988___   Date Tested___3/27/17___
P Max___50k___   Deflection Max _____
Measurements
          Circumference
          Butt:___38.75___   Weight:___469___
          Load 1:___38___   MC:___12.5%___
          Load 2:___37___   Length:___242___
          Tip:___31.375___
Edge Distance
          Max Compression Face___N/A___   Min Compression Face___N/A___
          Max Tension Face___N/A___   Min Tension Face___N/A___
Disk
          Distance from butt end _____
          Diameter in_____
          Thickness_____
          Weight: Wet___278.5, 601.6, 1090.7___
                    Dry___242.7, 530.9, 945.1___
          Total # of rings ___28___
          Total # of rings in outer 2"___15___
          Heartwood Diameter___8___
Defects:_____
          Beginning of C Failure. No Ts Tension

	Time	Load	Cause	Location				Type				
			Knot		KC	Hole	Other	Ten	Comp	Shear	Brash	Oth
Initial		50000		114			Check		✓			
Second												
Second												
Ultimate												

Knot Map

Knot #	Diameter	Position (in)	Arc Distance (in)	Knot #	Diameter	Position (in)	Arc (in)
1	.4	0-16	7	14	1	40	-6.5
2	.28	16-31	↓	15	1.25	37	-14
3	.32	25-34	↓	16	6	73	-9
4	.47	36-46	6	17	.5	75	-1
5	.22	52-58		18	1	77	-6.5
6	.33	58-67		19	.25	108-128	0
7	.42	04-87	7.5	20			
8	.3	86-96		21			
9	1	37.5	3	22			
10	1.25	39	9	23			
11	1.5	37	14	24			
12	1	74	6.5	25			
13	1.25	74	17.5	26			

Pole #_____4995_____   Date Tested____4/7/17_____

P Max____495/8_____   Deflection Max ____2.?64.04____

Measurements

Circumference

Butt:___34.125_____   Weight:__565_____

Load 1:_39.625_____   MC:____14.4_____

Load 2:_39.0_____   Length:__241.5_____

Tip:___33.5_____

Edge Distance

Compression Hole _2 - 1.45 - 2.25_   Hole _3 - 2.25 1.85_

Tension Hole _2 - 2.05 - 1.95_   Hole _3 - 2.1 - 1.95_

Disk

Distance from butt end _____

Weight: Wet____5.55_____

Dry____4.6595_____

Volume_____

Specific Gravity____.522_____

Total # of rings ____30_____

Total # of rings in outer 2"__12_____

Heartwood Diameter___9_____

Defects:_____

Shearing @ Butt 38.7K. 48.5 more Shear @ Butt. Along New Crack. Some Shelling Near Hole Ultimate @ 495 k. Tensile @ 42". Shelled Through Hole 1 Partially Because of Tensile Crack

	Time	Load	Cause	Location				Type				
			Knot		KC	Hole	Other	Ten	Comp	Shear	Brash	Oth
Initial												
Second												
Second												
Ultimate												

Knot Map

Knot #	Diameter	Position (in)	Arc Distance (in)	Knot #	Diameter	Position (in)	Arc (in)
1	1.25	40.5	0	14	1.1	91.5	9.5
2	1.1	43.0	7.5	15	.46	24-115	17.0
3	0.8	43.0	20.0	16			
4	1.2	42.0	-10.5	17			
5	1	43.0	-17.0	18			
6	1.2	63.6	2.0	19			
7	1.2	67.0	8.5	20			
8	.5	64.0	19.0	21			
9	1.45	66.0	-7.25	22			
10	1.6	90-	-1	23			
11	1.4	66	-18	24			
12	1.25	91	-11	25			
13	1.0	84.5	-19	26			

Pole #__4994_____   Date Tested __3/30/17____

P Max__30.7____   Deflection Max _____

Measurements

Circumference

Butt: _36_____

Load 1: _37_____   Weight: _458_____

Load 2: _35.75_____   MC: _12 %_____

Tip: _32.5_____   Length: _248.5_____

Edge Distance

$$\frac{5}{2.2} \quad \frac{2}{2.1}$$
$$1.7 \quad 1.5$$

Max Compression Face _____ Min Compression Face_____

Max Tension Face_____ Min Tension Face_____

$$\frac{5}{1.9} \quad \frac{2}{1.9}$$
$$1.8 \quad 1.7$$

Disk

Distance from butt end _____

Diameter in_____

Thickness_____

Weight: Wet _480.4, 720.9, 864_____

Dry _424.8, 626.7, 753.7_____

Total # of rings ___42_____

Total # of rings in outer 2" _24_____

Heartwood Diameter(Radius) _5"_____

Defects: Cracks in Tension Face. Crack running near holes._____

• Small Cracks Forming Butt @ 47 k, continues to extend through test

Moe failures at Butt. Hole/Knot. Butt Failure Extended Through Bone Zone in Shear

	Time	Load	Cause	Location				Type				
			Knot		KC	Hole	Other	Ten	Comp	Shear	Brash	Oth
Initial		16.8		Butt			Check			✗		
Second		30.7		Butt			" "			✗		
Second												
Ultimate												

Knot Map

Knot #	Diameter	Position (in)	Arc Distance (in)	Knot #	Diameter	Position (in)	Arc (in)
1	1	34	0	14	.95	99	-1
2	.80	26	11	15	.75	96	-5.5
3	.9	49	7.5	16	.75	97	-13
4	.55	52	10	17	.1-.38	0-80	-18
5	1.35	61	2.5	18	.2-.3	71-117	14
6	1.25	90	1	19			
7	1.10	96	8.5	20			
8	1.65	95	-18	21			
9	.5	89	-16	22			
10	.65	26	-12	23			
11	.5	50	-6	24			
12	.7	58	-8.5	25			
13	.8	60	-15	26			

Pole # 4445

P Max 22.29 K

Measurements *2

    Circumference

    Butt: 37.5

    Load 1: 37.0

    Load 2: 36.5

    Tip: 32.625

Date Tested 3/29/17

Deflection Max 3.4 in

Weight: 478

MC: 13.9

Length: 230"

6   Hole 1

| .9 / .9 | .75 / 1.25 |

Edge Distance

    Max Compression Face _____ Min Compression Face_____

    Max Tension Face_____ Min Tension Face_____

1.3   1.4

.5   .5

Disk

    Distance from butt end _____

    Diameter in_____

    Thickness_____

    Weight: Wet 1291.8

          Dry 1130

    Total # of rings 44

    Total # of rings in outer 2" 24

    Heartwood Diameter 9.2

Defects:_____

Initial Butt Shearing at 17.5K. 2 holes failed at 19 K in T. Some T above hole. Final Cause of failure at 22.3 k, shearing from butt to 70", following part of original

	Time	Load	Cause Knot	Location	KC	Hole	Other	Type Ten	Comp	Shear	Brash	Oth
Initial		17.5		0		x				o		
Second				61, 70, 79		x		x				
Second		22.3		0-70			X Chrd					
Ultimate												

Knot Map

Knot #	Diameter	Position (in)	Arc Distance (in)	Knot #	Diameter	Position (in)	Arc (in)
1	.67	43	~7.5	14	.1-.25	0-50	3.5-5
2	.75	52	~12.5	15	.1-.25	45-89	0- -2
3	.9	53	-2.5	16	.1-.25	87	2
4	1	54	-18	17			
5	.625	92	-2.5	18			
6	1	93	-12	19			
7	.75	94	-18	20			
8	1.125	96	-8	21			
9	1	54	10	22			
10	1	56	4	23			
11	1.04	95	9.5	24			
12	1.25	96	5.5	25			
13				26			

Pole #_4996_____   Date Tested _4/5/17_____
P Max_ 45 K_____   Deflection Max _3.2_____

Measurements

    <u>Circumference</u>
    Butt: _38.5_____   Weight: _241.5 508_____
    Load 1:_38.0_____   MC:_____15.6_____
    Load 2: _36.375____   Length: _241.5_____
    Tip: _33.25_____

Edge Distance

    Compression Hole _2 - 3.5 - 2.4_   Hole _6 - 2.3 - 3.3 -_____
    Tension Hole _6 - 3.3 - 2.6_   Hole _3 - 2.55 2.7-_____ _4 - 2.55 - 2.7_ _1 - 2.75, 3.1_

Disk

    Distance from butt end _____
    Weight: Wet_ 4.689_____
    Dry_ 3.9750_____
    Volume_____
    Specific Gravity _.55_____
    Total # of rings ____50_____
    Total # of rings in outer 2" _21_
    Heartwood Diameter _8.25____

Defects:_____

Shear at Butt. Shear Through Holes 2, 3

	Time	Load	Cause	Location				Type					
			Knot		KC	Hole	Other	Ten	Comp	Shear	Brash	Oth
Initial													
Second													
Second													
Ultimate													

Knot Map

Knot #	Diameter	Position (in)	Arc Distance (in)	Knot #	Diameter	Position (in)	Arc (in)
1	.65	31	-1	14	.25	42-60	2
2	.5	31	2	15	.25	66-80	2
3	.5	31.5	16	16			
4	.75	32	-6	17			
5	.65	31	-9.5	18			
6	.75	56.5	-4.5	19			
7	.85	59	-9.5	20			
8	.60	58	-18	21			
9	.85	85	-2	22			
10	.9	83	-8	23			
11	.85	85	-11.5	24			
12	Splinters	101		25			
13	.32	21-47	1	26			

Appendix 4: Derivations

MOE Derivation

The modulus of elasticity was determined for an asymmetric, unequal four-point loading using two methods. The 1st method was for a prismatic beam, and the second for a tapered beam. The equations for a tapered beam were taken from a Forest Products Laboratory Publication (Maki and Kuenzi 1956).

$$y = \frac{P * L^3}{E * I_0 * \gamma^3}$$

$$* \left(-.5 * \left(1 - \frac{z}{L}\right) * \gamma * \left(\frac{1}{1 + \gamma * \frac{x}{L}} + \frac{1}{1 + \gamma * \frac{z}{L}}\right) * \frac{x}{L} + \left(1 - \frac{z}{L}\right) * \ln\left(1 + \gamma * \frac{x}{L}\right) \right.$$

$$\left. - \frac{x}{L} * \ln\left(1 + \gamma * \frac{z}{L}\right) + \frac{x * z}{L^2} * \ln(1 + \gamma) \right)$$

Where

$$\gamma = \frac{d_c - d_0}{d_0}$$

And

$$z = 15.5 \ or \ 11.5 \ ft$$

$$x = 9 ft$$

$$L = 18 ft$$

The coefficients were found for each pole using formulas in an excel sheet, as γ changes for each pole based on end diameters. Using superposition, the modulus of elasticity can be found for the beam.

$$y = y_1 + y_2 = \frac{P_1}{E}() + \frac{P_2}{E}()$$

$$E = \frac{P_1}{y}() + \frac{P_2}{y}()$$

For an example, the deflection and load in the linear region for pole 4771 was found to be 30000 lb and 1.58 inches. The pole tip diameter is 12.18 inches and the butt diameter is 14.49 inches. The resultant MOE is 1.333E6 lb/in^2. When the geometry of the pole and MOE in inputted into the finite four-point bending model, the resultant deflection is 1.61 in. The difference in

deflection is less than 5%. The above equation is validated by the finite model, with a similar relationship of MOE and deflection.

Shear Deflection

$P_1 := \dfrac{1}{6}$ Loading Scenario

$P_2 := \dfrac{5}{6}$

$P := P_1 + P_2$

     $L := 18$ $a := 11.5$ $b := 4$ $c := 2.5$

Sum Moments

$-P_1 \cdot a - P_2 \cdot (a + b) + R_2 \cdot L \text{ solve}, R_2 \rightarrow 0.82407407407407407407$

$R_2 := 0.82407407407407407407$

Sum Forces

     $R_1 := P - R_2 = 0.176$

$V(x) := \begin{vmatrix} -R_1 & \text{if } x < a \\ -(R_1 - P_1) & \text{if } (a < x) \wedge [(a + b) > x] \\ (R_2) & \text{if } (a + b) < x \end{vmatrix}$ Shear for the loading scenario

$v(x) := \begin{vmatrix} -.5 & \text{if } x < 9 \\ .5 & \text{if } x > 9 \end{vmatrix}$ Shear for unit virtual load at 9 ft, the location of string LVDT

$v_c(x) := \begin{vmatrix} -.176 & \text{if } x < 14.83 \\ .824 & \text{if } x > 14.83 \end{vmatrix}$ Shear for unit virtual load at 3.17 ft, location of cylinder LVDT

$$\int_0^9 V(x) \cdot v(x)\, dx + \int_9^{11.5} V(x) \cdot v(x)\, dx + \int_{11.5}^{15.5} V(x) \cdot v(x)\, dx + \int_{15.5}^{18} V(x) \cdot v(x)\, dx$$

$$S := \int_0^9 V(x) \cdot v(x)\, dx + \int_9^{11.5} V(x) \cdot v(x)\, dx + \int_{11.5}^{15.5} V(x) \cdot v(x)\, dx + \int_{15.5}^{18} V(x) \cdot v(x)\, dx$$

     $S = 1.583$ String Coefficient

$$C := \int_0^{11.5} V(x) \cdot v_c(x)\, dx + \int_{11.5}^{14.83} V(x) \cdot v_c(x)\, dx + \int_{14.83}^{15.5} V(x) \cdot v_c(x)\, dx + \int_{15.5}^{18} V(x) \cdot v_c(x)\, dx$$

$C = 2.054$ Cylinder Coefficient

$F := \dfrac{10}{9}$ Shear Coeffeicent for Circle

$P := 45000\text{lb}$ Load at Failure

$A := 121\text{in}^2$ Area of Pole 755

$G := 114860\,\dfrac{\text{lb}}{\text{in}^2}$ Use Shear Modulus in LT direction, 10-20 times less than E

$\Delta_S := \dfrac{F \cdot S \cdot P \cdot 1\text{ft}}{A \cdot G}$

$\Delta_C := \dfrac{F \cdot C \cdot P \cdot 1\text{ft}}{A \cdot G}$

$\Delta_S = 0.068 \cdot \text{in}$ Shear Deflection for Pole 77

Orthotropic SCF in Bending

Find : The Orthotropic Stess Concentration for a Thin Douglas-Fir Plate using the derivation from Smith (1944)

Given : The Following Elastic Patameters are from the Wood Handbok

$E_z := 1780$ Longitudional Modulus

$E_x := .058 \cdot E_z = 103.24$

$v_{zx} := .383$ $v_{xz} := .464$ Poisson's Ratio

$u_{LT} := 112$ Modulus of Rigidity $G_{zx} := 122$

$G_{zx} := .071 \cdot E_z$ $G_{zx} = 126.38$ Shear Modulus

Solution:

$$\sqrt{2\left(\sqrt{\frac{E_z}{E_x}} - v_{zx} + \frac{E_z}{2 \cdot G_{zx}}\right)} = 4.65$$

$$\varepsilon := \left(\frac{E_z}{E_x}\right)^{\frac{1}{4}} = 2.038$$

$$k := \frac{\sqrt{E_z \cdot E_x}}{2} \cdot \left(\frac{1}{u_{LT}} - 2 \cdot \frac{v_{zx}}{E_z}\right) = 1.822$$

The following identity is identical to the area hyperbolic cosine   +

$$\alpha := \sqrt{k + \sqrt{k^2 - 1}} = 1.829$$

$$\beta := \sqrt{k - \sqrt{k^2 - 1}} = 0.547$$

$T := \alpha \cdot \varepsilon + \beta \cdot \varepsilon + 1 = 5.841$

This is the Orthotropic Stress Concentran at a Hole. The maximum SCF for an isotropic is 3. Therefore the multiplier for orthotropicity is.

$$\frac{T}{3} = 1.947$$

Moment Derivation

Unit Load of 1 lb is distributed to the two load heads below

$$P_1 := \frac{1}{6} lb$$

$$P_2 := \frac{5}{6} lb$$

$$P := P_1 + P_2$$

L := 18ft   a := 11.5ft   b := 4ft   c := 2.5ft

Sum Moments

$$-P_1 \cdot a - P_2 \cdot (a + b) + R_2 \cdot L \; solve, R_2 \; \rightarrow 0.82407407407407407407 \cdot lb$$

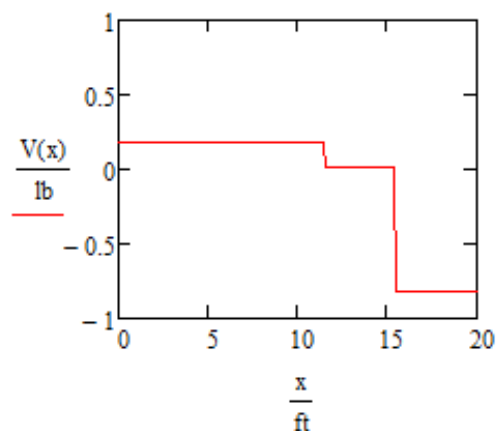$$R_2 := .824lb$$

Sum Forces

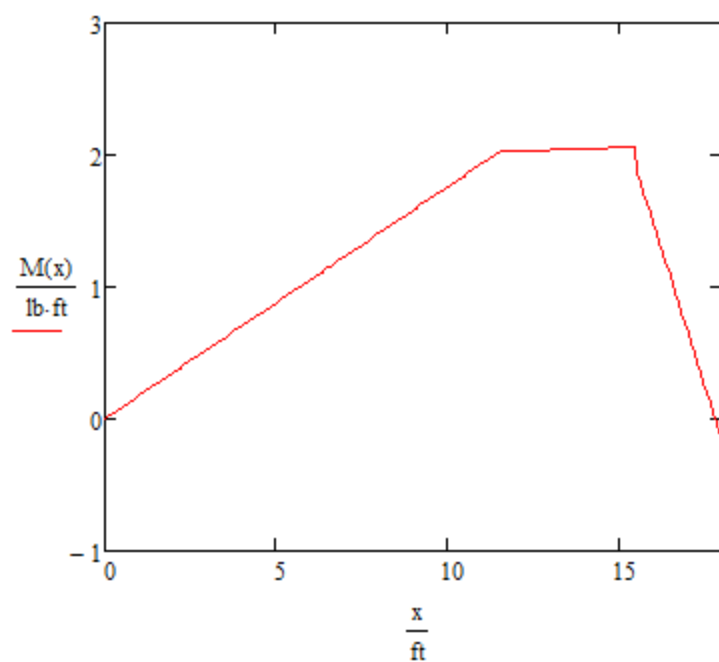$$R_1 := P - R_2 = 0.176 \cdot lb$$

$$V(x) := \begin{vmatrix} R_1 & \text{if } x < a \\ (R_1 - P_1) & \text{if } (a < x) \wedge [(a + b) > x] \\ (R_1 - P_1 - P_2) & \text{if } (a + b) < x \end{vmatrix}$$

$$V(10ft) = 0.176 \cdot lb$$

$$M(x) := \begin{cases} R_1 \cdot x & \text{if } x < a \\ R_1 \cdot a + (R_1 - P_1) \cdot (x - a) & \text{if } (a < x) \wedge [(a + b) > x] \\ [R_1 \cdot a - (R_1 - P_1) \cdot (a + b)] + (R_1 - P_1 - P_2) \cdot (x - a - b) & \text{if } (a + b) < x \end{cases}$$

$M(13\text{ft}) = 24.456\,\text{lb}\cdot\text{in}$